INFORMATION TO USERS

This reproduction was made from a copy of a document sent to us for microfilming. While the most advanced technology has been used to photograph and reproduce this document, the quality of the reproduction is heavily dependent upon the quality of the material submitted.

The following explanation of techniques is provided to help clarify markings or notations which may appear on this reproduction.

1. The sign or "target" for pages apparently lacking from the document photographed is "Missing Page(s)". If it was possible to obtain the missing page(s) or section, they are spliced into the film along with adjacent pages. This may have necessitated cutting through an image and duplicating adjacent pages to assure complete continuity.

2. When an image on the film is obliterated with a round black mark, it is an indication of either blurred copy because of movement during exposure, duplicate copy, or copyrighted materials that should not have been filmed. For blurred pages, a good image of the page can be found in the adjacent frame. If copyrighted materials were deleted, a target note will appear listing the pages in the adjacent frame.

3. When a map, drawing or chart, etc., is part of the material being photographed, a definite method of "sectioning" the material has been followed. It is customary to begin filming at the upper left hand corner of a large sheet and to continue from left to right in equal sections with small overlaps. If necessary, sectioning is continued again—beginning below the first row and continuing on until complete.

4. For illustrations that cannot be satisfactorily reproduced by xerographic means, photographic prints can be purchased at additional cost and inserted into your xerographic copy. These prints are available upon request from the Dissertations Customer Services Department.

5. Some pages in any document may have indistinct print. In all cases the best available copy has been filmed.

University Microfilms International
300 N. Zeeb Road
Ann Arbor, MI 48106

Murthy, Subbaiah Sridhara

A TRIANGULAR ANISOTROPIC THIN SHELL ELEMENT BASED ON DISCRETE KIRCHHOFF THEORY

The University of Arizona PH.D. 1983

PLEASE NOTE:

In all cases this material has been filmed in the best possible way from the available copy. Problems encountered with this document have been identified here with a check mark __√__.

1. Glossy photographs or pages _____
2. Colored illustrations, paper or print _____
3. Photographs with dark background _____
4. Illustrations are poor copy _____
5. Pages with black marks, not original copy _____
6. Print shows through as there is text on both sides of page _____
7. Indistinct, broken or small print on several pages __✓__
8. Print exceeds margin requirements _____
9. Tightly bound copy with print lost in spine _____
10. Computer printout pages with indistinct print _____
11. Page(s) _____ lacking when material received, and not available from school or author.
12. Page(s) _____ seem to be missing in numbering only as text follows.
13. Two pages numbered _____. Text follows.
14. Curling and wrinkled pages _____
15. Other Page 196 missing print. Not available from author or school. Filmed as received.

University Microfilms International

A TRIANGULAR ANISOTROPIC THIN SHELL ELEMENT BASED ON DISCRETE KIRCHHOFF THEORY

by

Subbaiah Sridhara Murthy

A Dissertation Submitted to the Faculty of the

DEPARTMENT OF CIVIL ENGINEERING AND ENGINEERING MECHANICS

In Partial Fulfillment of the Requirements
For the Degree of

DOCTOR OF PHILOSOPHY
WITH A MAJOR IN ENGINEERING MECHANICS

In the Graduate College

THE UNIVERSITY OF ARIZONA

1 9 8 3

THE UNIVERSITY OF ARIZONA
GRADUATE COLLEGE

As members of the Final Examination Committee, we certify that we have read the dissertation prepared by Subbaiah Sridhara Murthy

entitled A TRIANGULAR ANISOTROPIC THIN SHELL ELEMENT BASED ON DISCRETE KIRCHHOFF THEORY

and recommend that it be accepted as fulfilling the dissertation requirement for the Degree of DOCTOR OF PHILOSOPHY.

	Oct. 13, 83 Date
	10/13/83 Date
	10/13/83 Date
	10/13/83 Date
	10/13/83 Date

Final approval and acceptance of this dissertation is contingent upon the candidate's submission of the final copy of the dissertation to the Graduate College.

I hereby certify that I have read this dissertation prepared under my direction and recommend that it be accepted as fulfilling the dissertation requirement.

Dissertation Director	10/13/83 Date

STATEMENT BY AUTHOR

This dissertation has been submitted in partial fulfillment of requirements for an advanced degree at The University of Arizona and is deposited in the University Library to be made available to borrowers under rules of the Library.

Brief quotations from this dissertation are allowable without special permission, provided that accurate acknowledgment of source is made. Requests for permission for extended quotation from or reproduction of this manuscript in whole or in part may be granted by the head of the major department or the Dean of the Graduate College when in his judgment the proposed use of the material is in the interests of scholarship. In all other instances, however, permission must be obtained from the author.

SIGNED: 

To My Parents

ACKNOWLEDGMENTS

The author is deeply indebted to Dean Richard H. Gallagher who as chairman of his doctoral committee provided the author with invaluable guidance and advice throughout his graduate study. His deep insight and vast knowledge of the finite element method have been instrumental in successful completion of this research. His kindness, patience and understanding toward the author is gratefully acknowledged.

The author is also indebted to Professor Donald A. DaDeppo for his invaluable help during various stages of the research. His great enthusiasm and dedication to graduate teaching have left indelible mark on the author.

Acknowledgments are also due to Professors C. S. Desai, R. M. Richard, and B. R. Simon for their encouragement and kind help as members of the author's committee.

The author is also highly thankful to Mrs. Blanche A. Seferlis, Coordinator, Engineering Administration for her kind help and cooperation during the course of this study. Thanks also to Mrs. Terry Clark for the final typing of the manuscript.

The Graduate study program of the author at The University of Arizona was fully supported by the Government of India by awarding him "The Government of India National Scholarship for Study Abroad." This financial help is gratefully acknowledged.

TABLE OF CONTENTS

TABLE OF CONTENTS--Continued

TABLE OF CONTENTS--Continued

LIST OF ILLUSTRATIONS

LIST OF ILLUSTRATIONS--Continued

LIST OF ILLUSTRATIONS--Continued

LIST OF TABLES

LIST OF TABLES--Continued

ABSTRACT

The research work presented here deals with problems associated with finite element analysis of laminated composite thin-shell structures. The specific objective was to develop a thin shell finite element to model the linear elastic behavior of these shells, which would be efficient and simple to use by the practicing engineer.

A detailed discussion of the issues associated with the development of thin shell finite element has been presented. It has been pointed out that the problems encountered with formulation of these elements stem from the need for satisfaction of the interelement normal slope continuity and the rigid body displacement condition by the assumed displacement functions. These difficulties have been surmounted by recourse to the discrete Kirchhoff theory approach and an isoparametric representation of the shell middle surface.

A detailed derivation of the strain energy density in a thin laminated composite shell, based on a linear shear deformation theory formulated in a general curvilinear coordinate system, has been presented. The strain-displacement relations are initially derived in terms of the displacement and rotation vectors of the shell middle surface, and are subsequently expressed in terms of the cartesian components of these vectors to enable an isoparametric representation of the shell geometry.

A three-node curved triangular element with the tangent and normal displacement components and their first-order derivatives as

the final nodal degrees of freedom has been developed. The element formulation, however, starts with the independent interpolation of cartesian components of the displacement and rotation vectors using complete cubic and quadratic polynomials, respectively. The rigid-body displacement condition is satisfied by isoparametric interpolation of the shell geometry within an element. A convergence to the thin shell solution is achieved by enforcement of the Kirchhoff hypothesis at a discrete number of points in the element.

A detailed numerical evaluation through a number of standard problems has been carried out. Results of application of the "patch test solutions" to spherical shells demonstrate a satisfactory performance of the element under limiting states of deformation.

It is concluded that the DKT approach in conjunction with isoparametric representation results in a simple and efficient thin shell element.

CHAPTER 1

INTRODUCTION

In nature shells have evolved as the most efficient among the structural forms to withstand the effects of the natural forces to which they are subjected. Most shells occurring in nature are doubly curved. Sea shells, shells of eggs, nuts and human skulls are typical examples.

The shells derive their strength through form as opposed to strength through mass. The efficiency of the shell structural form stems from the coupling of the stretching and bending actions of the shell due to the curvature of the shell surface.

The earliest use of the shell structural form by the human civilization can be traced to the historical domes of ancient times as found in the Indian and Roman architecture. The modern thin-shell dome may be regarded as an evolution of the massive masonry dome.

The modern use of thin shells as roof coverings over large-span buildings providing large column-free space, as we know today, had its beginnings in the cylindrical barrel shells built in Germany in the 1920s. Since then the use of shells as an efficient structural form has grown into the other areas of engineering applications. Their extensive use in automobile bodies, ship hulls, aircraft fuselages, boilers and pressure vessels, liquid storage tanks and cooling towers are but a few examples.

The increasing use of shells in engineering applications has kept pace with the developments of modern materials of construction and efficient design and analysis procedures. While development of reinforced concrete led to the extensive use of thin shells in civil engineering architecture, the advent of high strength sheet metal suggested metallic thin shells as a better alternative in other industrial applications. Fiber reinforced composites are emerging as the materials of the future. Their high strength and low weight have prompted their use in aerospace applications which more often take the form of thin shells. The acceptance of shell structural form by the engineering fraternity is also due to the developments of design procedures and analysis tools to establish their structural integrity and cost effectiveness.

The earliest effort toward the analysis of shells was based on the assumption of membrane behavior of shells which led to the membrane or momentless theory of shells, where the bending resistance of the shell is neglected. While the origin of this theory is found in the work of Lame and Clapeyron [1], a general form of the equations of the membrane theory was due to Beltrami [2]. These theories were simple, and in certain cases gave a completely correct picture of the shell mechanism. However, there was need for a general shell theory accounting for the bending of the shell. The development of such a theory was motivated by the successful development of plate theory by Kirchhoff [3].

The plate theory developed by Kirchhoff [3] was based on the hypothesis that a normal to the undeformed reference surface remains

normal to the deformed reference surface and unstretched. Using the same assumption, Aron [4] in 1874 made the first attempt to develop a bending theory of thin shells from the general equations of elasticity. This was followed by the successful development of such a theory in 1888 by Love [5], known as Love's first approximation. It was shown that the strain energy in a thin shell undergoing small elastic deformations can be expressed as the sum of stretching and bending energies. However, it was soon discovered that, for general shells, the strain-displacement relations of Love's first approximation do not give zero strains under rigid body rotations. Nevertheless, Love's first approximation remained, for 70 years, the basis for the analysis of thin shells. The definitive work of Koiter [6] was very significant in establishing the nature of Love's first approximation.

Koiter [6] established that Love's expression for strain energy for a thin shell as the sum of stretching and bending energies is indeed a consistent first approximation on the basic assumption of plane stress; and the relative error in this approximation does not exceed h/R where h and R are, respectively, the thickness and the minimum radius of curvature of the shell. The strain-displacement relations given by Koiter [6] and independently by Sanders [7] give zero strains under rigid body movements. This theory is popularly known as Koiter-Sanders theory, and is generally considered as the best linear thin-shell theory. These theories, however, neglect the transverse shear deformation effects.

The neglected transverse shear energy may be of considerable importance in some classes of problems. This led to the development of

shell theories including the effects of transverse shear deformation [8, 9]. These theories resulted in complicated differential equations and associated boundary conditions.

The differential equations of the general shell theory were not, even in special cases, amenable to analytical treatment. However, for shells of revolution satisfying certain conditions, it was shown by Reissner [10] and Meissner [11] that the general fourth-order differential equation can be reduced to two second-order equations. They were recast by Reissner [12], offering certain advantages over those of Reissner-Meissner equations. The integration of the Reissner-Meissner equation for the general shell of revolution by the classical methods of asymptotic integration was given by Hilderbrand [13]. Such solutions, however, were not valid near the singular points of the differential equations.

Langer [14] proposed a method of asymptotic integration. The Reissner equations for the shell of revolution were readily amenable to treatment by this method, even at the singular points of integration. Such solutions were obtained for toroidal [15], ellipsoidal [16] and paraboloidal [17] shells of revolution. Such solutions for general shells under general boundary conditions and arbitrary loading were practically impossible, however; and, to that end, numerical solutions were sought. Although finite difference techniques and the methods of direct integration of the differential equations were established much earlier, it was not until the advent of modern digital computers in the 1950s that their applications to the analysis of practical shells were successful.

With the introduction of high-speed digital computers the finite element method was developed as a powerful numerical method for the analysis of structures. This method is versatile in its application to practical problems of complex geometry, boundary conditions and loading. It lends itself to easy incorporation of the effects of geometric and material nonlinearities, and is suitable for the development of general-purpose computer programs for large classes of problems which can be used without the comprehensive knowledge of their theoretical basis.

The finite element method was founded in the works of Courant [18], Argyris and Kelsey [19], and Turner et al. [20]. Since then the finite element technology has advanced through a number of indistinct phases; a detailed review of this progress is given by Zienkiewicz [21]. Many excellent textbooks on the subject have appeared [22-24], and are continuing to appear.

Motivated by the development of finite element formulation for plane stress problems, researchers developed formulations for three-dimensional and axisymmetric solids, problems of plate bending, and axisymmetric and general thin shells. While the developments of plane stress and solid elements did not encounter difficult problems, the development of satisfactory plate and shell elements had to go through a long period of research effort, which also led to the opening of new avenues of research in the finite element theory, including hybrid methods and isoparametric elements with selective and reduced integration.

One of the sought-after applications of the finite element method was its employment in the analysis of general thin shells. The potential of the finite element method for the design analysis of thin shells was foreseen by researchers in the field. The success of the method in this direction has been less than completely satisfactory. This can be attributed to the rigorous mathematical requirements demanded by the finite element theory as well as to the underlying shell theory for the development of a satisfactory curved thin shell element. Some of these requirements are also shared by the formulation for a plate bending finite element. It may be observed that the lack of a good plate bending element inhibited the development of a good thin shell element, and the developmental histories of the plate and thin-shell elements are parallel. Many thin-shell curved elements have been developed in the literature. They are of varying complexity, and each is aimed at an improvement over its predecessor, either in its performance or computational advantage. All of them, however, leave something to be desired.

The objective of the present research work is to develop a curved general thin-shell element for anisotropic shells of multi-layered laminated construction.

In the following, at the outset, the problems associated with the development of thin-shell elements are presented. This is followed by a survey of the general thin-shell finite elements, leading to the rationale behind the development of the new shell element. In the next section, the criteria for the development of the new thin shell element are summarized, followed by a brief description of the element

formulation. Finally, the scope of the present study is outlined at the end of the chapter.

1.1 Finite Elements for Thin Shells

A general thin shell structure can be discretized as an assemblage of curved elements which can take the shape of a quadrilateral or triangle. The latter shape is generally preferred due to its advantage in modeling shell surfaces of various geometries with irregular boundaries, and its relative ease in accommodating cutouts and mesh refinements near regions of significant response. The mathematical basis for the discretization of the primary field variables is usually based on one of the well-known variational principles of the structural mechanics.

The commonly used variational basis for the element formulations include, among others, the Principle of Minimum Potential Energy (PMPE), the Principle of Minimum Complementary Energy (PMCE), and Reissner's mixed variational principle. These principles lead, respectively, to displacement, force and mixed methods for the formulation of element force-displacement relations. Among these, the displacement or the stiffness method has been most successful, especially for curved thin-shell elements.

The advantages of the displacement method include the relative ease of choice of displacement trial functions to satisfy continuity as demanded by the PMPE, the symmetric-positive definite nature of the resulting algebraic equations, and its ease in extension to the study of dynamic response and nonlinear behavior including elastic stability.

These advantages have resulted in the development of large general-purpose structural analysis programs based on the displacement method. The development of a new finite element, therefore, cannot discount the advantage of existing programs. Thus, the research effort toward the development of a new thin-shell element was focused on the displacement method. The following discussions and the survey of the curved thin-shell elements primarily refer to this class of elements.

There are three associated issues in the development of thin-shell elements, namely, (a) shell theory, (b) displacement field and (c) geometric representation.

1.1.1 Shell Theory

The element formulation involves the discretization of the strain energy of the thin shell which is obtained by employing one of the classical shell theories. Such a theory could be a deep shell theory, resulting in a deep shell element, or a shallow shell theory leading to a shallow shell element. In this work the interest is in deep shell theory where the shell behavior is described with reference to curvilinear coordinates embedded on the middle surface of the shell. As noted by Morris [25], according to Truesdell and Toupin [26] for general field theories, any set of constitutive equations must satisfy certain mathematical principles. Among these, in the context of shell theories, Gol'denveizer [27] and Naghdi [28] point out three significant principles: consistency, rigid displacement invariance and coordinate invariance.

Consistency requires that any set of constitutive equations should be consistent with the principles of energy and equilibrium. As Gol'denveizer [27] points out, this implies the existence of reciprocity analogous to Betti's principle.

Rigid displacement invariance requires that the constitutive relations should remain invariant under rigid body displacement, which implies that such displacements should give rise to zero strain energy.

Coordinate invariance requires that the equations should be stated by a rule which holds equally well in all coordinate descriptions. This condition can easily be satisfied if the appropriate equations are stated in tensorial form or by the aid of direct notation without employing coordinates.

It may be noted that many thin-shell elements have relied on the theories of Love [5] and Novozhilov [29], neither of which gives a satisfactory compliance with all the above principles [25]. However, it is argued that the degree of rigor created by the requirement of the satisfaction of all the above principles is not necessary in view of the fact that numerical methods give approximate answers. The best course would seem to lie in choosing a theory which already satisfies these conditions.

1.1.2 Displacement Fields

The choice of representations for displacements within an element is another important aspect requiring careful consideration. In order to have theoretical assurance of convergence of the numerical

solution these trial functions should meet certain conditions. They are as follows:

1. The displacement trial functions should be able to represent constant strain states.
2. The displacement trial functions should give zero strain energy under rigid body displacements.
3. The displacement trial functions should satisfy the required degree of interelement continuity; this is one less than the highest order of derivative occurring in the functional to be minimized.

These conditions are to be satisfied in addition to the requirements on the underlying shell theory.

The constant strain condition can be easily satisfied if the displacement functions are assumed as polynomials in the curvilinear coordinates embedded on the shell middle surface. However, the use of lower order polynomials should be avoided since they usually lead to excess stiffness in response to inextensional bending modes [30].

An accurate representation of the rigid body modes must be included in the displacement functions for an acceptable rate of convergence [31]. Noncompliance with this condition, however, does not preclude convergence to the correct solution [32], although the convergence rate, from practical considerations, might not be acceptable.

Some of the earlier thin-shell elements [e.g., 33, 34] did not contain an explicit representation of the rigid body modes. It was

argued, however, that the higher order (cubic or quintic) polynomial representations for the displacement components in the curvilinear coordinates would result in a good approximation for the rigid body modes which contain trigonometric functions of the curvilinear coordinates [34]. It was observed by Morley [35] that, in order to retain the accuracy associated with the first approximation theory, if the tangential displacements are limited to quadratic polynomials, it is generally necessary that the linear dimensions of the finite element be of the same order of magnitude as the shell thickness, provided that the rigid body displacements are accommodatingly small. However, the use of quartic expressions would increase the linear dimension to $(Rxh)^{1/2}$, where R is the minimum radius, and h is the thickness of the shell. Thus, simply increasing the order of the approximating polynomial does not remove the rigid-body errors but reduces their influence. Notwithstanding, an exact representation of the rigid body modes can be achieved by taking recourse to "iso-parametric" representation of the shell middle surface and displacement components within an element.

In the development of the SHEBA shell element, Argyris and Scharpf [36] showed that, if the global cartesian components of the displacement vector and the position vector to the shell middle surface are interpolated by same set of shape functions, then the rigid body modes can be exactly represented. In the development of SHEBA element a special nonshallow shell theory using "natural strain" concept was adopted. Later, Dupuis [31] employed the isoparametric representation in conjunction with Koiter-Sanders thin-shell theory.

The displacement functions should also meet the conformity requirement. This requirement demands that the displacement function, and its derivatives up to one order less than the highest derivative occurring in the functional, be continuous across the interelement boundary. The order of the highest derivative in the potential energy expression depends on the underlying shell theory.

Since the beginning, due to their well-established nature, the theories based on the Kirchhoff hypothesis have formed the basis for the formulation of plate and shell elements. In conjunction with the PMPE, they demand the continuity of normal slope across the inter-element boundaries for a conforming plate or shell element.

Irons and Draper [37] showed that it is impossible to form Kirchhoff-theory conforming triangular plate or shell elements with simple nodal connections. It requires at least a quintic polynomial, with the function and all of its first-order and second-order derivatives as nodal degrees of freedom, to form a three-node conforming triangular plate or shell element. But these higher order derivatives, which lack direct physical significance, are not desirable from practical considerations. Notwithstanding, conforming three-node triangular elements were developed using various artifices, such as the subdomain approach [38], use of rational polynomials [39] or the Lagrangian multiplier technique [40]. Some of these formulations were also extended to thin-shell elements [34, 41].

An alternative approach is to seek formulations based on plate or shell theories which relax the Kirchhoff assumption. Here, the displacements of the reference surface and the rotations of the

normals to the reference surface are independently assumed. Melosh [42] employed it for plate bending problems, and Utku [43] applied it to shallow shell elements. Later, Key and Beisinger [44] developed a quadrilateral element for thin shells. All of these elements, however, inherited the problems of excessive stiffness for coarse meshes and slow convergence rates.

To overcome the above disadvantages of an otherwise attractive approach, the imposition of Kirchhoff constraints at a discrete number of points in the structure was proposed and used by Wempner, Oden and Kross [45]; this scheme later became known as the Discrete Kirchhoff Theory (DKT). In this theory, the bending energy is calculated from the independently assumed normal rotations. To force the convergence of the solution to that of Kirchhoff theory, Kirchhoff constraints are enforced at the nodal points in the structure. Thus, at the nodal points, the normal rotations are expressed in terms of the reference surface displacements, and one arrives at a conforming plate or shell element with conventional degrees of freedom as nodal connection quantities. The development of the new shell element in the present work is based on the "discrete Kirchhoff theory" approach.

1.1.3 Geometric Representation

The problem of geometric representation in finite element shell analysis is one of its most important aspects, and is drawing increasing attention. In case of the general shell, the geometry of the middle surface is described by the cartesian components of the position vector to any point on the shell surface and, depending on the shell theory,

their derivatives up to third-order, as functions of the curvilinear coordinates embedded on the shell surface.

The geometric description is usually provided at the nodal points, and the geometry within the shell is interpolated from these nodal data. For a shell surface of regular geometry the geometric description of the shell surface can be readily obtained using the parametric equations of the shell surface. However, for shells of arbitrary geometry one has recourse to mathematical techniques of curved surface representation.

In the beginning, the mathematical basis of the representation of curved surfaces was realized in the work of Coons [46], Ferguson [47], Bezier [48] and others. Lien [49] applied the Coons' surface-patch technique to finite element thin shell analysis. More recently Wu [50] developed a unified approach to the geometric problems of finite element thin-shell analysis based on a closed-form bivariate expression. This work also includes a survey of different techniques for shape representation.

In the present work, it is assumed that the shell geometric representation is available at the nodal points in a curvilinear coordinate system which need be neither principal nor orthogonal. Such nodal data are provided either by the analytical equation of the shell surface or from the numerical data obtained by a suitable mathematical representation of the shell surface.

In the next section, a brief survey of the triangular curved thin-shell element is presented.

1.2 A Survey of Curved Thin-Shell Elements

The evolution of the finite element method for thin shell structural analysis has been traced by Gallagher [51]. Three distinct approaches to the finite element representation of thin shells can be identified: (a) by the "facet" representation where the shell surface is modeled as an assemblage of flat elements, (b) by the use of three-dimensional solid or thick-shell isoparametric elements and (c) by the curved elements based on a thin shell theory. The relative advantages and disadvantages as well as limitations of the first two approaches have been extensively discussed in literature [50-52].

An excellent and comprehensive review of the development of thin shell elements until 1969 is given by Gallagher [52]. Further progress in the development of curved finite elements until 1971 is presented by Dawe [53], and the later developments until the middle of the 1970s are summarized in the articles of Gallagher [54] and Bushnell [55].

In view of these comprehensive surveys, and since the present work is focused on the development of a curved shell element, a discussion of some of the earlier formulations as well as the recent developments of curved thin shell elements are presented to bring out the rationale for the development of the new element.

Cowper, Lindberg and Olson [56] presented the "CURSHL" element as an extension of their original conforming shallow shell element [57]. The tangential displacements are interpolated by complete cubic polynomials, and the normal displacement by a restricted quintic polynomial with cubic variation of normal slope along the

element sides. The centroidal values of the tangential displacements are initially used as nodal degrees of freedom which are later removed by static condensation. The resulting stiffness matrix has thirty-six degrees of freedom, twelve at each of the corner nodes, consisting of the values of three translations, their six first-order derivatives and three second-order derivatives of the normal displacement. The user has the option to generate the element matrices based on either Koiter-Sanders or Donnell-Vlasov shell theory.

Published results [56] indicate that CURSHL gives extremely accurate results and has a high convergence rate. The element does not contain an explicit representation of rigid body modes, however. Also, the element is overconforming, and the nodal continuity of the second derivatives of the normal displacement lead to practical difficulties in the analysis of nonsmooth shells and shells with curvature discontinuity.

Argyris and Scharpf [36] formulated the so-called SHEBA element, where a complete quintic polynomial with twenty-one terms is used for each of the three displacement components. Interelement continuity is satisfied by the use of midside nodes having all three normal derivatives as degrees of freedom. An exact representation of the rigid body modes is achieved by isoparametric representation of the shell surface and the displacements. The stiffness matrices are derived using a special nonshallow shell theory based on the "natural strain" concept due to Argyris. The resulting stiffness matrix has sixty-three degrees of freedom, eighteen at each of the corner nodes (three translational displacements, all six first derivatives, and all

nine second derivatives), and three normal derivatives at each of the three midside nodes.

SHEBA element gives extremely accurate solutions [58]. Earlier critics [34] have raised questions about its efficiency in obtaining a solution of given accuracy as compared to other simpler elements, since the midside nodes in the SHEBA element lead to large bandwidths for the resulting algebraic equations. Due to the large size of the element matrices the computational cost for nonlinear analysis would be prohibitive. Also, it is difficult to detect the relation of the approach of the shell theory using triangular coordinates, and that based on mathematical models of thin elastic shells expressed in tensor notations [31].

Dupuis [31] presented a curved triangular element based on the Koiter-Sanders model where the shell surface is described in a curvilinear coordinate system. The rigid body motion condition is satisfied by interpolating the displacements and the shell geometry in a global cartesian coordinate system by same set of shape functions. To enable such an isoparametric interpolation, the potential energy functional in the curvilinear coordinates has been transformed into a global cartesian coordinate system. The element derivation utilizes cubic shape functions with three rational polynomials [59] for conforming interpolation of all the displacement components, with nine degrees of freedom at each of the corner nodes. The element formulation, apparently, satisfies all the mathematical requirements of Ritz's method [31]. The "standard" cylindrical shell roof problem is the only numerical solution available.

The displacement solution for the cylindrical shell roof problem presented in reference [31] converges to a value about thirty-five percent above the shallow shell solution of Scordelis and Lo [60]. Other deep shell solutions [34, 50] converge to a value about three percent below the shallow shell solution. No attention seems to be given to this in the literature. The lack of extensive numerical comparisons, and the high-order of numerical integration required for the rational polynomials has made this element less attractive for practical applications.

Thomas and Gallagher [61] formulated a curved triangular element described in curvilinear coordinates based on the generalized potential energy concept [23]. The element tangential and normal displacements are approximated by complete cubic polynomials, which satisfy neither the interelement admissibility conditions, nor the criterion of zero strain energy under rigid body motion. The continuity of normal derivatives across the interelement boundaries is enforced in the global representation using the Lagrange multiplier technique, which also represents a modification of the potential energy. These Lagrange multipliers, which have the units of force, quantify the normal moments required to restore the normal slope continuity. Thus, the element has a total of thirty degrees of freedom, with nine at the corner nodes, and one Lagrange multiplier at each of the three midside nodes. The formulation has also been extended to nonlinear and stability analyses [62]. Extensive numerical results are presented for a variety of shells for both linear and nonlinear analyses [34, 61-63].

The numerical solutions show a satisfactory prediction of results for the displacements; but the same conclusion cannot be drawn for stress predictions. The use of Lagrange multipliers has not only resulted in increase of the problem size, but also requires careful pivotal strategy in the solution of the resulting algebraic equations to avoid a zero pivot [61]. The element lacks explicit rigid body representation, and also the midside freedoms are undesirable.

More recently, Wu [50] developed a curved triangular thin shell element closely following the theoretical basis of SHEBA element [36]. The natural coordinate systems, the isoparametric representation of the element geometry, and the shell theory based on the natural strain concept are directly adopted from the SHEBA element. The major difference between the two formulations is in the interpolation scheme for the element geometry and displacements. While the SHEBA element employs complete quintic polynomials for each of the global cartesian components, the element under discussion uses the cubic interpolation scheme proposed by Birkhoff and Mansfield [64]. The latter scheme uses nine cubic polynomial shape functions and three singular shape functions in the natural area coordinates to achieve a C^1-continuous interpolation of a function over a triangular region. This approximation for the displacements results in a total of thirty-six degrees of freedom for the element, nine at each corner node and three at each midside node. The degrees of freedom at the corner nodes are the three components of the displacements along the directions of principal curvature and shell normal, and their six first-order derivatives with respect to the principal curvilinear coordinates. The degrees of freedom at the

midside node are $u_{,s_n}$, $v_{,s_n}$, and $w_{,s_n}$, where u and v are, respectively, the displacement components along the tangent and normal to the element curved edge lying in the tangent plane of the shell surface at the midside node, and w is the component along the shell normal. s_n is the unit vector in the direction of the u-displacement.

Although the rational polynomials used in the displacement approximation provide the desired C^1-continuity, they also result in singular second-order derivatives required to define the curvature terms. To alleviate this difficulty, a set of substitute second-order derivatives, similar to those used by Irons and Razzaque [65] in their plate bending elements, is adopted. These substitute shape functions provide C^1-interelement compatibility for the constant strain state and thus satisfy the conditions of the patch test [66]. However, the interpolation scheme violates the C^1-continuity of the displacement field in a general state of deformation where the strains are not constant. This discrepancy is reduced by minimizing the difference between the two sets of second-order derivatives in a least square sense, as suggested by Irons and Razzaque [65].

Extensive numerical results are presented [50] to show that the element gives accurate results for various classes of shells, and the computational costs are modest. More recently, the formulation has been extended to nonlinear analysis [67].

The element stiffness matrix, however, has a rank deficiency of two beyond that allowed for rigid body modes. This additional rank deficiency is due to the lack of linear independence in the choice of

the substitute shape functions, which is reflected in the representation of the bending behavior by the substitute derivatives. For a curved shell surface, this does not result in a singular stiffness matrix, due to the inherent coupled membrane-bending action. In this case, the two linearly-dependent modes, termed "pseudo zero-energy modes" [67], blend to give a zero value for the combined membrane and bending energies. Nevertheless, the contribution of these two bending modes to the global energy is lost.

The above deficiency has, apparently, not resulted in loss of the performance of the linear element. However, for linear buckling and geometrically nonlinear analyses, the adverse effect is more pronounced. In the case of highly nonlinear problems, the deficiency of the energy in the global level leads to undesirable flexibility [67]. Also, for the special case of a flat plate, with no rotational degrees of freedom suppressed and with uniform element sizes, the global stiffness matrix is singular.

The curved thin shell elements covered in the discussion presented so far belong to the class of elements based on thin shell theories, which accept in one form or another the Love-Kirchhoff hypothesis. The adherence to the latter has led to the difficulties associated with the C^1-continuous interpolation over a triangle. This difficulty prompted the development of plate and shell elements based on shell theories which relax the Kirchhoff hypothesis. Here, we may recall the earlier discussion on the development of elements which led to the discrete Kirchhoff theory (DKT) approach. This approach has been highly successful for triangular elements [68], and a few

applications to curved thin shell development have appeared in the literature.

Wempner et al. [45] proposed a rectangular element in the reference surface coordinates based on DKT. Although the formulation was for a general shell, the applications were limited to plates and cylindrical shells.

Key and Beisinger [44] recognized the potential of the formulation based on DKT, and sought to develop an arbitrary thin shell element. Although the linear shear theory for an arbitrary shell was presented, their "KB6" quadrilateral element with thirty-six degrees of freedom is embedded on the middle surface of a shell of revolution.

Batoz, Dhatt and their coworkers have developed a number of curved triangular elements for the analysis of shallow and deep shells, which they have summarized in reference [69]. The representation of bending behavior in all these formulations is based on the DKT approach for triangular plate elements, simultaneously developed by Stricklin et al. [70] and Dhatt [71]. The latter approach consists essentially in assuming, as a starting point, a nine-term cubic polynomial for the transverse displacement, and complete quadratic polynomials for the two independent normal rotations, with a total of twenty-one generalized displacements. By introducing discrete Kirchhoff constraints and the constraints of a linear variation of the normal rotations, the total degrees of freedom for the element are reduced to nine, consisting of the transverse displacement and its two first derivatives at each corner node. This representation will be subsequently referred to as the DKT representation.

Dhatt [72] presented a curved triangular element with twenty-seven degrees of freedom based on a linear shear theory applicable to thin shallow shells. The vertical distance to a point on the shell surface above the horizontal base was approximated as that of a quadratic surface. The tangential displacements are interpolated by nine-term cubic polynomials, and DKT representation is used for the normal displacement. Two illustrative examples show that the displacements slowly converge to shallow shell solution.

In a later presentation [73] the above element was modified so as to satisfy the shallow shell rigid body conditions. The latter condition is satisfied by representing the tangential displacements by linear polynomials coupled with transverse displacement terms. The DKT representation is retained for the bending behavior, and the element has a total of fifteen degrees of freedom. The results of the application of the element to the cylindrical shell roof problem show that the element is too stiff. The deflection solution for the cylindrical roof problem converges to a value which is about five percent below the shallow shell solution, even after using more than 1200 degrees of freedom. However, satisfactory results are obtained for a shallow square hypar. Thus, the element seems to be limited to shallow shell applications.

Batoz [74] has formulated a curved triangular thin shell element in a curvilinear coordinate system using the DKT approach. Linear shear theory in a general curvilinear system, as derived by Wempner et al. [45], is used to calculate the element strain energy. Tangential displacements are interpolated by cubic Hermitian

polynomials, while the DKT representation is used for normal displacement. The element has a total of twenty-seven degrees of freedom, nine at each corner node. The analysis of cylindrical shells under point and distributed loads, and a spherical shell under pinching loads at the poles are presented as example problems. The finite element solutions converge to those based on deep shell theory. Although the formulation is presented for anisotropic laminated shells, numerical results are limited to isotropic shells. The shallow-shell version of the element has also been extended for nonlinear and stability analyses [74, 75].

The above element formulation does not contain an explicit representation of the rigid body modes. Also, no verification of adequate compliance with the convergence conditions through a "patch" test has been provided. There is a need to demonstrate that the element can acequately represent the limiting states of behavior, typical of inextensional bending and pure membrane states of deformation, and those accompanied with large rigid-body-type displacements.

DKT approach has been, thus, established as a practical and viable alternative for the development of conforming curved thin shell elements with simple nodal connections. The only curved triangular thin shell element formulated in a curvilinear coordinate system for deep shell applications known to the author is that due to Batoz [74]. It is desirable to develop a new curved triangular thin shell element based on the DKT approach for deep shell applications with the explicit representation of the rigid body modes, and suitable for the

analysis of general anisotropic shells. This, indeed, is the objective of the research work presented here.

In the next section, the desired features and the requirements of a curved thin shell element are presented.

1.3 Requirements for a Curved Thin Shell Element

The development of a new thin shell element should consider the criteria drawn from different perspectives, including those of geometric and material modeling, relative ease of use for practical applications, satisfaction of the mathematical requirements to achieve reliable solutions with modest computational costs, and potential for extension to include nonlinear effects. The important requirements for a curved thin shell element are summarized in the following list.

1. The element should result in an accurate and reliable prediction of shell behavior.
2. The element should preferably be triangular in shape, and with corner nodes alone.
3. The nodal connection quantities should be simple with physical significance to aid the easy application of boundary conditions.
4. The underlying shell theory should be simple and suitable for deep shell applications.
5. The shape functions should be simple, avoiding rational or singular polynomials.
6. The element formulation should preferably be in a general curvilinear coordinate system (neither principal nor

orthogonal) for the direct utilization of surface representation algorithms which often result in such a coordinate system.

7. The element should be suitable for application to anisotropic shells of laminated composite construction.
8. The element should be computationally efficient.
9. The formulation should be capable of being easily extended to include the effects of geometric and material nonlinearities.

The development of the new shell element was guided by the objective of meeting a majority of the above requirements.

In the next section, a brief description of the formulation of the new curved thin shell element developed in the present work is given.

1.4 A Brief Description of the New Curved Thin Shell Element

The curved thin shell element formulated herein is a three-node triangular element with twenty-seven degrees of freedom, nine at each of the corner nodes. The degrees of freedom are u, $u_{,x}$, $u_{,y}$, v, $v_{,x}$, $v_{,y}$, w, $w_{,x}$, $w_{,y}$, where u, v, and w are, respectively, the tangential and normal components of the displacement in the (x,y) curvilinear coordinate system, and a comma denotes a partial derivative.

The element formulation is based on the principle of minimum potential energy using the discrete Kirchhoff theory approach. An explicit representation of the rigid body modes is achieved by isoparametric representation of the shell middle surface. The linear

shear theory for arbitrary thin shells in a general curvilinear coordinate system, as presented by Wempner et al. [45] is used for the calculation of the element strain energy. However, the component of the strain energy due to transverse shear deformation is neglected, in order to have convergence to the thin shell solution. In this theory, the membrane strains and the curvature changes of the shell middle surface are expressed in terms of the two independent vectors of the displacement and the rotation of the shell normal at any point on the shell middle surface. To enable the isoparametric representation of the shell geometry, the strain-displacement relations are transformed into a global cartesian coordinate system. The geometry within an element is interpolated from the nodal geometric data by the same set of shape functions as those used for the displacement interpolation. The nodal geometric data are obtained either from the parametric equations of the shell surface, or from a suitable mathematical representation of the shell surface in the case of arbitrary shells.

The cartesian components of the displacement and rotation vectors are interpolated by polynomial shape functions in the natural area coordinates. Complete (ten-term) cubic polynomials are used for the interpolation of all three components of the displacement vector, where the value of the displacement component and its two first-order derivatives at each of the corner nodes, and the centroidal values are used as nodal degrees of freedom. Complete (six-term) quadratic polynomials are used for the interpolation of the three components of the rotation vector, where the value of the rotation component at each

of the corner nodes and three midside nodes are used as nodal degrees of freedom. This representation for the displacement and rotation components results in a total of forty-eight degrees of freedom for the element, twelve at each of the corner nodes, three at each of the midside nodes and three centroidal values. These interpolation functions provide C^0-continuity for the displacement and rotation components across the interelement boundaries. Since only first-order derivatives of the displacement and rotation components occur in the element strain energy expression based on the linear shear theory, this results in a conforming thin shell element. However, the displacement components are C^1-continuous at the corner nodes of the element. Three types of constraints are imposed at a discrete number of points in the element to obtain the thin shell results in the convergence limit. These are: (a) discrete Kirchhoff constraints, (b) surface-normal rotation constraints and (c) the constraints of linear variation of the normal rotation.

The discrete Kirchhoff constraints represent the conditions of vanishing of the transverse shearing strain components. A total of nine of these constraints are imposed at the corner and midside nodes, with six of them at the corner nodes.

The surface-normal rotation constraints represent the equality of the two values of the rotation of the shell about the shell normal, which has been doubly defined. One value of the latter rotation results from the independently-assumed cartesian components of the rotation vector of the shell normal. Another value for the same rotation is defined in terms of the displacement gradients. A total of

six of these constraints, one at each of the corner and midside nodes, are imposed.

The condition of linear variation of the normal rotation along the element side is imposed so as to eliminate the degrees of freedom at the midside nodes. This gives rise to three more constraints.

Thus we have a total of eighteen constraints, which, in conjunction with the static condensation of the centroidal freedoms, will result in a total of twenty-seven degrees of freedom for the element.

Finally, the degrees of freedom are transformed into a local orthogonal curvilinear coordinate system located at the corner nodes for the easy application of symmetry and support conditions. It may be noted that all the nodes meeting at a common point share the same set of orthogonal curvilinear coordinates.

1.5 Scope of the Study

The scope of the presentation of the subsequent chapters is as follows.

In the second chapter, the details of the linear shear deformation theory for an arbitrary thin shell in a general curvilinear coordinate system is presented, using tensorial notation. This is followed by the development of the strain-displacement relations expressed in terms of the cartesian components of the displacement and rotation vectors. The chapter concludes with the presentation of strain energy density for an anisotropic shell of laminated composite construction.

In the third chapter, the development of the new curved triangular thin shell element is presented. The details of the interpolation functions, the isoparametric representation of the shell middle surface, the development of the various constraints and the procedure to calculate the element matrices are discussed. A brief description of the computer program is also included.

In the fourth chapter, extensive numerical solutions are presented to demonstrate the accuracy and the computational efficiency of the new element. Various "patch" test solutions are also included to demonstrate the satisfactory compliance with the conditions of conformity and convergence.

Concluding remarks and suggestions for future work are presented in the fifth chapter.

CHAPTER 2

LINEAR SHEAR DEFORMATION THEORY FOR ANISOTROPIC LAMINATED COMPOSITE THIN SHELLS

The equations of the linear shear deformation theory for anisotropic laminated composite thin shells are presented in the following sections. Attention is focused on the derivation of the expression for the strain energy density when the shell is undergoing small extensional and bending deformations.

The strain energy density in a thin shell, based on linear shear deformation theory for an isotropic material, was presented by Wempner et al. [45]. These equations developed in a tensorial notation, were applicable to thin arbitrary shells described in a general curvilinear coordinate system. These equations will be extended to include anisotropic materials, representative of multi-layered, multi-directonally oriented laminated composite construction. Also, the strain-displacement relations will be transformed into a global cartesian system to enable the isoparametric representation of the shell middle surface.

The linear shear deformation theory is based on the fundamental assumption that normals to the undeformed shell middle surface remain straight but do not necessarily remain normal to the deformed shell middle surface. It is also assumed that the displacement gradients are small. The first assumption results in a linear variation of the bending strain, and a constant transverse shearing

strain across the shell thickness; the latter assumption results in linear strain-displacement relations.

The formulation starts with the section on the differential geometry of a curved surface. This is followed by the presentation of the kinematics of deformation, leading to the strain-displacement relations in the curvilinear coordinate system. The latter relations are transformed into a global cartesian frame. The chapter concludes with the derivation of strain energy expression for isotropic and laminated composite shells.

2.1 Differential Geometry of a Curved Surface

2.1.1 Indicial Notation

Indicial notation will be used to represent the components of vectors and tensors. The Standard Summation Convention, where a repeated index implies a summation over the range of the index, is also adopted. Lower case Latin indices (i,j, ...) have a range 1 to 3, and the Greek indices (α,β,γ, ...) have a range 1 to 2. A subscript indicates a covariant component, and a superscript indicates a contravariant component. The mixed variance components are represented by combination of subscript and superscript; the order of the latter indices is indicated by preceding the indices with a period. However, the period will be dropped if the order of the indices is of no consequence.

2.1.2 Base Vectors and Metric Tensors of the Curved Surface

Figure 1a shows the geometry of the shell middle surface, and a surface parallel to that surface.

The position vector to a point, P, on the undeformed reference surface is $\bar{R}_o(\theta^1,\theta^2)$, which is defined as a function of the curvilinear coordinates (θ^1,θ^2), in which θ^α = constant (α = 1,2) are curvilinear coordinate lines embedded on the middle surface of the shell.

The position vector, $\bar{R}_o$, is defined in terms of its components in a global cartesian coordinate system, (x^1,x^2,x^3), as

$$\bar{R}_o(\theta^1,\theta^2) = x^1(\theta^1,\theta^2)\hat{e}_1 + x^2(\theta^1,\theta^2)\hat{e}_2 + x^3(\theta^1,\theta^2)\hat{e}_3 \qquad (2.1)$$

$$= x^i\hat{e}_i (i = 1,2,3) \qquad (2.2)$$

where $\hat{e}_i$ are the cartesian unit base vectors. The caret (^) placed over the symbol signifies a unit vector.

Let θ^3 be the distance along the normal to the middle surface ($\theta^3 = 0$) and let $\hat{a}_3$ denote a unit normal vector to the undeformed middle surface. Then the position vector to an arbitrary point, Q, is

$$\bar{R}(\theta^1,\theta^2) = \bar{R}_o(\theta^1,\theta^2) + \theta^3\hat{a}_3 \qquad (2.3)$$

The tangent base vectors, $\bar{g}_i$, of the coordinate system θ^i follow from the partial differentiation of the Eq. (2.3):

$$\bar{g}_\alpha = \bar{R}_{,\alpha} = \bar{R}_{o,\alpha} + \theta^3\hat{a}_{3,\alpha} \qquad \bar{g}_3 = \bar{R}_{,3} = \hat{a}_3 \qquad (2.4a,b)$$

where a comma denotes partial differentiation with respect to θ^α (e.g., $\bar{R}_{o,\alpha} = \partial\bar{R}_o/\partial\theta^\alpha$). The Greek indices have the range 1,2.

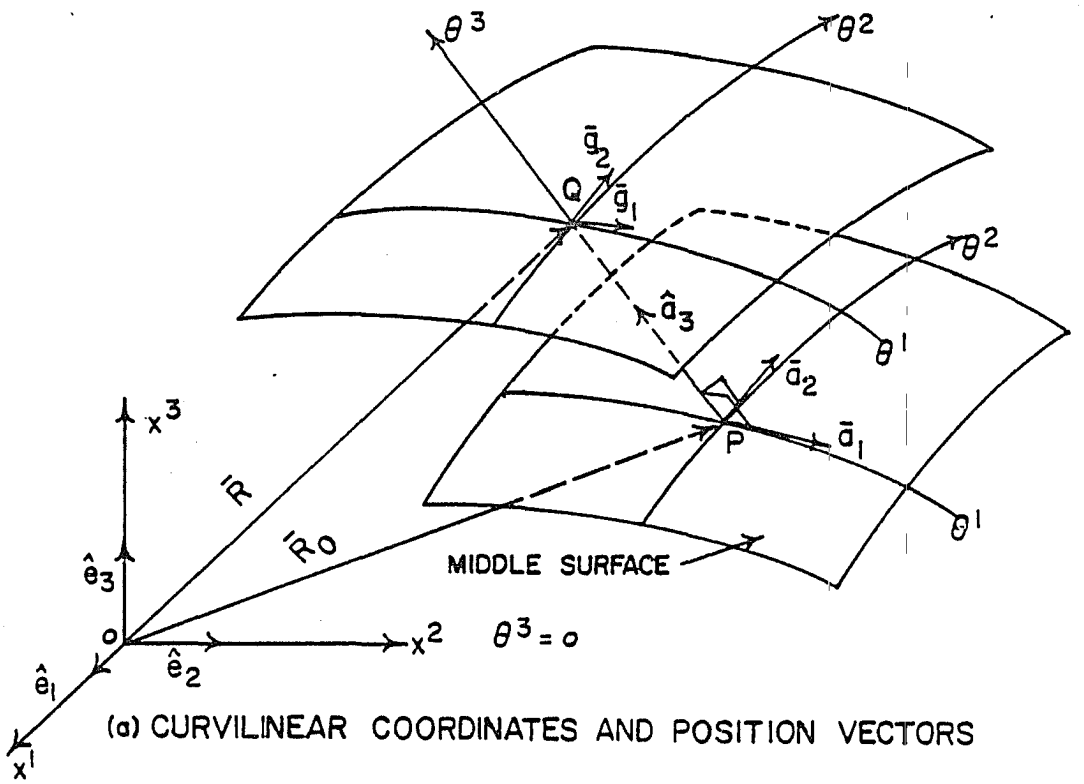

(a) CURVILINEAR COORDINATES AND POSITION VECTORS

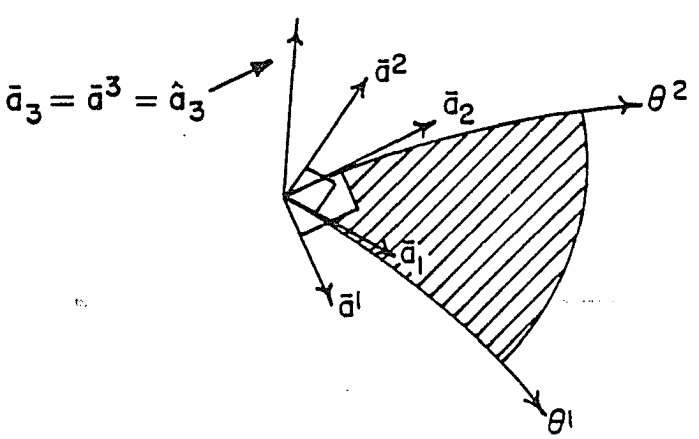

(b) THE TWO BASE VECTOR TRIADS

Figure 1. Curvilinear coordinates and base vectors.

The tangent vectors at the middle surface are denoted by $\bar{a}_i$, and are defined as follows:

$$\bar{a}_i(\theta^1,\theta^2) \equiv \bar{g}_i(\theta^1,\theta^2,0) \tag{2.5}$$

It follows from Eqs. (2.4) and (2.5) that

$$\bar{a}_\alpha = \bar{R}_o\,,\alpha \qquad \bar{a}_3 = \bar{g}_3 = \hat{a}_3 \tag{2.6a,b}$$

$$\bar{g}_\alpha = \bar{a}_\alpha + \theta^3 \hat{a}_3\,,\alpha \tag{2.7}$$

We define the reciprocal base vectors, $\bar{a}^i$, which are normal to the θ^i surface:

$$\bar{a}^i \equiv \bar{g}^i(\theta^1,\theta^2,0) \tag{2.8}$$

$$\bar{a}^i \cdot \bar{a}_j = \delta^i_j \tag{2.9}$$

where a period ($\cdot$) denotes the dot product, and δ^i_j is the Kronecker delta defined as

$$\delta^i_j \equiv \begin{cases} 0 \text{ if } i \neq j \\ \\ 1 \text{ if } i = j \end{cases} \tag{2.10}$$

Since θ^3 is the distance along the normal to the middle surface, it follows that $\bar{a}^3 = \bar{g}^3 = \hat{a}_3$.

The two basic triads of vectors, $\bar{a}_i$ and $\bar{a}^i$ are shown in Fig. 1b. The vectors $\bar{a}_\alpha$ and $\bar{a}^\alpha$ are tangent to the surface, and $\bar{a}_3 = \bar{a}^3 = \hat{a}_3$ is the unit normal vector. $\bar{a}_\alpha$ is tangent to the θ^α line, and $\bar{a}^\alpha$ is normal to the θ^α surface.

Each of the vector triads $\bar{a}_\alpha$ and $\bar{a}^\alpha$ can be expressed as a linear combination of the other:

$$\bar{a}^\alpha = a^{\alpha\beta}\bar{a}_\beta \qquad \bar{a}_\alpha = a_{\alpha\beta}\bar{a}^\beta \tag{2.11a,b}$$

The coefficients $a_{\alpha\beta}$ and $a^{\alpha\beta}$ are the covariant and the contravariant components of the metric tensor of the surface coordinates θ^α.

From Eqs. (2.11) and (2.9) it follows that

$$a^{\alpha\beta} = \bar{a}^\alpha \cdot \bar{a}^\beta \qquad a_{\alpha\beta} = \bar{a}_\alpha \cdot \bar{a}_\beta \tag{2.12a,b}$$

$$a^{\alpha\beta}a_{\beta\gamma} = \delta^\alpha_\gamma \tag{2.13}$$

Equations (2.12) and (2.13) show that $a^{\alpha\beta}$ and $a_{\alpha\beta}$ are symmetric tensors, and one is the reciprocal or the inverse of the other.

Using Eq. (2.13), $a^{\alpha\beta}$ can be expressed in terms of $a_{\alpha\beta}$ as

$$a^{11} = \frac{a_{22}}{a} \qquad a^{22} = \frac{a_{11}}{a} \qquad a^{12} = \frac{-a_{12}}{a} = a^{21} \tag{2.14}$$

where a is the determinant of the covariant metric tensor:

$$a = |a_{\alpha\beta}| = a_{11}a_{22} - a_{12}^2 \tag{2.15}$$

It also follows from Eq. (2.13) that

$$|a^{\alpha\beta}| = \frac{1}{a} \tag{2.16}$$

An incremental change of position on the surface is accompanied by a change in the position vector $\bar{R}_o$. The first-order differential change in $\bar{R}_o$ is

$$d\bar{R}_o = \bar{R}_{o\,,\alpha}d\theta^\alpha = \bar{a}_\alpha d\theta^\alpha \tag{2.17a,b}$$

The incremental distance, ds, between two points on the middle surface is

$$ds^2 = d\bar{R}_o \cdot d\bar{R}_o = \bar{a}_\alpha \cdot \bar{a}_\beta d\theta^\alpha d\theta^\beta \qquad (2.18a,b,c)$$

It follows from Eqs. (2.12) and (2.18) that

$$ds^2 = a_{\alpha\beta} d\theta^\alpha d\theta^\beta \qquad (2.19)$$

Equation (2.19) is known as the first fundamental form. The coefficients of this quadratic form are the components of the metric tensor of surface coordinates. These components serve to measure distances on the surface, and hence the name metric tensor.

2.1.3 Curvature Tensor and the Second Fundamental Form

The normal vector $\hat{a}_3$ is a unit vector, and hence its direction, but not its length, depends on the coordinates θ^α. Its derivative lies in the plane of $\bar{a}^\alpha$. Hence the partial derivative $\hat{a}_{3\,,\beta}$ can be expressed as a linear combination of $\bar{a}^\alpha$ in the form

$$\hat{a}_{3\,,\beta} = -b_{\alpha\beta}\bar{a}^\alpha \qquad (2.20a)$$

where the quantities $b_{\alpha\beta}$ are the covariant components of a surface tensor; $b_{\alpha\beta}$ is called the <u>curvature tensor</u>.

From Eq. (2.20a) it follows that

$$\hat{a}_{3\,,\beta} \cdot \bar{a}_\alpha = -b_{\alpha\beta} \qquad (2.20b)$$

Differentiating the orthogonality condition $\hat{a}_3 \cdot \bar{a}_3 = 0$ with respect to α, and using Eq. (2.6a) we obtain

$$\hat{a}_{3\,,\alpha}\cdot\bar{a}_{\beta} = -\hat{a}_{3}\cdot\bar{a}_{\beta\,,\alpha} = -\hat{a}_{3}\cdot\bar{R}_{o\,,\beta\alpha} \tag{2.21}$$

From Eqs. (2.20b) and (2.21) it follows that $b_{\alpha\beta}$ is symmetric

$$b_{\alpha\beta} = b_{\beta\alpha} \tag{2.22}$$

The mixed variant components of the curvature tensor are obtained by raising the index of $b_{\alpha\beta}$

$$b^{\alpha}_{\beta} = b_{\gamma\beta}a^{\gamma\alpha} \tag{2.23}$$

Using Eqs. (2.11a) and (2.23), the derivative in Eq. (2.20a) can also be expressed in terms of b^{α}_{β}

$$\hat{a}_{3\,,\beta} = -b^{\alpha}_{\beta}\bar{a}_{\alpha} \tag{2.24}$$

Equations (2.20) and (2.24) are known as Weingarten's formulas for the derivative of the normal vector.

The first-order differential change in $\hat{a}_3$ due to incremental change of position on the surface is

$$d\hat{a}_{3} = \hat{a}_{3\,,\alpha}d\theta^{\alpha} \tag{2.25}$$

According to Eqs. (2.17b), (2.25) and (2.20b)

$$d\bar{R}_{o}\cdot d\bar{a}_{3} = -b_{\alpha\beta}d\theta^{\alpha}d\theta^{\beta} \tag{2.26}$$

Equation (2.26) is known as the second fundamental form. The coefficients of this quadratic form are the components of the curvature tensor of the middle surface. These components serve to measure the normal curvature and the torsion of the coordinate lines on the middle surface.

There are two scalar invariants of the curvature tensor, namely the mean curvature, H, and the Gaussian curvature, K.

$$K \equiv |b_\beta^\alpha| = b_1^1 b_2^2 - b_2^1 b_1^2 \tag{2.27}$$

$$H \equiv \frac{1}{2} b_\alpha^\alpha = \frac{1}{2}(b_1^1 + b_2^2) \tag{2.28}$$

The directions in which the normal curvatures have extremum values are the principal curvature directions. The corresponding normal curvatures are called the principal curvatures. If the principal curvatures are distinct, the principal directions are orthogonal. The torsion of the surface vanishes in the principal directions.

It can be shown that the mean and Gaussian curvatures are, respectively, half the sum and the product of the principal curvatures.

2.1.4 Metric Tensor of the Spatial System

After employing Eq. (2.24), the base vectors, g_α, of the spatial system, Eq. (2.7), can be expressed as

$$\bar{g}_\alpha = \bar{a}_\alpha - \theta^3 b_\alpha^\beta \bar{a}_\beta \tag{2.29}$$

$$= \bar{a}_\alpha - \theta^3 b_{\alpha\beta} \bar{a}^\beta \tag{2.30}$$

The components of the metric tensor of the spatial system, $g_{\alpha\beta}$, are defined as

$$g_{\alpha\beta} = \bar{g}_\alpha \cdot \bar{g}_\beta \qquad g_{\alpha 3} = \bar{g}_\alpha \cdot \bar{g}_3 \tag{2.31a,b}$$

Substituting for $\bar{g}_\alpha$ from Eqs. (2.29) and (2.30), and with the aid of

Eqs. (2.12) we have

$$g_{\alpha\beta} = a_{\alpha\beta} - 2\theta^3 b_{\alpha\beta} + (\theta^3)^2 b_{\alpha\gamma} b^{\gamma}_{\beta} \tag{2.32a}$$

$$g_{\alpha 3} = 0 \tag{2.32b}$$

2.2 Kinematics of Deformation

2.2.1 Metric Tensor of the Deformed Coordinates

Figure 2 shows the configuration of the shell element before and after deformation. $\bar{R}_o(\theta^1,\theta^2)$ is the position vector of a particle, P, on the middle surface of the undeformed shell, and $\bar{R}(\theta^1,\theta^2)$ is that of an arbitrary particle, Q, on the normal line through the point P. Here we may recall the relation between $\bar{R}_o$ and $\bar{R}$ as

$$\bar{R}(\theta^1,\theta^2) = \bar{R}_o(\theta^1,\theta^2) + \theta^3 \hat{a}_3 \tag{2.33}$$

After deformation, the particle P moves to P*, and the position vector to P* is denoted as $\bar{R}^*_o(\theta^1,\theta^2)$. Similarly, the position of the particle Q* in the deformed configuration is denoted as $\bar{R}^*(\theta^1,\theta^2)$.

It is our basic assumption that after deformation the θ^3 line, which is normal to the undeformed middle surface, remains <u>straight</u> and undergoes <u>negligible stretching</u>, but need not necessarily be normal to the deformed middle surface of the shell. Let $\hat{A}_3$ denote the unit vector along the deformed θ^3 line, where the deformation is due to rotation alone. Since θ^3 line remains unstretched we have

$$\bar{R}^* = \bar{R}^*_o + \theta^3 \hat{A}_3 \tag{2.34}$$

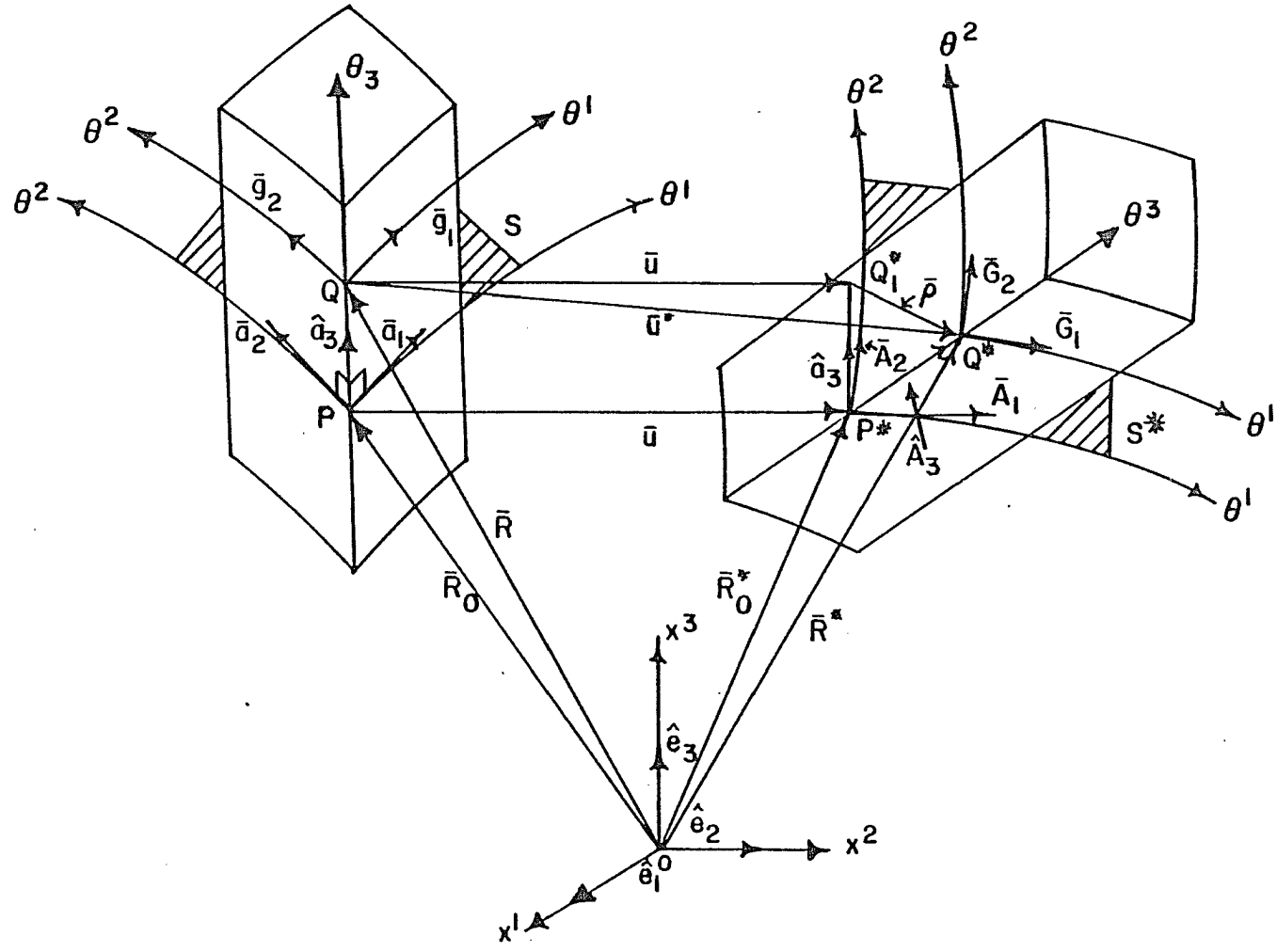

Figure 2. Motion of a shell element.

Let $\bar{u}$ and $\bar{u}^*$ be the displacement vectors of the points P and Q respectively. From Figure 2 it follows that

$$\bar{R}_o + \bar{u} = \bar{R}_o^* \tag{2.35}$$

and

$$\bar{R} + \bar{u}^* = \bar{R}^* \tag{2.36}$$

The vectors $\bar{u}$ and $\bar{u}^*$ differ by a vector $\bar{o}$ (see Figure 2), which represents the displacement caused by the rotation of $\hat{a}_3$ into $\hat{A}_3$. If the rotations of the normal are sufficiently small, they can be represented by a rotation vector $\bar{\Phi}$ [45]. Then we can write

$$\bar{o} = \bar{\Phi} \times (\theta^3 \hat{a}_3) \tag{2.37}$$

$$\hat{A}_3 = \hat{a}_3 + \bar{\Phi} \times \hat{a}_3 \tag{2.38}$$

and

$$\bar{u}^* = \bar{u} + \bar{\Phi} \times (\theta^3 \hat{a}_3)$$

where $\times$ denotes vector cross product. Substituting Eq. (2.35) and Eq. (2.38) into Eq. (2.34), we obtain,

$$\bar{R}^* = \bar{R}_o + \bar{u} + \theta^3(\hat{a}_3 + \bar{\Phi} \times \hat{a}_3) \tag{2.39}$$

Employing Eq. (2.33) and Eq. (2.37), we can also write

$$\bar{R}^* = \bar{R} + \bar{u} + \theta^3 \bar{\lambda} \tag{2.40}$$

where

$$\bar{\lambda} = \bar{\Phi} \times \hat{a}_3 \tag{2.41}$$

The base vectors of the deformed spatial coordinates are

$$\bar{G}_\alpha = \bar{R}^*{}_{,\alpha} = \bar{R}_{,\alpha} + \bar{u}^{\bullet}{}_{,\alpha} + \theta^3 \bar{\lambda}_{,\alpha} \tag{2.42a}$$

$$\bar{G}_3 = \bar{R}^*_{\ ,3} = \bar{R}_{\ ,3} + \bar{\lambda} \tag{2.42b}$$

In view of Eqs. (2.4) and (2.37) we obtain

$$\bar{G}_\alpha = \bar{g}_\alpha + \bar{u}_{\ ,\alpha} + \theta^3\bar{\lambda}_{\ ,\alpha} \tag{2.43a}$$

$$\bar{G}_3 = \hat{a}_3 + \bar{\lambda} \tag{2.43b}$$

According to Eq. (2.31), the covariant components of the metric tensor, G_{ij}, of the spatial coordinates of the deformed shell are given by

$$G_{\alpha\beta} = \bar{G}_\alpha \cdot \bar{G}_\beta \qquad G_{\alpha 3} = \bar{G}_\alpha \cdot \bar{G}_3 \tag{2.44a,b}$$

Substituting for $\bar{G}_\alpha$ from Eq. (2.43a) we have

$$G_{\alpha\beta} = (\bar{g}_\alpha + \bar{u}_{\ ,\alpha} + \theta^3\bar{\lambda}_{\ ,\alpha}) \cdot (\bar{g}_\beta + \bar{u}_{\ ,\beta} + \theta^3\bar{\lambda}_{\ ,\beta}) \tag{2.45}$$

After carrying out the multiplication in Eq. (2.45), and neglecting the nonlinear terms in $\bar{u}_{\ ,\alpha}$ and $\bar{\lambda}_{\ ,\alpha}$, and in view of Eq. (2.31) we obtain

$$G_{\alpha\beta} = g_{\alpha\beta} + \bar{g}_\alpha \cdot \bar{u}_{\ ,\beta} + \bar{g}_\beta \cdot \bar{u}_{\ ,\alpha} + \theta^3(\bar{g}_\alpha \cdot \bar{\lambda}_{\ ,\beta} + \bar{g}_\beta \cdot \bar{\lambda}_{\ ,\alpha}) \tag{2.46}$$

After substituting for $\bar{g}_\alpha$ from Eq. (2.29), the equation for $G_{\alpha\beta}$ is obtained as

$$\begin{aligned} G_{\alpha\beta} &= g_{\alpha\beta} + \bar{a}_\alpha \cdot \bar{u}_{\ ,\beta} + \bar{a}_\beta \cdot \bar{u}_{\ ,\alpha} \\ &\quad + \theta^3(\bar{a}_\alpha \cdot \bar{\lambda}_{\ ,\beta} + \bar{a}_\beta \cdot \bar{\lambda}_{\ ,\alpha} - b_\alpha^\gamma \bar{a}_\gamma \cdot \bar{u}_{\ ,\beta} - b_\beta^\gamma \bar{a}_\gamma \cdot \bar{u}_{\ ,\alpha}) \\ &\quad - (\theta^3)^2 (b_\alpha^\gamma \bar{a}_\gamma \cdot \bar{\lambda}_{\ ,\beta} + b_\beta^\gamma \bar{a}_\gamma \cdot \bar{\lambda}_{\ ,\alpha}) \end{aligned} \tag{2.47}$$

Defining

$$\gamma_{\alpha\beta} = \frac{1}{2}(\bar{a}_\alpha \cdot \bar{u}_{,\beta} + \bar{a}_\beta \cdot \bar{u}_{,\alpha}) \tag{2.48}$$

and

$$\chi_{\alpha\beta} = \frac{1}{2}(\bar{a}_{,\alpha} \cdot \bar{\lambda}_{,\beta} + \bar{a}_\beta \cdot \bar{\lambda}_{,\alpha} - b_\alpha^\gamma \bar{a}_\gamma \cdot \bar{u}_{,\beta} - b_\beta^\gamma \bar{a}_\gamma \cdot \bar{u}_{,\alpha}) \tag{2.49}$$

Equation (2.47) for $G_{\alpha\beta}$ takes the simple form

$$G_{\alpha\beta} = g_{\alpha\beta} + 2\gamma_{\alpha\beta} + 2\theta^3 \chi_{\alpha\beta} - (\theta^3)^2 (b_\alpha^\gamma \bar{a}_\gamma \cdot \bar{\lambda}_{,\beta} + b_\beta^\gamma \bar{a}_\gamma \cdot \bar{\lambda}_{,\alpha}) \tag{2.50}$$

Similarly, the components $G_{\alpha 3}$ are given by

$$G_{\alpha 3} = \bar{G}_\alpha \cdot \bar{G}_3 \tag{2.51}$$

Substituting for $\bar{G}_\alpha$ and $\bar{G}_3$ from Eqs. (2.43)

$$G_{\alpha 3} = (\bar{g}_\alpha + \bar{u}_{,\alpha} + \theta^3 \bar{\lambda}_{,\alpha}) \cdot (\hat{a}_3 + \bar{\lambda}) \tag{2.52}$$

After carrying out the multiplication in Eq. (2.52) and neglecting the nonlinear terms in $\bar{u}$ and $\bar{\lambda}$ we obtain

$$G_{\alpha 3} = \bar{g}_\alpha \cdot \hat{a}_3 + \bar{g}_\alpha \cdot \bar{\lambda} + \bar{u}_{,\alpha} \cdot \hat{a}_3 + \theta^3 \bar{\lambda}_{,\alpha} \cdot \hat{a}_3 \tag{2.53}$$

Substituting for $\bar{g}_\alpha$ from Eq. (2.7), and recalling that $\bar{a}_\alpha$ and $\bar{a}_3$ are orthogonal, Eq. (2.53) may be written as

$$G_{\alpha 3} = \bar{a}_\alpha \cdot \bar{\lambda} + \hat{a}_3 \cdot \bar{u}_{,\alpha} + \theta^3 (\hat{a}_{3,\alpha} \cdot \bar{\lambda} + \hat{a}_3 \cdot \bar{\lambda}_{,\alpha}) \tag{2.54}$$

The θ^3-term in Eq. (2.54), using Eq. (2.41), vanishes:

$$\theta^3 (\hat{a}_{3,\alpha} \cdot \bar{\lambda} + \hat{a}_3 \cdot \bar{\lambda}_{,\alpha}) = \theta^3 (\hat{a}_3 \cdot \bar{\lambda})_{,\alpha} = \theta^3 (\hat{a}_3 \cdot \bar{\xi} \times \bar{a}_3) = 0$$

Thus, equation for $G_{\alpha 3}$ takes the simple form

$$G_{\alpha 3} = \bar{a}_\alpha \cdot \bar{\lambda} + \hat{a}_3 \cdot \bar{u}_{,\alpha} \tag{2.55}$$

2.2.2 Strain Tensor

The strain tensor is defined as

$$\bar{\gamma}_{ij} = \frac{1}{2}(G_{ij} - g_{ij}) \tag{2.56}$$

Substituting Eq. (2.32), Eq. (250), and Eq. (2.55) into Eq. (2.56), the equation for strain tensor is obtained as

$$\bar{\gamma}_{\alpha\beta} = \gamma_{\alpha\beta} + \theta^3 \chi_{\alpha\beta} - (\theta^3)^2 (b_\alpha^\gamma \bar{a}_\gamma \cdot \bar{\lambda}_{,\beta} + b_\beta^\gamma \bar{a}_\gamma \cdot \bar{\lambda}_{,\alpha}) \tag{2.57}$$

$$\bar{\gamma}_{\alpha 3} = \frac{1}{2}(\bar{a}_\alpha \cdot \bar{\lambda} + \hat{a}_3 \cdot \bar{u}_{,\alpha}) \tag{2.58}$$

In the case of thin shells, the term containing $(\theta^3)^2$ is negligible compared to the term containing θ^3. Then, Eq. (2.57) and Eq. (2.58) reduce to

$$\bar{\gamma}_{\alpha\beta} = \gamma_{\alpha\beta} + \theta^3 \chi_{\alpha\beta} \tag{2.59}$$

$$\bar{\gamma}_{\alpha 3} = \frac{1}{2}(\bar{a}_\alpha \cdot \bar{\lambda} + \hat{a}_3 \cdot \bar{u}_{,\alpha}) \tag{2.60}$$

The component $\gamma_{\alpha\beta}$ is the strain of the middle surface, and $\chi_{\alpha\beta}$ is the bending strain component with a linear variation over the shell thickness. The component $\gamma_{\alpha 3}$ is the transverse shear strain component. It may be noted that the strain components $\bar{\gamma}_{ij}$ throughout the shell are determined by the deformation of the middle surface, and

is expressed in terms of the displacement vector, $\bar{u}$, and the vector of normal rotation, $\bar{\Phi}$.

In the next section, the strain tensor components will be expressed in terms of cartesian components of the displacement and the normal rotation vectors.

2.3 Strain Tensor in Cartesian Coordinates

The position vector to the undeformed middle surface, $\bar{R}_o(\theta^1,\theta^2)$ according to Eq. (2.2) is

$$\bar{R}_o(\theta^1,\theta^2) = x^1\hat{e}_1 + x^2\hat{e}_2 + x^3\hat{e}_3 = x^i\hat{e}_i \tag{2.61}$$

The tangent base vectors at the middle surface are

$$\bar{a}_\alpha = \bar{R}_{o\ ,\alpha} = x^i{}_{,\alpha}\hat{e}_i \tag{2.62}$$

The unit normal vector to the middle surface is

$$\hat{a}_3 = n^i\hat{e}_i = \bar{a}_1 \times \bar{a}_2/|\bar{a}_1 \times \bar{a}_2| \tag{2.63}$$

It can be shown that

$$|\bar{a}_1 \times \bar{a}_2| = \sqrt{a} \tag{2.64}$$

where a is the determinant of the covariant metric tensor defined in Eq. (2.15).

With the aid of Eq. (2.62) and Eq. (2.64), Eq. (2.63) for the unit normal vector is obtained as

$$\hat{a}_3 = \frac{1}{\sqrt{a}} e_{ijk}x^i{}_{,1}x^j{}_{,2}\hat{e}_k \tag{2.65}$$

where e_{ijk} is the permutation symbol.

The displacement vector and the rotation vector are expressed in terms of the cartesian components as

$$\bar{u} = u^i \hat{e}_i \tag{2.66}$$

$$\bar{\phi} = \phi^i \hat{e}_i \tag{2.67}$$

It follows from Eq. (2.66) and Eq. (2.67) that

$$\bar{u}_{,\alpha} = u^i{}_{,\alpha} \hat{e}_i \tag{2.68}$$

$$\bar{\phi}_{,\alpha} = \phi^i{}_{,\alpha} \hat{e}_i \tag{2.69}$$

2.3.1 Membrane Strain Tensor of the Middle Surface

According to Eq. (2.59) and Eq. (2.48), the components of the membrane strain tensor are

$$2\gamma_{\alpha\beta} = \bar{a}_\alpha \cdot \bar{u}_{,\beta} + \bar{a}_\beta \cdot \bar{u}_{,\alpha} \tag{2.70}$$

In view of Eqs. (2.62) and (2.68)

$$2\gamma_{\alpha\beta} = (x^i{}_{,\alpha} \hat{e}_i) \cdot (u^j{}_{,\beta} \hat{e}_j) + (x^i{}_{,\beta} \hat{e}_i) \cdot (u^j{}_{,\alpha} \hat{e}_j) \tag{2.71}$$

After carrying out the dot multiplication we obtain

$$2\gamma_{\alpha\beta} = x^i{}_{,\alpha} u^i{}_{,\beta} + x^i{}_{,\beta} u^i{}_{,\alpha} \tag{2.72}$$

2.3.2 Bending Strain Tensor of the Middle Surface

According to Eq. (2.59) and Eq. (2.49), the components of the bending strain tensor are

$$2\chi_{\alpha\beta} = \bar{a}_\alpha \cdot \bar{\lambda}_{,\beta} + \bar{a}_{,\beta} \cdot \bar{\lambda}_{,\alpha} - b_\alpha^\mu \bar{a}_\mu \cdot \bar{u}_{,\beta} - b_\beta^\mu \bar{a}_\mu \cdot \bar{u}_{,\alpha} \tag{2.73}$$

According to Eq. (2.41)

$$\bar{\lambda}_{,\alpha} = (\bar{\phi} \times \hat{a}_3)_{,\alpha} \tag{2.74}$$

$$= \bar{\Phi}_{,\alpha} \times \hat{a}_3 + \bar{\Phi} \times \hat{a}_{3,\alpha} \tag{2.75}$$

In view of Eq. (2.67) and Eq. (2.63) we have

$$\bar{\phi}_{,\alpha} \times \hat{a}_3 = e_{ijk}\phi^i{}_{,\alpha} n^j \hat{e}_k \tag{2.76}$$

and using Eq. (2.24) for $\hat{a}_{3,\alpha}$ we have

$$\bar{\phi} \times \hat{a}_{3,\alpha} = (\phi^i \hat{e}_i) \times (-b_\alpha^\beta x^j{}_{,\beta} \hat{e}_j)$$

$$= -b_\alpha^\beta e_{ijk}\phi^i x^j{}_{,\beta} \hat{e}_k \tag{2.77}$$

Using Eq. (2.76) and Eq. (2.77) in Eq. (2.75) we get

$$\bar{\lambda}_{,\alpha} = (e_{ijk}\phi^i{}_{,\alpha} n^j - b_\alpha^\mu e_{ijk}\phi^i x^j{}_{,\mu})\hat{e}_k \tag{2.78}$$

Consider term by term in the bending strain tensor, Eq. (2.73)

$$\bar{a}_\alpha \cdot \bar{\lambda}_{,\beta} = x^m{}_{,\alpha} \hat{e}_m \cdot \bar{\lambda}_{,\beta} \tag{2.79}$$

$$= (e_{ijk}\phi^i{}_{,\beta} n^j - b_\beta^\mu e_{ijk}\phi^i x^j{}_{,\mu}) x^k{}_{,\alpha} \tag{2.80}$$

Similarly

$$\bar{a}_\beta \cdot \bar{\lambda}_{,\alpha} = (e_{ijk}\phi^i{}_{,\alpha} n^j - b_\alpha^\mu e_{ijk}\phi^i x^j{}_{,\mu}) x^k{}_{,\beta} \tag{2.81}$$

and

$$-(b_\alpha^\mu \bar{a}_\mu \cdot \bar{u}_{,\beta} + b_\beta^\mu \bar{a}_\mu \cdot \bar{u}_{,\alpha}) = -(b_\alpha^\mu x^i{}_{,\mu} u^i{}_{,\beta} + b_\beta^\mu x^i{}_{,\mu} u^i{}_{,\alpha}) \tag{2.82}$$

Using Eqs. (2.80)-(2.82) in Eq. (2.73), we obtain

$$2\chi_{\alpha\beta} = (e_{ijk}\phi^i{}_{,\alpha}n^j x^k{}_{,\beta} + e_{ijk}\phi^i{}_{,\beta}n^j x^k{}_{,\alpha})$$
$$- (b^\mu_\alpha e_{ijk}\phi^i x^j{}_{,\mu}x^k{}_{,\beta} + b^\mu_\beta e_{ijk}\phi^i x^j{}_{,\mu}x^k{}_{,\alpha})$$
$$- (b^\mu_\alpha x^i{}_{,\mu}u^i{}_{,\beta} + b^\mu_\beta x^i{}_{,\mu}u^i{}_{,\alpha}) \qquad (2.83)$$

2.3.3 Transverse Shear Strain Tensor

According to Eq. (2.60) the components of the transverse shear strain tensor are

$$2\gamma_{\alpha 3} = (\bar{a}_\alpha\cdot\bar{\lambda} + \hat{a}_3\cdot\bar{u}_{,\alpha}) \qquad (2.84)$$

According to Eq. (2.41)

$$\bar{\lambda} = \bar{\phi} \times \bar{a}_3 = e_{ijk}\phi^i n^j \hat{e}_k \qquad (2.85)$$

Substituting for the vectors in Eq. (2.84) in terms of their components, it is found that

$$2\gamma_{\alpha 3} = e_{ijk}\phi^i n^j x^k{}_{,\alpha} + n^i u^i{}_{,\alpha} \qquad (2.86)$$

For the later use, in the next section we examine the rotation of the shell element about the shell normal.

2.3.4 Rotation of the Shell Element

If the rotation of the shell element is small, the rotation can be represented as a vector. The rotation vector, $\bar{\Omega}$, can be obtained in terms of the displacement gradients as follows. $\bar{\Omega}$ can be expressed in terms of the components resolved along the base

vectors $\bar{g}_i$ or $\bar{g}^i$ as

$$\bar{\Omega} = \Omega^i \bar{g}_i = \Omega_i \bar{g}^i \qquad (2.86a,b)$$

The Ω^i components are related to the components of the rotation tensor, ω_{ij}, as [76]

$$\Omega^p = \frac{1}{2} \frac{1}{\sqrt{g}} e_{pij} \omega_{ji} \qquad (2.87)$$

where ω_{ij} is given in terms of the displacement gradients as [76]

$$\omega_{ij} = \frac{1}{2} (\bar{g}_i \cdot \bar{u}_{,j} - \bar{g}_j \cdot \bar{u}_{,i}) \qquad (2.88)$$

From Eq. (2.87), in particular, we obtain

$$\Omega^3 = \frac{1}{2\sqrt{g}} (\bar{g}_2 \cdot \bar{u}_{,1} - \bar{g}_1 \cdot \bar{u}_{,2}) \qquad (2.89)$$

When Eq. (2.89) is applied to a point on the shell middle surface, where the direction "3" coincides with the shell normal direction, θ^3, it is found that

$$\Omega^3 = \Omega_3 = \frac{1}{2\sqrt{a}} (\bar{a}_2 \cdot \bar{u}_{,1} - \bar{a}_1 \cdot \bar{u}_{,2}) \qquad (2.90)$$

Use of Eq. (2.62) and Eq. (2.66) in Eq. (2.90) leads to

$$\Omega_3 = \frac{1}{2\sqrt{a}} (x^i{}_{,2} u^i{}_{,1} - x^i{}_{,1} u^i{}_{,2}) \qquad (2.91)$$

2.4 Strain Energy Density in a Laminated Composite Shell

The construction details of a laminated composite shell is shown in Figure 3b. The shell wall is made up of stacking of

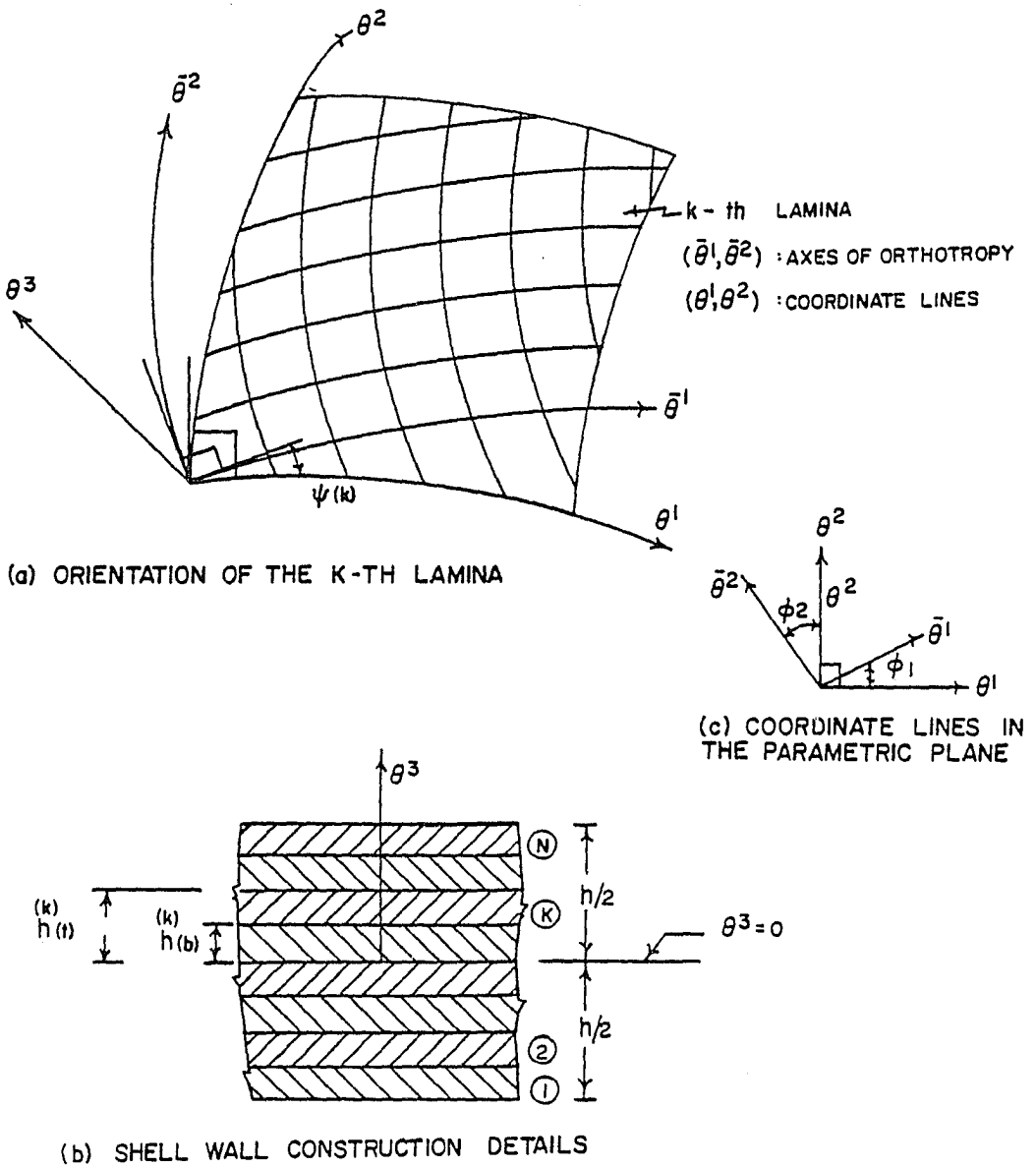

Figure 3. Laminated composite shell: construction details.

orthotropic laminae, total N in number. The distances to the bottom and top faces of the kth lamina from the middle surface in the θ^3 direction are denoted, respectively, by $h^{(k)}_{(b)}$ and $h^{(k)}_{(t)}$. The axes of orthotropy of the kth lamina are rotated from the curvilinear coordinate directions by an angle $\psi^{(k)}$ considered positive in the counterclockwise direction as shown in Figure 3a.

The axes of orthotropy of an individual lamina are usually orthogonal. The constitutive tensor in the curvilinear coordinate directions will be obtained by transforming the corresponding tensor in the orthotropy directions. At this stage, to simplify the transformation, it is assumed that the curvilinear coordinate directions are orthogonal, but not necessarily principal.

The strain energy density per unit volume in a three dimensional linear elastic body is of the form

$$u = \frac{1}{2}\, \tau^{k\ell} \bar{\gamma}_{k\ell} \tag{2.92}$$

where $\tau^{k\ell}$ are the contravariant components of the stress tensor. The three dimensional stress-strain relations for linear elastic behavior are given by

$$\tau^{ij} \equiv E^{ijk\ell} \bar{\gamma}_{k\ell} \tag{2.93}$$

where $E^{ijk\ell}$ (i,j,k,ℓ:1,2,3) are the contravariant components of the constitutive tensor, which transforms as a fourth-order tensor. In general, the following symmetries exist for the coefficients $E^{ijk\ell}$

$$E^{ijk\ell} = E^{jik\ell} = E^{ij\ell k} = E^{k\ell ij} \tag{2.94}$$

The individual orthotropic lamina is elastically symmetric with respect to the θ^3 coordinate. Therefore, the transformation $\bar{\theta}^3 = -\theta^3$, $\bar{\theta}^1 = \theta^1$, $\bar{\theta}^2 = \theta^2$ does not alter the strain energy function, that is, $u(\theta^1,\theta^2,\theta^3) = \bar{u}(\bar{\theta}^1,\bar{\theta}^2,\bar{\theta}^3)$. The above transformations, however, transform the strain components as $\bar{\gamma}_{3\alpha} = -\gamma_{3\alpha}$, $\bar{\gamma}_{33} = \gamma_{33}$, $\bar{\gamma}_{\alpha\beta} = \gamma_{\alpha\beta}$. Such terms should vanish to maintain the elastic symmetry. Therefore we have

$$E^{333\alpha} = E^{3\alpha\beta\gamma} = 0 \tag{2.95}$$

Then the equation for the strain energy in an individual lamina takes the form

$$u = \frac{1}{2} E^{\alpha\beta\gamma\eta}\bar{\gamma}_{\alpha\beta}\bar{\gamma}_{\gamma\eta} + E^{33\gamma\eta}\bar{\gamma}_{33}\bar{\gamma}_{\gamma\eta} + 2E^{\alpha3\beta3}\bar{\gamma}_{\alpha3}\bar{\gamma}_{\beta3} + \frac{1}{2} E^{3333}\bar{\gamma}_{33}^2 \tag{2.96}$$

Also, in view of Eq. (2.94) and Eq. (2.95), Eq. (2.93) is replaced by

$$\tau^{\alpha\beta} = E^{\alpha\beta\gamma\eta}\bar{\gamma}_{\gamma\eta} + E^{\alpha\beta33}\bar{\gamma}_{33} \tag{2.97a}$$

$$\tau^{\alpha3} = 2E^{\alpha3\beta3}\bar{\gamma}_{\beta3} \tag{2.97b}$$

$$\tau^{33} = E^{33\gamma\eta}\bar{\gamma}_{\gamma\eta} + E^{3333}\bar{\gamma}_{33} \tag{2.97c}$$

The tensorial components $E^{ijk\ell}$ vary with the θ^3 coordinate. It would be convenient to express these tensorial components in terms of the physical components which, being material constants, do not vary within a lamina. The physical components, σ^{ij}, of the stress tensor τ^{ij}, and the physical components, ε_{ij} of the strain tensor $\bar{\gamma}_{ij}$, when

the displacement gradients are small, are related as follows:

$$\sigma^{ij} = \sqrt{\frac{g_{(jj)}}{g^{(ii)}}}\,\tau^{ij} \tag{2.98}$$

$$\bar{\varepsilon}_{ij} = \frac{\bar{\gamma}_{ij}}{\sqrt{g_{(ii)}g_{(jj)}}} \tag{2.99}$$

where the parentheses around the indices indicate that with respect to these indices the summation convention is suspended. The linear elastic stress-strain relations between the physical components is defined similar to Eqs. (2.97)

$$\sigma^{\alpha\beta} \equiv G^{\alpha\beta\gamma\eta}\bar{\varepsilon}_{\gamma\eta} + G^{\alpha\beta 33}\bar{\varepsilon}_{33} \tag{2.100a}$$

$$\sigma^{\alpha 3} \equiv 2G^{\alpha 3\beta 3}\bar{\varepsilon}_{\beta 3} \tag{2.100b}$$

$$\sigma^{33} \equiv G^{33\gamma\eta}\bar{\varepsilon}_{\gamma\eta} + G^{3333}\bar{\varepsilon}_{33} \tag{2.100c}$$

where $G^{ijk\ell}$ are the physical components of the constitutive tensor. Substituting Eq. (2.98) and Eq. (2.99) in Eq. (2.93) we obtain

$$\sigma^{(ij)} = \sqrt{\frac{g_{(jj)}g_{(kk)}g_{(\ell\ell)}}{g^{(ii)}}}\,E^{ijk\ell}\bar{\varepsilon}_{k\ell} \tag{2.101}$$

Comparing Eqs. (2.100) and Eq. (2.101) it is seen that the physical and tensorial components of the constitutive tensor are related as

$$G^{ijk\ell} = \sqrt{\frac{g_{(jj)}g_{(kk)}g_{(\ell\ell)}}{g^{(ii)}}}\,E^{ijk\ell} \tag{2.102}$$

Since the shell is thin, we can assume that it is in a state of plane stress, and neglect the transverse normal stress. Setting

σ^{33} in Eq. (2.100c) to zero, it is seen that

$$\bar{\varepsilon}_{33} = - \frac{G^{33\gamma\eta}}{G^{3333}} \bar{\varepsilon}_{\gamma\eta} \tag{2.103}$$

Using Eq. (2.103) in Eq. (2.100a) we obtain

$$\sigma^{\alpha\beta} = G^{\alpha\beta\gamma\eta}\bar{\varepsilon}_{\gamma\eta} - \frac{G^{\alpha\beta 33}G^{33\gamma\eta}}{G^{3333}} \bar{\varepsilon}_{\gamma\eta} \tag{2.104a}$$

$$\sigma^{\alpha 3} = 2G^{\alpha 3\beta 3}\bar{\varepsilon}_{\beta 3} \tag{2.104b}$$

Letting

$$F^{\alpha\beta\gamma\eta} = G^{\alpha\beta\gamma\eta} - \frac{G^{\alpha\beta 33}G^{33\gamma\eta}}{G^{3333}} \tag{2.105}$$

we obtain

$$\sigma^{\alpha\beta} = F^{\alpha\beta\gamma\eta}\bar{\varepsilon}_{\gamma\eta} \tag{2.106a}$$

$$\sigma^{\alpha 3} = 2G^{\alpha 3\beta 3}\bar{\varepsilon}_{\beta 3} \tag{2.106b}$$

Using Eq. (2.102), Eq. (2.106a) can be written in terms of the tensorial components, $C^{\alpha\beta\gamma\eta}$, of the plane constitutive tensor, $F^{\alpha\beta\gamma\eta}$.

$$\tau^{\alpha\beta} = C^{\alpha\beta\gamma\eta}\bar{\gamma}_{\gamma\eta} \tag{2.107a}$$

$$\tau^{\alpha 3} = 2E^{\alpha 3\beta 3}\tau_{\beta 3} \tag{2.107b}$$

where

$$C^{\alpha\beta\gamma\eta} = \sqrt{\frac{g^{(\alpha\alpha)}}{g_{(\beta\beta)}g_{(\gamma\gamma)}g_{(\eta\eta)}}}\, F^{\alpha\beta\gamma\eta} \tag{2.108}$$

$$E^{\alpha 3\beta 3} = \sqrt{\frac{g^{(\alpha\alpha)}}{g_{(\beta\beta)}}}\, G^{\alpha 3\beta 3} \tag{2.109}$$

and the strain energy density in an individual lamina, Eq. (2.96),

$$u = \frac{1}{2} C^{\alpha\beta\gamma\eta} \bar{\gamma}_{\alpha\beta} \bar{\gamma}_{\gamma\eta} + 2E^{\alpha 3\beta 3} \bar{\gamma}_{\alpha 3} \bar{\gamma}_{\beta 3} \tag{2.110}$$

The total strain energy in the shell is obtained by integration of the strain energy density over the volume of the shell

$$U = \int_{vol} u dv \tag{2.111}$$

where the differential volume element dv is expressed in terms of the differential area element, ds, as

$$dv = ds d\theta^3 \tag{2.112}$$

The differential area at any point θ^3 from the middle surface can be expressed in terms of its projection on the middle surface, ds_o, as [76]

$$ds = \sqrt{\frac{g}{a}}\, ds_o \tag{2.113}$$

where g and a are the determinants of the metric tensors $g_{\alpha\beta}$ and $a_{\alpha\beta}$ respectively. In view of Eq. (2.112) and Eq. (2.113), Eq. (2.111) takes the form

$$U = \int_{vol} \sqrt{\frac{g}{a}}\, u ds_o d\theta^3 \tag{2.114}$$

or

$$U = \int_{A_o} u_s ds_o \tag{2.115}$$

where u_s is the strain energy density per unit area of the middle surface, and A_o is the total middle surface area of the shell. It follows from Eq. (2.114) and Eq. (2.115) that

$$u_s = \int_{\theta^3} \sqrt{\frac{\bar{g}}{a}}\, u d\theta^3 \tag{2.116}$$

where the integration is carried over the thickness of the shell. For a multi-layered laminated shell with N layers, Eq. (2.116) can be written as

$$u_s = \sum_{k=1}^{N} \int_{h_{(b)}^{(k)}}^{h_{(t)}^{(k)}} \sqrt{\frac{\bar{g}}{a}}\, u^{(k)} d\theta^3 \tag{2.117}$$

where $u^{(k)}$ is the value of u in the kth layer, and the integral over the shell thickness has been expressed as sum of the integrals over the individual lamina. It follows from Eq. (2.110) that

$$u^{(k)} = \frac{1}{2} C_{(k)}^{\alpha\beta\gamma\eta} \bar{\gamma}_{\alpha\beta} \bar{\gamma}_{\gamma\eta} + 2E_{(k)}^{\alpha 3 \beta 3} \bar{\gamma}_{\alpha 3} \bar{\gamma}_{\beta 3} \tag{2.118}$$

where the suffix k signifies the kth layer. Also, from the differential geometry of the curved surfaces it is known [76, Chap. 11] that

$$\sqrt{\frac{\bar{g}}{a}} = (1 - 2H\theta^3 + K(\theta^3)^2) \tag{2.119}$$

where H and K are, respectively, the mean and Gaussian curvatures of the middle surface defined by Eq. (2.27) and Eq. (2.28). Further, if χ denotes the maximum curvature of the middle surface, Eq. (2.32a) can be replaced by the approximate relations

$$g_{\alpha\beta} \simeq a_{\alpha\beta}[1 + 0(\chi\theta^3)] \qquad g^{\alpha\beta} \simeq a^{\alpha\beta}[1 + 0(\chi\theta^3)] \tag{2.120}$$

where the notation 0(--) stands for order of (--). In view of Eq. (2.120), Eq. (2.108) and Eq. (2.109) can be written as

$$C^{\alpha\beta\gamma\eta}_{(k)} = \sqrt{\frac{a^{(\alpha\alpha)}}{a_{(\beta\beta)}a_{(\gamma\gamma)}a_{(\eta\eta)}}}\, F^{\alpha\beta\gamma\eta}_{(k)} \,[1 + 0(\chi\theta^3)] \tag{2.121a}$$

$$= C^{\alpha\beta\gamma\eta}_{(k_o)} \,[1 + 0(\chi\theta^3)] \tag{2.121b}$$

and

$$E^{\alpha 3\beta 3}_{(k)} = \sqrt{\frac{a^{(\alpha\alpha)}}{a_{(\beta\beta)}}}\, G^{\alpha 3\beta 3}_{(k)} \tag{2.122a}$$

$$= E^{\alpha 3\beta 3}_{(k_o)} \tag{2.122b}$$

Using Eq. (2.118) and Eq. (2.119) in Eq. (2.117), and in view of Eq. (2.121b) and Eq. (2.122b), the strain energy density u_s is obtained as

$$\begin{aligned} u_s = &\sum_{k=1}^{N} \frac{1}{2} C^{\alpha\beta\gamma\eta}_{(k_o)} \int_{h^{(k)}_{(b)}}^{h^{(k)}_{(t)}} \bar{\gamma}_{\alpha\beta}\bar{\gamma}_{\gamma\eta}[1 + 0(\chi\theta^3)]d\theta^3 \\ &+ \sum_{k=1}^{N} 2E^{\alpha 3\beta 3}_{(k_o)} \int_{h^{(k)}_{(b)}}^{h^{(k)}_{(t)}} \bar{\gamma}_{\alpha 3}\bar{\gamma}_{\beta 3}d\theta^3 \end{aligned} \tag{2.123}$$

Substituting the strain distribution from Eq. (2.59), Eq. (2.123) becomes

$$\begin{aligned} u_s = &\sum_{k=1}^{N} \frac{1}{2} C^{\alpha\beta\gamma\eta}_{(k_o)} \int_{h^{(k)}_{(b)}}^{h^{(k)}_{(t)}} (\gamma_{\alpha\beta} + \theta^3\chi_{\alpha\beta})(\gamma_{\gamma\eta} + \theta^3\chi_{\gamma\eta})[1 + 0(\chi\theta^3)]d\theta^3 \\ &+ \sum_{k=1}^{N} 2E^{\alpha 3\beta 3}_{(k_o)} \int_{h^{(k)}_{(b)}}^{h^{(k)}_{(t)}} \bar{\gamma}_{\alpha 3}\bar{\gamma}_{\beta 3}d\theta^3 \end{aligned} \tag{2.124}$$

Carrying out the multiplication in Eq. (2.124),

$$u_s = \sum_{k=1}^{N} \frac{1}{2} C^{\alpha\beta\gamma\eta}_{(k_o)} \int_{h^{(k)}_{(b)}}^{h^{(k)}_{(t)}} [\gamma_{\alpha\beta}\gamma_{\gamma\eta} + (\gamma_{\alpha\beta}\chi_{\gamma\eta} + \gamma_{\gamma\eta}\chi_{\alpha\beta})\theta^3 + \chi_{\alpha\beta}\chi_{\gamma\eta}(\theta^3)^2]d\theta^3$$

$$+ \sum_{k=1}^{N} 2E^{\alpha 3\beta 3}_{(k_o)} \int_{h^{(k)}_{(b)}}^{h^{(k)}_{(t)}} \bar{\gamma}_{\alpha 3}\bar{\gamma}_{\beta 3} d\theta^3$$

$$+ (\text{terms quadratic in strains})(\chi h) \tag{2.125}$$

In the case of thin shells $\chi h << 1$; and hence the last parenthetical term in Eq. (2.125) is negligible in comparison with the other. Since the strain components $\gamma_{\alpha\beta}$, $\chi_{\alpha\beta}$ and $\bar{\gamma}_{\alpha 3}$ do not vary with θ^3, after carrying out the integration Eq. (2.125) can be written in the simpler form:

$$u_s = \frac{1}{2}[A^{\alpha\beta\gamma\eta}\gamma_{\alpha\beta}\gamma_{\gamma\eta} + B^{\alpha\beta\gamma\eta}(\gamma_{\alpha\beta}\chi_{\gamma\eta} + \gamma_{\gamma\eta}\chi_{\alpha\beta}) + D^{\alpha\beta\gamma\eta}\chi_{\alpha\beta}\chi_{\gamma\eta}] + 2H^{\alpha 3\beta 3}\bar{\gamma}_{\alpha 3}\bar{\gamma}_{\beta 3} \tag{2.126}$$

where

$$A^{\alpha\beta\gamma\eta} = \sum_{k=1}^{N} C^{\alpha\beta\gamma\eta}_{(k_o)} (h^{(k)}_{(t)} - h^{(k)}_{(b)}) \tag{2.127a}$$

$$B^{\alpha\beta\gamma\eta} = \frac{1}{2} \sum_{k=1}^{N} C^{\alpha\beta\gamma\eta}_{(k_o)} [(h^{(k)}_{(t)})^2 - (h^{(k)}_{(b)})^2] \tag{2.127b}$$

$$D^{\alpha\beta\gamma\eta} = \frac{1}{3} \sum_{k=1}^{N} C^{\alpha\beta\gamma\eta}_{(k_o)} [(h^{(k)}_{(t)})^3 - (h^{(k)}_{(b)})^3] \tag{2.127c}$$

$$H^{\alpha 3 \beta 3} = \sum_{k=1}^{N} E^{\alpha 3 \beta 3}_{(k_o)} \left(h^{(k)}_{(t)} - h^{(k)}_{(b)}\right) \tag{2.127d}$$

Equations (2.127a) to (2.127d) are the laminate constitutive tensors. The tensors $A^{\alpha\beta\gamma\eta}$ and $D^{\alpha\beta\gamma\eta}$ represent the extensional and bending rigidities; and the rigidity due to extensional-bending coupling is represented by $B^{\alpha\beta\gamma\eta}$. $H^{\alpha 3 \beta 3}$ is the transverse shear rigidity. It may be noted that, in general, $B^{\alpha\beta\gamma\eta}$ are non-zero. However, for particular laminate constructions, such as symmetric laminates, extensional-bending coupling will be completely absent.

The lamina constitutive tensors in Eqs. (2.127) are directly obtained by transformation of the corresponding tensors in the principal material directions of the individual lamina. The lamina stress-strain relations in the principal material directions, $\bar{\theta}^i$, can be expressed in terms of the basic elastic constants of the orthotropic lamina.

Let E_1, E_2 and E_3 be the Young's moduli in the directions of orthotropy; G_{12}, G_{23} and G_{13} be the rigidity moduli between the directions indicated by the indices; and ν_{12}, ν_{23}, ν_{13} be the corresponding Poisson's ratios, where ν_{12} gives the transverse strain in the direction $\bar{\theta}^2$ due to the longitudinal strain in the direction $\bar{\theta}^1$. The strain components in the directions $\bar{\theta}^i$ are given by Hooke's law:

$$\bar{\varepsilon}_{11} = \frac{\bar{\sigma}_{11}}{E_1} - \nu_{21} \frac{\bar{\sigma}_{22}}{E_2} - \nu_{31} \frac{\bar{\sigma}_{33}}{E_3} \tag{2.128a}$$

$$\bar{\varepsilon}_{22} = -\nu_{12} \frac{\bar{\sigma}_{11}}{E_1} + \frac{\bar{\sigma}_{22}}{E_2} - \nu_{32} \frac{\bar{\sigma}_{33}}{E_3} \tag{2.128b}$$

$$\bar{\varepsilon}_{33} = -\nu_{13}\frac{\bar{\sigma}_{11}}{E_1} - \nu_{23}\frac{\bar{\sigma}_{22}}{E_2} + \frac{\bar{\sigma}_{33}}{E_3} \tag{2.128c}$$

$$2\bar{\varepsilon}_{12} = \frac{\bar{\sigma}_{12}}{G_{12}} \tag{2.128d}$$

$$2\bar{\varepsilon}_{23} = \frac{\bar{\sigma}_{23}}{G_{23}} \tag{2.128e}$$

$$2\bar{\varepsilon}_{13} = \frac{\bar{\sigma}_{13}}{G_{13}} \tag{2.128f}$$

Inverting these equations the stress-strain relations can be obtained in the form

$$\bar{\sigma}_{ij} = \bar{G}^{ijk\ell}\bar{\varepsilon}_{k\ell} \tag{2.129}$$

where $\bar{G}^{ijk\ell}$ forms the symmetric array

$$\begin{array}{cccccc} \bar{G}^{1111} & \bar{G}^{1122} & \bar{G}^{1133} & 0 & 0 & 0 \\ & \bar{G}^{2222} & \bar{G}^{2233} & 0 & 0 & 0 \\ & & \bar{G}^{3333} & 0 & 0 & 0 \\ \text{symmetric} & & & \bar{G}^{1212} & 0 & 0 \\ & & & & \bar{G}^{2323} & 0 \\ & & & & & \bar{G}^{1313} \end{array} \tag{2.130}$$

The coefficients of the above array in terms of the basic elastic constants of the lamina are given below:

$$\bar{G}^{1111} = \frac{E_1}{F}(1 - \nu_{23}\nu_{32}) \qquad \bar{G}^{1122} = \frac{E_2}{F}(\nu_{12} + \nu_{13}\nu_{32}) \tag{2.131a,b}$$

$$\bar{G}^{1133} = \frac{E_3}{F}(\nu_{13} + \nu_{12}\nu_{23}) \qquad \bar{G}^{2222} = \frac{E_2}{F}(1 - \nu_{13}\nu_{31}) \tag{2.132a,b}$$

$$\bar{G}^{2233} = \frac{E_3}{F}(\nu_{23} + \nu_{21}\nu_{13}) \qquad \bar{G}^{3333} = \frac{E_3}{F}(1 - \nu_{12}\nu_{21}) \tag{2.133a,b}$$

$$\bar{G}^{1212} = G_{12} \qquad \bar{G}^{2323} = G_{23} \qquad \bar{G}^{1313} = G_{13} \tag{2.134a,b,c}$$

where

$$F = (1 - \nu_{12}\nu_{21} - \nu_{23}\nu_{32} - \nu_{13}\nu_{31} - \nu_{12}\nu_{23}\nu_{13} - \nu_{21}\nu_{32}\nu_{31}) \tag{2.135}$$

Also

$$\nu_{21} = \nu_{12}\frac{E_2}{E_1} \qquad \nu_{32} = \nu_{23}\frac{E_3}{E_2} \qquad \nu_{31} = \nu_{13}\frac{E_3}{E_1} \tag{2.136}$$

It may be noted that $\bar{G}^{ijk\ell}$ are the physical components in the directions of orthotropy, $\bar{\theta}^i$. When the plane stress condition prevails, according to Eq. (2.105), we can write

$$\bar{F}^{\alpha\beta\gamma\eta} = \bar{G}^{\alpha\beta\gamma\eta} - \frac{\bar{G}^{\alpha\beta 33}\bar{G}^{33\gamma\eta}}{\bar{G}^{3333}} \tag{2.137}$$

The corresponding tensorial components follow from Eqs. (2.121) and (2.122). For the kth lamina we can write

$$\bar{C}^{\alpha\beta\gamma\eta}_{(k_o)} = \sqrt{\frac{\bar{a}^{(\alpha\alpha)}}{\bar{a}^{(\beta\beta)}\bar{a}^{(\gamma\gamma)}\bar{a}^{(\eta\eta)}}}\,\bar{F}^{\alpha\beta\gamma\eta}_{(k)} \tag{2.138}$$

and

$$\bar{E}^{\alpha 3\beta 3}_{(k_o)} = \sqrt{\frac{\bar{a}^{(\alpha\alpha)}}{\bar{a}^{(\beta\beta)}}}\,\bar{G}^{\alpha 3\beta 3}_{(k)} \tag{2.139}$$

where $\bar{a}_{\alpha\beta}$ and $\bar{a}^{\alpha\beta}$ are the components of the metric tensor in the $\bar{\theta}^i$ direction. The metric tensors in the directions θ^i and $\bar{\theta}^i$ are related by the second-order tensor transformation law

$$\bar{a}_{\alpha\beta} = \frac{\partial\theta^\lambda}{\partial\bar{\theta}_\alpha}\frac{\partial\theta^\mu}{\partial\bar{\theta}_\beta}\, a_{\lambda\mu} \tag{2.140}$$

$$\bar{a}^{\alpha\beta} = \frac{\partial\bar{\theta}^\alpha}{\partial\theta^\lambda}\frac{\partial\bar{\theta}^\beta}{\partial\theta^\mu}\, a^{\lambda\mu} \tag{2.141}$$

where the coefficients of transformation, $\frac{\partial\theta^\alpha}{\partial\bar{\theta}^\beta}$ etc. will be derived in the later part of this section. Finally, the constitutive tensor in the $\bar{\theta}^i$ direction is transformed into the θ^i direction, following the fourth-order tensor transformation law.

$$C^{\alpha\beta\gamma\eta}_{(k_o)} = \frac{\partial\theta^\alpha}{\partial\bar{\theta}^\lambda}\frac{\partial\theta^\beta}{\partial\bar{\theta}^\mu}\frac{\partial\theta^\gamma}{\partial\bar{\theta}^\phi}\frac{\partial\theta^\eta}{\partial\bar{\theta}^\psi}\,\bar{C}^{\lambda\mu\phi\psi}_{(k_o)} \tag{2.142}$$

$$E^{\alpha 3\beta 3}_{(k_o)} = \frac{\partial\theta^\alpha}{\partial\bar{\theta}^\lambda}\frac{\partial\theta^\beta}{\partial\bar{\theta}^\mu}\,\bar{E}^{\lambda 3\mu 3}_{(k_o)} \tag{2.143}$$

To derive the formulae for the coefficients of transformation in Eq. (2.140)-Eq. (2.143), consider the orientation of the kth lamina in Figure 3a. The principal material directions $\bar{\theta}^\alpha$ are rotated from the orthogonal curvilinear coordinate directions θ^α by the angle $\psi^{(k)}$. Figure 3c shows the mapping of these lines in the parametric space. Let

$$\bar{\theta}^\alpha = \bar{\theta}^\alpha(\theta^1,\theta^2) \tag{2.144}$$

Since the $\bar{\theta}^\alpha$ lies on the middle surface of the shell, the position vector to a point on the $\bar{\theta}^\alpha$ line is given by

$$\bar{R}(\bar{\theta}^{\alpha}) = \bar{R}[\bar{\theta}^{\alpha}(\theta^1,\theta^2)] \tag{2.145}$$

Tangent vector to the $\bar{\theta}^{\alpha}$ line is denoted as $\bar{a}^{*}_{\alpha}$, which is given by

$$\bar{a}^{*}_{\alpha} = \frac{\partial \bar{R}}{\partial \bar{\theta}^{\alpha}} = \frac{\partial \bar{R}}{\partial \theta^1}\frac{\partial \theta^1}{\partial \bar{\theta}^{\alpha}} + \frac{\partial \bar{R}}{\partial \theta^2}\frac{\partial \theta^2}{\partial \bar{\theta}^{\alpha}} \tag{2.146}$$

or

$$\bar{a}^{*}_{\alpha} = \bar{a}_1 \frac{\partial \theta^1}{\partial \bar{\theta}^{\alpha}} + \bar{a}_2 \frac{\partial \theta^2}{\partial \bar{\theta}^{\alpha}} \quad (\alpha = 1,2) \tag{2.147}$$

Thus we have

$$\bar{a}^{*}_1 = \bar{a}_1 \frac{\partial \theta^1}{\partial \bar{\theta}^1} + \bar{a}_2 \frac{\partial \theta^2}{\partial \bar{\theta}^1} = k_1\bar{a}_1 + k_2\bar{a}_2 \tag{2.148a}$$

$$\bar{a}^{*}_2 = \bar{a}_1 \frac{\partial \theta^1}{\partial \bar{\theta}^2} + \bar{a}_2 \frac{\partial \theta^2}{\partial \bar{\theta}^2} = k_3\bar{a}_1 + k_4\bar{a}_2 \tag{2.148b}$$

Since the angle between the vectors $\bar{a}_{\alpha}$ and $\bar{a}^{*}_{\alpha}$ is $\psi^{(k)}$ and both lie on the tangent plane, we have the relations

$$\bar{a}_1 \times \bar{a}^{*}_1 = \sqrt{a_{11}}\,\sqrt{a^{*}_{11}}\,\sin\psi^{(k)}\,\hat{n} \tag{2.149}$$

$$\bar{a}_1 \cdot \bar{a}^{*}_1 = \sqrt{a_{11}}\,\sqrt{a^{*}_{11}}\,\cos\psi^{(k)} \tag{2.150}$$

where $\hat{n}$ is the outward unit normal vector to the middle surface.

Substituting for $\bar{a}^{*}_1$ from Eq. (2.148a), Eq. (2.149), and Eq. (2.150), recalling that $\bar{a}_1$ and $\bar{a}_2$ are orthogonal, leads to

$$\frac{k_1}{k_2} = \frac{\sqrt{a_{22}}}{\sqrt{a_{11}}}\frac{\cos\psi^{(k)}}{\sin\psi^{(k)}} \tag{2.151}$$

Similar consideration of the vectors $\bar{a}_2$ and $\bar{a}^*_2$ leads to

$$\frac{k_3}{k_4} = \frac{-\sqrt{a_{22}}\sin\psi^{(k)}}{\sqrt{a_{11}}\cos\psi^{(k)}} \tag{2.152}$$

Since Eqs. (2.148) imply a rotation of the $\bar{\theta}^\alpha$ lines relative to θ^α coordinate lines in the parametric plane, as shown in Figure 3c, we have the normality conditions

$$k_1^2 + k_2^2 = 1 \qquad k_3^2 + k_4^2 = 1 \tag{2.153a,b}$$

Solution of Eqs. (2.151)-(2.153) leads to the following values for the parameters k_1 to k_4:

$$k_1 = \frac{\partial\theta^1}{\partial\bar{\theta}^1} = \frac{\sqrt{a_{22}}}{p} \cdot \cos\psi^{(k)} \tag{2.154a}$$

$$k_2 = \frac{\partial\theta^2}{\partial\bar{\theta}^1} = \frac{\sqrt{a_{11}}}{p} \sin\psi^{(k)} \tag{2.154b}$$

$$k_3 = \frac{\partial\theta^1}{\partial\bar{\theta}^2} = \frac{-\sqrt{a_{22}} \cdot \sin\psi^{(k)}}{p} \tag{2.154c}$$

$$k_4 = \frac{\partial\theta^2}{\partial\bar{\theta}^2} = \frac{\sqrt{a_{11}}}{p} \cos\psi^{(k)} \tag{2.154d}$$

where

$$p = \sqrt{(a_{22}\cos^2\psi^{(k)} + a_{11}\sin^2\psi^{(k)})} \tag{2.155}$$

Using these values for the transformation coefficients, we can obtain the covariant metric tensor $\bar{a}_{\alpha\beta}$ in Eq. (2.140) and the constitutive tensors $C^{\alpha\beta\gamma\eta}_{(k_o)}$ and $E^{\alpha 3\beta 3}_{(k_o)}$ in Eq. (2.142) and Eq. (2.143). The

contravariant metric tensor $\bar{a}^{\alpha\beta}$ in Eq. (2.141) is directly obtained, according to Eq. (2.14), as

$$\bar{a}^{11} = \frac{\bar{a}_{22}}{\bar{a}} \ , \ \bar{a}^{22} = \frac{\bar{a}_{11}}{\bar{a}} \ , \ \bar{a}_{12} = \frac{-\bar{a}_{12}}{\bar{a}} = \bar{a}^{21} \tag{2.156a}$$

where

$$\bar{a} = |\bar{a}_{\alpha\beta}| \tag{2.156b}$$

If the material is isotropic, the constitutive relations are much simpler and can be expressed in terms of the two elastic constants of the material. For an isotropic material the constitutive tensor $E^{ijk\ell}$ of Eq. (2.93) is given by [76]

$$E^{ijk\ell} = \frac{E}{2(1+\nu)} \left(g^{ik}g^{j\ell} + g^{i\ell}g^{jk} + \frac{2\nu}{1-\nu} g^{ij}g^{k\ell}\right) \tag{2.157}$$

where E is the Young's modulus and ν is the Poisson's ratio. The strain energy density of Eq. (2.126) takes the simple form

$$u_s = \frac{1}{2} h \, C^{\alpha\beta\gamma\eta}\gamma_{\alpha\beta}\gamma_{\gamma\eta} + \frac{1}{2}\frac{h^3}{12} C^{\alpha\beta\gamma\lambda}\chi_{\alpha\beta}\chi_{\gamma\eta} + 2hE^{\alpha 3\beta 3}\gamma_{\alpha 3}\gamma_{\beta 3} \tag{2.158}$$

where

$$C^{\alpha\beta\gamma\eta} = \frac{E}{2(1+\nu)} \left[a^{\alpha\gamma}a^{\beta\eta} + a^{\alpha\eta}a^{\beta\gamma} + \frac{2\nu}{1-\nu} a^{\alpha\beta}a^{\gamma\eta}\right] \tag{2.159}$$

This completes the presentation of the strain energy density evaluation in a laminated composite as well as an isotropic thin shell. In the next chapter, the development of the new triangular curved shell element will be presented, where the important equations from the present chapter will be presented in the matrix notation.

CHAPTER 3

CURVED TRIANGULAR ANISOTROPIC THIN SHELL FINITE ELEMENT

The formulation of the new curved triangular anisotropic thin shell element based on the "discrete Kirchhoff theory" approach is presented in this chapter. Element matrices for linear elastic behavior are derived based on the principle of minimum potential energy. The element formulation is capable of modeling anisotropic material behavior, representative of multi-layered, multi-directionally oriented laminated composite shells. A brief description of the element, and the approach to the formulation of the element matrices was presented in Section 1.4 of Chapter 1. The complete formulational details are presented in the following.

The formulation starts with a section describing the various coordinate systems used during the element development. The details of the interpolation of the components of the displacement and rotation vectors, and that of the isoparametric representation of the shell middle surface form the next two sections. This is followed by the calculation of the finite element strain energy. Here the strain-displacement relations and the lamina constitutive relations will be recast using conventional symbols (dropping the indices) and matrix notation. The task of derivation of the discrete Kirchoff constraints, and the surface rotation constraints is addressed in Section 3.5. The details of the numerical implementation of the

various constraints leading to the element matrices, and their subsequent transformation into the local orthogonal curvilinear coordinate system are presented in Sections 3.6 and 3.7. The chapter concludes with a brief description of the computer program.

3.1 Coordinate Systems

Figure 4 shows the various coordinate systems used. The curvilinear coordinates are denoted by (α,β). Figure 4b shows the element definition in the α-β parametric plane. The element nodes are specified by their (α,β) coordinate values, and the element sides are specified as straight lines in the α-β parametric plane. This plane triangle is mapped onto the curvilinear element in the Euclidean space by the parametric equation of the shell middle surface, as shown in Figure 4a. The equation of the middle surface is described by the components of the position vector, $\bar{R}_o(\alpha,\beta)$, to the shell middle surface referred to the global cartesian coordinate system, denoted by (x,y,z). Thus

$$\bar{R}_o(\alpha,\beta) = x(\alpha,\beta)\hat{e}_1 + y(\alpha,\beta)\hat{e}_2 + z(\alpha,\beta)\hat{e}_3 \qquad (3.1)$$

where $\hat{e}_1$, $\hat{e}_2$ and $\hat{e}_3$ are the cartesian unit base vectors. Figure 4c shows the natural coordinate system (ξ,η), where the triangle in the parametric plane is mapped onto the unit right-angled triangle. These coordinates are also referred to as barycentric coordinates. It is also noted that ξ and η are two of the three area coordinates, the third one being $(1 - \xi - \eta)$. The mapping between the α-β and ξ-η planes is defined by the relations

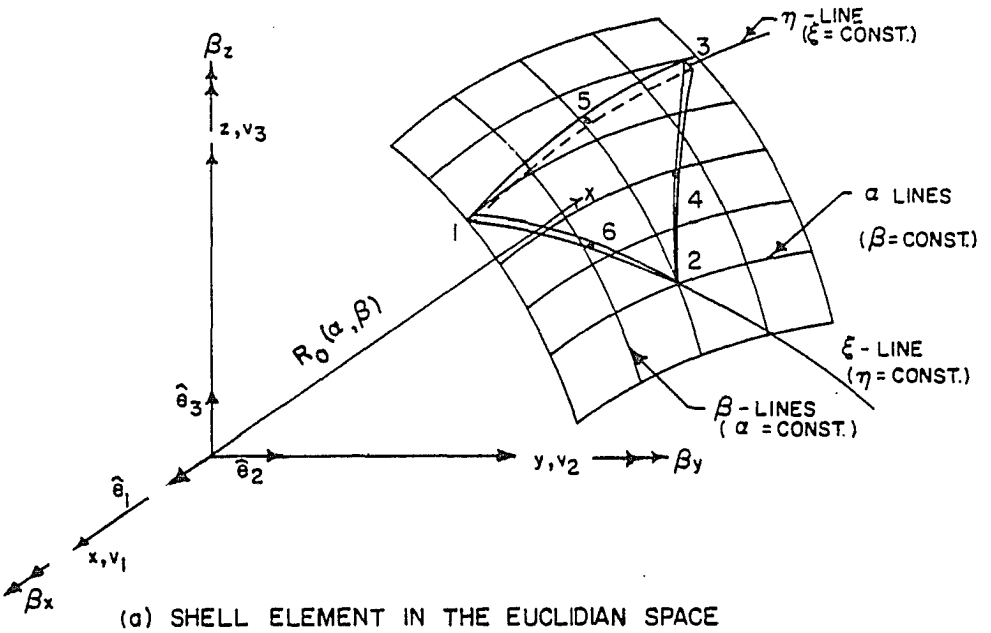

(a) SHELL ELEMENT IN THE EUCLIDIAN SPACE

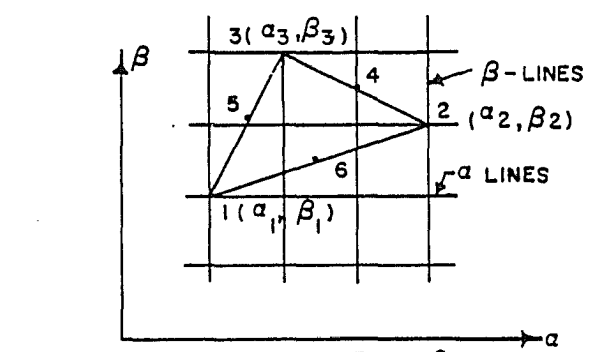

(b) SHELL ELEMENT IN THE $\alpha-\beta$ PARAMETRIC PLANE

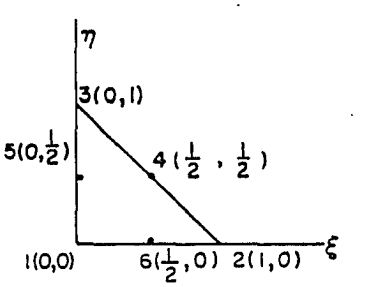

(c) SHELL ELEMENT IN THE NATURAL COORDINATES

Figure 4. Coordinate systems.

$$\alpha = \alpha_1 + (\alpha_2 - \alpha_1)\xi + (\alpha_3 - \alpha_1)\eta \tag{3.2a}$$

$$\beta = \beta_1 + (\beta_2 - \beta_1)\xi + (\beta_3 - \beta_1)\eta \tag{3.2b}$$

where ξ and η vary between 0 and 1. The derivatives in the two coordinate systems are related as follows:

$$\frac{\partial}{\partial \xi} = R_{11}\frac{\partial}{\partial \alpha} + R_{12}\frac{\partial}{\partial \beta} \tag{3.3a}$$

$$\frac{\partial}{\partial \eta} = R_{21}\frac{\partial}{\partial \alpha} + R_{22}\frac{\partial}{\partial \beta} \tag{3.3b}$$

where

$$R_{11} = \alpha_2 - \alpha_1 \quad R_{12} = \beta_2 - \beta_1 \tag{3.4a}$$

$$R_{21} = \alpha_3 - \alpha_1 \quad R_{22} = \beta_3 - \beta_1 \tag{3.4b}$$

The inverse relations follow from Eqs. (3.3)

$$\frac{\partial}{\partial \alpha} = d_{11}\frac{\partial}{\partial \xi} + d_{12}\frac{\partial}{\partial \eta} \tag{3.5a}$$

$$\frac{\partial}{\partial \beta} = d_{21}\frac{\partial}{\partial \xi} + d_{22}\frac{\partial}{\partial \eta} \tag{3.5b}$$

where

$$d_{11} = (\beta_3 - \beta_1)/f \quad d_{12} = -(\beta_2 - \beta_1)/f \tag{3.6a}$$

$$d_{21} = -(\alpha_3 - \alpha_1)/f \quad d_{22} = (\alpha_2 - \alpha_1)/f \tag{3.6b}$$

where f is the Jacobian of the transformation:

$$f = \frac{\partial(\alpha,\beta)}{\partial(\xi,\eta)} = (\alpha_2 - \alpha_1)(\beta_3 - \beta_1) - (\alpha_3 - \alpha_1)(\beta_2 - \beta_1) \tag{3.7}$$

For future use, the inverse relations between the second-order derivatives are also noted below:

$$\frac{\partial^2}{\partial\alpha^2} = (d_{11})^2 \frac{\partial^2}{\partial\xi^2} + 2d_{11}d_{12} \frac{\partial^2}{\partial\xi\partial\eta} + (d_{12})^2 \frac{\partial^2}{\partial\eta^2} \tag{3.8a}$$

$$\frac{\partial^2}{\partial\alpha\partial\beta} = d_{11}d_{21} \frac{\partial^2}{\partial\xi^2} + (d_{11}d_{22} + d_{12}d_{21}) \frac{\partial^2}{\partial\xi\partial\eta} + d_{12}d_{22} \frac{\partial^2}{\partial\eta^2} \tag{3.8b}$$

$$\frac{\partial^2}{\partial\beta^2} = (d_{21})^2 \frac{\partial^2}{\partial\xi^2} + 2d_{21}d_{22} \frac{\partial^2}{\partial\xi\partial\eta} + (d_{22})^2 \frac{\partial^2}{\partial\eta^2} \tag{3.8c}$$

3.2 Interpolation of Displacements and Rotations

The cartesian components of the displacement and rotation vectors are interpolated by polynomial shape functions in the ξ-η natural coordinates. While complete (ten-term) cubic polynomials are used for all the three displacement components, the rotation components are interpolated by complete (six-term) quadratic polynomials. The details of interpolation are given below.

3.2.1 Interpolation of Displacement Components

Each of the cartesian components of the displacement, v_1, v_2, v_3 (see Figure 4a) is assumed as a complete cubic polynomial in the ξ,η coordinates as

$$v_i = a_1 + a_2\xi + a_3\eta + a_4\xi^2 + a_5\xi\eta + a_6\eta^2 + a_7\xi^3 + a_8\xi^2\eta + a_9\xi\eta^2 + a_{10}\eta^3 \quad (i = 1,2,3) \tag{3.9}$$

$$= \lfloor f(\xi,\eta) \rfloor \{a\} \tag{3.10}$$

where

$$\lfloor f(\xi,\eta) \rfloor = \lfloor 1,\xi,\eta,\xi^2,\xi\eta,\eta^2,\xi^3,\xi^2\eta,\xi\eta^2,\eta^3 \rfloor \tag{3.11}$$

$$\{a\} = \lfloor a_1, a_2, \ldots, a_{10} \rfloor^T \tag{3.12}$$

where the generalized displacements a_1, a_2, ..., a_{10} can be expressed in terms of the nodal values of v_i, $\frac{\partial v_i}{\partial \xi}$ and $\frac{\partial v_i}{\partial \eta}$ at the three corner nodes and the centroidal value, $(v_i)_G$. By evaluating the above nodal values using Eq. (3.9) at the corner nodes and the element centroid, and solving the resulting set of ten simultaneous equations we obtain

$$\{a\} = [T]\{\bar{V}_i\} \tag{3.13}$$

where

$$\underset{10X1}{\{\bar{V}_i\}} = \lfloor (v_i)_1, \left(\frac{\partial v_i}{\partial \xi}\right)_1, \left(\frac{\partial v_i}{\partial \eta}\right)_1, \ldots, \left(\frac{\partial v_i}{\partial \eta}\right)_3, (v_i)_G \rfloor^T \tag{3.14}$$

and the suffix following the parentheses indicates the node number or the centroid. The matrix [T] is found to be [33]:

$$\underset{10X10}{[T]} = \begin{bmatrix} 1 & 0 & 0 & 0 & 0 & 0 & 0 & 0 & 0 & 0 \\ 0 & 1 & 0 & 0 & 0 & 0 & 0 & 0 & 0 & 0 \\ 0 & 0 & 1 & 0 & 0 & 0 & 0 & 0 & 0 & 0 \\ -3 & -2 & 0 & 3 & -1 & 0 & 0 & 0 & 0 & 0 \\ -13 & -3 & -3 & -7 & 2 & -1 & -7 & -1 & 2 & 27 \\ -3 & 0 & -2 & 0 & 0 & 0 & 3 & 0 & -1 & 0 \\ 2 & 1 & 0 & -2 & 1 & 0 & 0 & 0 & 0 & 0 \\ 13 & 3 & 2 & 7 & -2 & 2 & 7 & 1 & -2 & -27 \\ 13 & 2 & 3 & 7 & -2 & 1 & 7 & 2 & -2 & -27 \\ 2 & 0 & 1 & 0 & 0 & 0 & -2 & 0 & 1 & 0 \end{bmatrix} \tag{3.15}$$

The ξ-η derivatives in Eq. (3.14) are transformed to α-β derivatives with the help of Eqs. (3.3), and Eq. (3.12) becomes

$$\{a\} = [S]\{V_i\} \tag{3.16}$$

where

$$\underset{10X10}{[S]} = [T][\bar{R}] \tag{3.17}$$

$$\{\bar{V}_i\} = [\bar{R}]\{V_i\} \tag{3.18}$$

and $[\bar{R}]$ is the diagonal super-matrix defined in terms of the sub-matrix [R] as

$$\underset{10X10}{[\bar{R}]} = \lceil [R],\ [R],\ [R],\ 1 \rfloor \tag{3.19}$$

with [R] matrix defined as

$$\underset{3X3}{[R]} = \begin{bmatrix} 1 & 0 & 0 \\ 0 & R_{11} & R_{12} \\ 0 & R_{21} & R_{22} \end{bmatrix} \tag{3.20}$$

where $R_{11}, \ldots, R_{22}$ are defined by Eqs. (3.4). The vector $\{V_i\}$ in Eq. (3.18) is defined below:

$$\underset{10X1}{\{V_i\}} = \left\lfloor (v_i)_1,\ \left(\frac{\partial v_i}{\partial \alpha}\right)_1,\ \left(\frac{\partial v_i}{\partial \beta}\right)_1,\ \ldots,\ \left(\frac{\partial v_i}{\partial \beta}\right)_3,\ (v_i)_G \right\rfloor^T \tag{3.21}$$

For a given set of values of the nodal degrees of freedom, $\{V_i\}$, we can obtain the corresponding set of the generalized displacements, $\{a\}$, by use of Eq. (3.16). The displacement component, v_i, and its derivatives at any point (ξ,η) within the element are obtained directly using Eq. (3.9). This method of computation is convenient

for the numerical implementation of the various constraints to be discussed later in detail.

By combining Eq. (3.10) and Eq. (3.16) we can also obtain the shape function representation for the displacement component v_i in the form

$$v_i = \lfloor N \rfloor \{V_i\} \tag{3.22}$$

where the row vector of shape functions is obtained as

$$\underset{1X10}{\lfloor N \rfloor} = \lfloor f(\xi,\eta) \rfloor [S] \tag{3.23}$$

3.2.2 Interpolation of Rotation Components

Each of the cartesian components of the rotation vector is assumed as a complete quadratic polynomial in the ξ-η coordinates. The rotation components are denoted as β_x, β_y and β_z which are positive in the right hand sense as shown in Figure 4a. Thus, typically,

$$\beta_x = b_1 + b_2\xi + b_3\eta + b_4\xi^2 + b_5\xi\eta + b_6\eta^2 \tag{3.24}$$

The generalized displacements $b_1, b_2, \ldots, b_6$ are eliminated in favor of the nodal values of β_x at the corner nodes and three mid-side nodes. Thus we obtain

$$\beta_x = \lfloor N' \rfloor \{\beta_x\} \tag{3.25}$$

where

$$\underset{6X1}{\{\beta_x\}} = \lfloor (\beta_x)_1, (\beta_x)_2, \ldots, (\beta_x)_6 \rfloor^T \tag{3.26}$$

$$\underset{1X6}{\lfloor N' \rfloor} = \lfloor N'_1, N'_2, \ldots, N'_6 \rfloor \tag{3.27}$$

where the shape functions, N_i' (i = 1,6), are listed below

$$N_1' = 2(1 - \xi - \eta)(\frac{1}{2} - \xi - \eta)$$

$$N_2' = \xi(2\xi - 1)$$

$$N_3' = \eta(2\eta - 1)$$

$$N_4' = 4\xi\eta \qquad (3.28a\text{-}f)$$

$$N_5' = 4\eta(1 - \xi - \eta)$$

$$N_6' = 4\xi(1 - \xi - \eta)$$

The β_y and β_z components are also interpolated by the same set of shape functions.

It may be noted that the above interpolations for the displacement and rotation components are C^o-continuous across the interelement boundaries. Since the highest order of the derivative of the displacements and rotations that occur in the element strain energy expression is one, the interpolation is conforming for displacements.

3.3 Isoparametric Representation of the Element Geometry

The geometry of the middle surface is described by the position vector and its derivatives up to second order at the corner nodes of the triangle. In the case of shells with regular geometry, the above nodal values are obtained from the parametric equations of the middle surface. But in the case of shells with arbitrary geometry, one has to take recourse to one of the mathematical surface

representation techniques, and obtain the above quantities numerically. However, in both the cases, the geometric quantities within the element are obtained by interpolating the position vector from the nodal value of the latter and its first order derivatives using the same set of shape functions as those used for the displacements. Thus the components of the position vector at any point within the element are obtained as

$$x(\xi,\eta) = \lfloor N(\xi,\eta) \rfloor \{x\} \tag{3.29}$$

$$y(\xi,\eta) = \lfloor N(\xi,\eta) \rfloor \{y\} \tag{3.30}$$

$$z(\xi,\eta) = \lfloor N(\xi,\eta) \rfloor \{z\} \tag{3.31}$$

where x, y, z are the cartesian components of the position vector to any point (ξ,η) within the element as indicated in Eq. (3.1); and the row vector of shape functions is defined in Eq. (3.23). Also, we have the definitions:

$$\{x\} = \left\lfloor (x)_1, \left(\frac{\partial x}{\partial \alpha}\right)_1, \left(\frac{\partial x}{\partial \beta}\right)_1, \ldots, \left(\frac{\partial x}{\partial \beta}\right)_3, (x)_G \right\rfloor^T \tag{3.32}$$

$$\{y\} = \left\lfloor (y)_1, \left(\frac{\partial y}{\partial \alpha}\right)_1, \left(\frac{\partial y}{\partial \beta}\right)_1, \ldots, \left(\frac{\partial y}{\partial \beta}\right)_3, (y)_G \right\rfloor^T \tag{3.33}$$

$$\{z\} = \left\lfloor (z)_1, \left(\frac{\partial z}{\partial \alpha}\right)_1, \left(\frac{\partial z}{\partial \beta}\right)_1, \ldots, \left(\frac{\partial z}{\partial \beta}\right)_3, (z)_G \right\rfloor^T \tag{3.34}$$

where the suffix following the parentheses indicates the node number or the centroid of the element at which the quantity is evaluated.

It may be noted that the cubic interpolation used in the representation of the middle surface within the element is C^1-continuous at the element nodes, but is only C^o-continuous across

the interelement boundaries. It has been shown by Ciarlet [77] that no higher order continuity is required to be satisfied for the element to be "conforming for geometry"; and, mathematically, C^o-continuity is sufficient to provide the "geometric conformity." Thus the element is conforming both for the displacements as well as for the geometry.

The isoparametric interpolation of the element geometry leads to an exact representation of the rigid body modes of the shell. To prove this consider a linearized rigid body displacement in the form

$$v_1^* = a_0 + a_1 x + a_2 y + a_3 z \tag{3.35a}$$

$$v_2^* = b_0 + b_1 x + b_2 y + b_3 z \tag{3.35b}$$

$$v_3^* = c_0 + c_1 x + c_2 y + c_3 z \tag{3.35c}$$

In view of Eqns. (3.29)-(3.31), Eq. (3.35a) can be written as

$$v_1^* = a_0 + a_1 \lfloor N \rfloor \{x\} + a_2 \lfloor N \rfloor \{y\} + a_3 \lfloor N \rfloor \{z\} \tag{3.36}$$

The row vector $\lfloor N \rfloor$ may be considered as an assemblage of sub-vectors, partitioned according to the nodes as

$$\underset{1X12}{N} = \left\lfloor \lfloor N_{(1)} \rfloor, \lfloor N_{(2)} \rfloor, \lfloor N_{(3)} \rfloor, \lfloor N_{(4)} \rfloor \right\rfloor \tag{3.37}$$

where the corner nodes are represented by the suffixes 1 to 3, and the centroid by the suffix 4. Each sub-vector is of length 3, the last two elements of $\lfloor N_{(4)} \rfloor$ are null. The column vectors $\{x\}$, $\{y\}$ and $\{z\}$ are considered to be partitioned in the same manner. Using this notation, Eq. (3.36) can be written as

$$v_1^* = a_o + \sum_{i=1}^{4} [a_1 \lfloor N_{(i)} \rfloor \{x_{(i)}\} + a_2 \lfloor N_{(i)} \rfloor \{y_{(i)}\} + a_3 \lfloor N_i \rfloor \{z_i\}] \quad (3.38)$$

If we define the vector $\{\alpha\}$ as

$$\{\alpha\} = \lfloor 1, 0, 0 \rfloor^T \quad (3.39)$$

from Eq. (3.23) and Eq. (3.17) it follows that

$$\sum_{i=1}^{4} \lfloor N_{(i)} \rfloor \{\alpha\} = 1 \quad (3.40)$$

In view of Eq. (3.40), Eq. (3.38) can be written as

$$v_1^* = \sum_{i=1}^{4} \lfloor N_{(i)} \rfloor [a_o\{\alpha\} + a_1\{x_{(i)}\} + a_2\{y_{(i)}\} + a_3\{z_{(i)}\}] \quad (3.41)$$

$$v_1^* = \sum_{i=1}^{4} \lfloor N_{(i)} \rfloor \{v_{1(i)}^*\} \quad (3.42)$$

where $\{v_{1(i)}^*\}$ is the column vector of displacement degrees of freedom at the ith node corresponding to the linearized rigid body displacement of Eq. (3.35a). This follows by comparing Eq. (3.35a) and the term in the brackets in Eq. (3.41). But Eq. (3.42) is exactly of the form as Eq. (3.22). Similarly, the exact representation of the displacement components v_2^* and v_3^* follows.

It is thus established that the above interpolation scheme for the displacements, and the isoparametric representation of the shell middle surface results in a conforming element with explicit representation of the rigid body modes.

In the next section, we consider the strain energy in the finite element.

3.4 Element Strain Energy

The total strain energy in the shell is expressed as the sum of the strain energies in the individual finite elements into which the shell is divided. An expression for the strain energy of the laminated composite shell was derived in Section 2.4 based on the linear shear deformation theory, using tensorial notation. Here, the details of the discretization of the strain energy are presented in matrix notation.

It may be observed from Eq. (2.126) that the strain energy in the shell is expressed as the sum of the energies associated with the stretching and bending of the shell and that due to transverse shear deformation. In the case of thin shells, the contribution of the transverse shear strain energy to the total strain energy is negligible when compared to that due to stretching and bending of the shell. Also, as our objective is to achieve a solution converging to the thin-shell solution, the transverse shear energy is subsequently neglected.

When the transverse shear energy is neglected, and with symmetry of the lamina constitutive tensors, the strain energy density per unit area of the undeformed middle surface, Eq. (2.126), can be written in the form

$$u_s = \frac{1}{2} \left[\lfloor \gamma \rfloor [A] \{\gamma\} + 2 \lfloor \gamma \rfloor [B] \{\chi\} + \lfloor \chi \rfloor [D] \{\chi\} \right] \tag{3.43}$$

where

$$\lfloor \gamma \rfloor = \lfloor \gamma_{11}, \gamma_{22}, \gamma_{12} \rfloor \tag{3.44}$$

$$\lfloor \chi \rfloor = \lfloor \chi_{11}, \chi_{22}, \chi_{12} \rfloor \tag{3.45}$$

and the matrices [A], [B], and [D] are formed by the components of the tensors $A^{\alpha\beta\gamma\eta}$, $B^{\alpha\beta\gamma\eta}$ and $D^{\alpha\beta\gamma\eta}$, respectively, defined by Eqs. (2.127). Typically we have

$$[A] = \begin{pmatrix} A^{1111} & A^{1122} & 2A^{1112} \\ A^{2211} & A^{2222} & 2A^{2212} \\ 2A^{1211} & 2A^{1222} & 4A^{1212} \end{pmatrix} \tag{3.46}$$

The elements of the strain vectors in Eqs. (3.44)-(3.45) are given by Eq. (2.72) and Eq. (2.83) in the indicial notation. With the conventional notations for the displacement and rotation components of the present chapter, and after carrying out the expansions of the dummy indices, the above equations are as found below.

Membrane Strains:

$$\gamma_{11} = \frac{\partial x}{\partial \alpha}\frac{\partial v_1}{\partial \alpha} + \frac{\partial y}{\partial \alpha}\frac{\partial v_2}{\partial \alpha} + \frac{\partial z}{\partial \alpha}\frac{\partial v_3}{\partial \alpha} \tag{3.46a}$$

$$\gamma_{22} = \frac{\partial x}{\partial \beta}\frac{\partial v_1}{\partial \beta} + \frac{\partial y}{\partial \beta}\frac{\partial v_2}{\partial \beta} + \frac{\partial z}{\partial \beta}\frac{\partial v_3}{\partial \beta} \tag{3.46b}$$

$$\gamma_{12} = \frac{1}{2}\left(\frac{\partial x}{\partial \alpha}\frac{\partial v_1}{\partial \beta} + \frac{\partial y}{\partial \alpha}\frac{\partial v_2}{\partial \beta} + \frac{\partial z}{\partial \alpha}\frac{\partial v_3}{\partial \beta}\right.$$

$$\left. + \frac{\partial x}{\partial \beta}\frac{\partial v_1}{\partial \alpha} + \frac{\partial y}{\partial \beta}\frac{\partial v_2}{\partial \alpha} + \frac{\partial z}{\partial \beta}\frac{\partial v_3}{\partial \alpha}\right) \tag{3.46c}$$

Curvature Changes:

$$\chi_{11} = -(c_1 \frac{\partial z}{\partial \alpha} - c_2 \frac{\partial y}{\partial \alpha})\beta_x - (c_2 \frac{\partial x}{\partial \alpha} - c_3 \frac{\partial z}{\partial \alpha})\beta_y$$

$$- (c_3 \frac{\partial y}{\partial \alpha} - c_1 \frac{\partial x}{\partial \alpha})\beta_z + a_1 \frac{\partial \beta_x}{\partial \alpha} + a_2 \frac{\partial \beta_y}{\partial \alpha} + a_3 \frac{\partial \beta_z}{\partial \alpha}$$

$$- (c_3 \frac{\partial v_1}{\partial \alpha} + c_1 \frac{\partial v_2}{\partial \alpha} + c_2 \frac{\partial v_3}{\partial \alpha}) \qquad (3.47a)$$

$$\chi_{22} = - (d_1 \frac{\partial z}{\partial \beta} - d_2 \frac{\partial y}{\partial \beta})\beta_x - (d_2 \frac{\partial x}{\partial \beta} - d_3 \frac{\partial z}{\partial \beta})\beta_y$$

$$- (d_3 \frac{\partial y}{\partial \beta} - d_1 \frac{\partial x}{\partial \beta})\beta_z + b_1 \frac{\partial \beta_x}{\partial \beta} + b_2 \frac{\partial \beta_y}{\partial \beta} + b_3 \frac{\partial \beta_z}{\partial \beta}$$

$$- (d_3 \frac{\partial v_1}{\partial \beta} + d_1 \frac{\partial v_2}{\partial \beta} + d_2 \frac{\partial v_3}{\partial \beta}) \qquad (3.47b)$$

$$\chi_{12} = \frac{1}{2} [-(c_1 \frac{\partial z}{\partial \beta} - c_2 \frac{\partial y}{\partial \beta})\beta_x - (c_2 \frac{\partial x}{\partial \beta} - c_3 \frac{\partial z}{\partial \beta})\beta_y$$

$$- (c_3 \frac{\partial y}{\partial \beta} - c_1 \frac{\partial x}{\partial \beta})\beta_z - (d_1 \frac{\partial z}{\partial \alpha} - d_2 \frac{\partial y}{\partial \alpha})\beta_x$$

$$- (d_2 \frac{\partial x}{\partial \alpha} - d_3 \frac{\partial z}{\partial \alpha})\beta_y - (d_3 \frac{\partial y}{\partial \alpha} - d_1 \frac{\partial x}{\partial \alpha})\beta_z$$

$$+ a_1 \frac{\partial \beta_x}{\partial \beta} + a_2 \frac{\partial \beta_y}{\partial \beta} + a_3 \frac{\partial \beta_z}{\partial \beta} + b_1 \frac{\partial \beta_x}{\partial \alpha} + b_2 \frac{\partial \beta_y}{\partial \alpha} + b_3 \frac{\partial \beta_z}{\partial \alpha}$$

$$- (c_3 \frac{\partial v_1}{\partial \beta} + c_1 \frac{\partial v_2}{\partial \beta} + c_2 \frac{\partial v_3}{\partial \beta} + d_3 \frac{\partial v_1}{\partial \alpha} + d_1 \frac{\partial v_2}{\partial \alpha} + d_2 \frac{\partial v_3}{\partial \alpha})] \qquad (3.47c)$$

where

$$a_1 = n_2 \frac{\partial z}{\partial \alpha} - n_3 \frac{\partial y}{\partial \alpha} \ , \ a_2 = n_3 \frac{\partial x}{\partial \alpha} - n_1 \frac{\partial z}{\partial \alpha} \ , \ a_3 = n_1 \frac{\partial y}{\partial \alpha} - n_2 \frac{\partial x}{\partial \alpha} \qquad (3.48a)$$

$$b_1 = n_2 \frac{\partial z}{\partial \beta} - n_3 \frac{\partial y}{\partial \beta} \ , \ b_2 = n_3 \frac{\partial x}{\partial \beta} - n_1 \frac{\partial z}{\partial \beta} \ , \ b_3 = n_1 \frac{\partial y}{\partial \beta} - n_2 \frac{\partial x}{\partial \beta} \tag{3.48b}$$

$$c_1 = b_1^1 \frac{\partial y}{\partial \alpha} + b_1^2 \frac{\partial y}{\partial \beta} \ , \ c_2 = b_1^1 \frac{\partial z}{\partial \alpha} + b_1^2 \frac{\partial z}{\partial \beta} \ , \ c_3 = b_1^1 \frac{\partial x}{\partial \alpha} + b_1^2 \frac{\partial x}{\partial \beta} \tag{3.48c}$$

$$d_1 = b_2^1 \frac{\partial y}{\partial \alpha} + b_2^2 \frac{\partial y}{\partial \beta} \ , \ d_2 = b_2^1 \frac{\partial z}{\partial \alpha} + b_2^2 \frac{\partial z}{\partial \beta} \ , \ d_3 = b_2^1 \frac{\partial x}{\partial \alpha} + b_2^2 \frac{\partial x}{\partial \beta} \tag{3.48d}$$

In the above equations, n_i $(i = 1,3)$ are the components of the surface unit normal vector, and b_α^β $(\alpha,\beta = 1,2)$ are the mixed variant components of the curvature tensor, defined by Eq. (2.23). Equations (3.46) and Eqs. (3.47) can be put in the matrix notation as

$$\{\gamma\} = [L_1]\{v\} \tag{3.49}$$

$$\{\chi\} = [L_2]\{v\} + [L_3]\{\beta\} \tag{3.50}$$

where

$$\underset{6X1}{\{v\}} = \left[\frac{\partial v_1}{\partial \alpha} \ , \ \frac{\partial v_2}{\partial \alpha} \ , \ \frac{\partial v_3}{\partial \alpha} \ , \ \frac{\partial v_1}{\partial \beta} \ , \ \frac{\partial v_2}{\partial \beta} \ , \ \frac{\partial v_3}{\partial \beta}\right]^T \tag{3.51}$$

$$\underset{9X1}{\{\beta\}} = \left[\beta_x, \ \beta_y, \ \beta_z, \ \frac{\partial \beta_x}{\partial \alpha} \ , \ \frac{\partial \beta_y}{\partial \alpha} \ , \ \frac{\partial \beta_z}{\partial \alpha} \ , \ \frac{\partial \beta_x}{\partial \beta} \ , \ \frac{\partial \beta_y}{\partial \beta} \ , \ \frac{\partial \beta_z}{\partial \beta}\right]^T \tag{3.52}$$

$$[L_1] \begin{pmatrix} \partial x/\partial\alpha & \partial y/\partial\alpha & \partial z/\partial\alpha & 0 & 0 & 0 \\ 0 & 0 & 0 & \partial x/\partial\beta & \partial y/\partial\beta & \partial z/\partial\beta \\ \frac{1}{2}\partial x/\partial\beta & \frac{1}{2}\partial y/\partial\beta & \frac{1}{2}\partial z/\partial\beta & \frac{1}{2}\partial x/\partial\alpha & \frac{1}{2}\partial y/\partial\alpha & \frac{1}{2}\partial z/\partial\alpha \end{pmatrix} \tag{3.53}$$

$$[L_2]_{3X6} = \begin{pmatrix} -c_3 & -c_1 & -c_2 & 0 & 0 & 0 \\ 0 & 0 & 0 & -d_3 & -d_1 & -d_2 \\ -\frac{1}{2}d_3 & -\frac{1}{2}d_1 & -\frac{1}{2}d_2 & -\frac{1}{2}c_3 & -\frac{1}{2}c_1 & -\frac{1}{2}c_2 \end{pmatrix} \tag{3.54}$$

$$[L_3]_{3X9} = \begin{pmatrix} -(c_1\frac{\partial z}{\partial\alpha} - c_2\frac{\partial y}{\partial\alpha}) & -(c_2\frac{\partial x}{\partial\alpha} - c_3\frac{\partial z}{\partial\alpha}) & -(c_3\frac{\partial y}{\partial\alpha} - c_1\frac{\partial x}{\partial\alpha}) & a_1 & a_2 & a_3 & 0 & 0 & 0 \\ -(d_1\frac{\partial z}{\partial\beta} - d_2\frac{\partial y}{\partial\beta}) & -(d_2\frac{\partial x}{\partial\beta} - d_3\frac{\partial z}{\partial\beta}) & -(d_3\frac{\partial y}{\partial\beta} - d_1\frac{\partial x}{\partial\beta}) & 0 & 0 & 0 & b_1 & b_2 & b_3 \\ -\frac{1}{2}(c_1\frac{\partial z}{\partial\beta} - c_2\frac{\partial y}{\partial\beta}) & -\frac{1}{2}(c_2\frac{\partial x}{\partial\beta} - c_3\frac{\partial z}{\partial\beta}) & -\frac{1}{2}(c_3\frac{\partial y}{\partial\beta} - c_1\frac{\partial x}{\partial\beta}) & \frac{b_1}{2} & \frac{b_2}{2} & \frac{b_3}{2} & \frac{a_1}{2} & \frac{a_2}{2} & \frac{a_3}{2} \\ +d_1\frac{\partial z}{\partial\alpha} - d_2\frac{\partial y}{\partial\alpha}) & +d_2\frac{\partial x}{\partial\alpha} - d_3\frac{\partial z}{\partial\alpha}) & +d_3\frac{\partial y}{\partial\alpha} - d_1\frac{\partial x}{\partial\alpha}) & & & & & & \end{pmatrix} \tag{3.55}$$

The use of finite element representations for the displacement and rotation components, Eq. (3.22) and Eq. (3.25), in Eqs. (3.49)-(3.50), leads to the strain-nodal degrees of freedom relations in the form:

$$\{\gamma\} = [L_1][B_1]\{V_{(T)}\} \tag{3.56}$$

$$\{\chi\} = [L_2][B_1]\{V_{(T)}\} + [L_3][B_2]\{V_{(R)}\} \tag{3.57}$$

where $\{V_{(T)}\}$ and $\{V_{(R)}\}$ are ensembles of vectors of translational and rotational degrees of freedom of the element, defined as

$$\underset{30X1}{\{V_{(T)}\}} = \left\lfloor \lfloor V_1 \rfloor, \lfloor V_2 \rfloor, \lfloor V_3 \rfloor \right\rfloor^T \tag{3.58}$$

$$\underset{18X1}{\{V_{(R)}\}} = \left\lfloor \lfloor \beta_x \rfloor, \lfloor \beta_y \rfloor, \lfloor \beta_z \rfloor \right\rfloor^T \tag{3.59}$$

where the sub-vectors in Eqs. (3.58)-(3.59) are defined in Eq. (3.21) and Eq. (3.26). The matrices $[B_1]$ and $[B_2]$ are defined in terms of the shape-function vectors of Eqs. (3.23) and (3.25) as found below.

$$\underset{6X30}{[B_1]} = \begin{pmatrix} \lfloor N,\alpha \rfloor & \lfloor 0 \rfloor & \lfloor 0 \rfloor \\ \lfloor 0 \rfloor & \lfloor N,\alpha \rfloor & \lfloor 0 \rfloor \\ \lfloor 0 \rfloor & \lfloor 0 \rfloor & \lfloor N,\alpha \rfloor \\ \lfloor N,\beta \rfloor & \lfloor 0 \rfloor & \lfloor 0 \rfloor \\ \lfloor 0 \rfloor & \lfloor N,\beta \rfloor & \lfloor 0 \rfloor \\ \lfloor 0 \rfloor & \lfloor 0 \rfloor & \lfloor N,\beta \rfloor \end{pmatrix} \tag{3.60}$$

and

$$[B_2]_{9X18} = \begin{pmatrix} \lfloor N' \rfloor & \lfloor 0 \rfloor & \lfloor 0 \rfloor \\ \lfloor 0 \rfloor & \lfloor N' \rfloor & \lfloor 0 \rfloor \\ \lfloor 0 \rfloor & \lfloor 0 \rfloor & \lfloor N' \rfloor \\ \lfloor N', \alpha \rfloor & \lfloor 0 \rfloor & \lfloor 0 \rfloor \\ \lfloor 0 \rfloor & \lfloor N', \alpha \rfloor & \lfloor 0 \rfloor \\ \lfloor 0 \rfloor & \lfloor 0 \rfloor & \lfloor N', \alpha \rfloor \\ \lfloor N', \beta \rfloor & \lfloor 0 \rfloor & \lfloor 0 \rfloor \\ \lfloor 0 \rfloor & \lfloor N', \beta \rfloor & \lfloor 0 \rfloor \\ \lfloor 0 \rfloor & \lfloor 0 \rfloor & \lfloor N', \beta \rfloor \end{pmatrix} \tag{3.61}$$

where the notation $\lfloor N, \alpha \rfloor$ stands for $\frac{\partial}{\partial \alpha} \lfloor N \rfloor$, and $\lfloor 0 \rfloor$ is a null vector of appropriate size (1X10 or 1X6).

The total strain energy in the element is obtained by integrating the strain energy density per unit area of the reference surface, Eq. (3.43), over the area of the element.

$$U^{(e)} = \int u_s \sqrt{a}\, d\alpha d\beta \tag{3.62}$$

where a is the determinant of the covariant metric tensor defined by Eq. (2.15). In view of Eqs. (3.56)-(3.57), it is seen that the strain energy of an element can be expressed as a quadratic form in terms of the 48 nodal degrees of freedom contained in the vectors $\{V_{(T)}\}$ and $\{V_{(R)}\}$.

Thus, the use of shear deformation theory has led to a conforming element with the use of simple polynomial shape functions. However, the use of independent assumptions for the displacement and

rotation components renders the element unduly stiff if the material resists the transverse shear strains inherent in the latter displacement representation. This also results in a slow convergence rate, and the thin-shell solution is achieved only in the convergence limit. It is desirable to alleviate the effects of the transverse shear deformation to achieve fast convergence to the thin-shell solution.

The first step toward minimizing the effects of the transverse shear deformation has already been taken in neglecting the transverse shear energy. To reduce the effects further, the constraints analogous to the Kirchhoff hypothesis are imposed at a discrete number of points on the element boundary. These constraints will be subsequently referred to as "Discrete Kirchhoff Constraints" (DKC).

It is also observed that the independent assumptions for the displacement and rotation components leaves the rotation of the shell about the surface normal doubly defined. One value is defined in terms of the displacement gradients, as derived in Eq. (2.91). A second value results from the independent rotation components. Six constraints representing the equality of these two values are imposed, one at each of the corner and mid-side nodes. These constraints will be referred to as "Surface Normal Rotation Constraints" (SNRC).

From the computational point of view, the mid-side nodes are undesirable. To that end, the rotation degrees of freedom at the mid-side nodes are eliminated by imposing a linear variation of the normal rotation along the element sides. These constraints will be referred to as "Linear Variation of Normal Rotation Constraints" (LVNRC).

The mathematical details of the above constraints are discussed in detail in the next section.

3.5 Constraint Conditions

3.5.1 Discrete Kirchhoff Constraints (DKC)

Discrete Kirchhoff constraints are the conditions of the vanishing of the transverse shear strains at discrete number of points on the boundary of the element. Six of these constraints at the corner nodes, and three at the mid-side nodes are imposed.

To derive the DKC at the corner nodes, consider the transverse shear strain components given by Eq. (2.86). In the notations of the present chapter, and after expanding the dummy indices, Eq. (2.86) becomes

$$2\gamma_{\lambda 3} = (\beta_y n_3 - \beta_z n_2)x_{,\lambda} + (\beta_z n_1 - \beta_x n_3)y_{,\lambda} + (\beta_x n_2 - \beta_y n_1)z_{,\lambda} + n_1 v_{1,\lambda} + n_2 v_{2,\lambda} + n_3 v_{3,\lambda} \qquad (3.63)$$

$$(\lambda = 1,2)$$

where $\lambda = 1,2$ corresponds to the coordinate directions α and β respectively; n_i $(i = 1,3)$ are the components of the unit normal vector to the middle surface. The six DKC at the corner nodes are given by the conditions

$$(\gamma_{\lambda 3})_j = 0 \quad j = 1,2,3 \quad \lambda = 1,2 \qquad (3.64)$$

where the suffix j indicates that the strain is evaluated at the jth corner node. Using Eq. (3.63), Eq. (3.64) takes the form

$$(\beta_{yj}n_{3j} - \beta_{zj}n_{2j})x_{,\lambda j} + (\beta_{zj}n_{1j} - \beta_{xj}n_{3j})y_{,\lambda j}$$

$$+ (\beta_{xj}n_{2j} - \beta_{yj}n_{1j})z_{,\lambda j} + n_{1j}v_{1,\lambda j} + n_{2j}v_{2,\lambda j} + n_{3j}v_{3,\lambda j} = 0 \tag{3.65}$$

$$j = 1,2,3 \quad \lambda = 1,2$$

where $\beta_{yj} = (\beta_y)_j$ and $x_{,\alpha j} = (\frac{\partial x}{\partial \alpha})_j$ etc.

To derive the DKC at the mid-side nodes, we have to obtain the equation for the transverse shear strain between the normal direction and the direction, s, along curvilinear edge of the element. Such an expression is easily obtained by observing that the sides of the unit triangle in the ξ-η natural coordinate plane is mapped onto the corresponding curvilinear sides of the element in the Euclidian space, as shown in Figure 4. Thus, we can consider (ξ-η) coordinates as an alternative set of parameters, and obtain the transverse shear components along the element sides by a second-order tensor transformation law. Consider the curvilinear side 12, which corresponds to the ξ-line (η = const). If we denote the transverse shear component (tensorial) along the ξ-direction as $\bar{\gamma}_{\xi 3}$, then we can write

$$\bar{\gamma}_{\xi 3} = \frac{\partial \theta^{\lambda}}{\partial \xi} \gamma_{\lambda 3} \qquad \text{sum on } \lambda, \ (\lambda = 1,2) \tag{3.66}$$

where θ^1 and θ^2 correspond to α and β directions. In view of Eqs. (3.2), after carrying out the summation, Eq. (3.66) can be written as

$$\bar{\gamma}_{\xi 3} = (\alpha_2 - \alpha_1)\gamma_{13} + (\beta_2 - \beta_1)\gamma_{23} \tag{3.67}$$

Equation (3.67) can be generalized to all the three sides. If s denotes the curvilinear direction through the nodes i-j of the

triangle, then we can write

$$\bar{\gamma}_{s3} = (\alpha_j - \alpha_i)\gamma_{13} + (\beta_j - \beta_i)\gamma_{23} \tag{3.68a}$$

or

$$\bar{\gamma}_{s3} = \alpha_{ji}\gamma_{13} + \beta_{ji}\gamma_{23} \tag{3.68b}$$

The three DKC at the mid-side nodes are given by the conditions

$$(\bar{\gamma}_{s3})_k = 0 \qquad k = 4,5,6 \tag{3.69}$$

where k is the mid-side node on the side passing through the corner nodes i and j. In view of Eq. (3.68b), we obtain the DKC at the mid-side nodes as

$$\alpha_{ji}(\gamma_{13})_k + \beta_{ji}(\gamma_{23})_k = 0 \qquad k = 4,5,6 \tag{3.70}$$

where $\gamma_{\lambda 3}$ ($\lambda = 1,2$), is defined in Eq. (3.63).

3.5.2 Surface Normal Rotation Constraints (SNRC)

The SNRC express the condition of the equality of the two values of the shell rotation about the surface normal, which has been doubly defined. The first value is defined in terms of the displacement gradients, as given by Eq. (2.91). In the notations of the present chapter, the first value is given by

$$\Omega^{(1)} = \frac{1}{2\sqrt{a}}\left[(x_{,\beta}v_{1,\alpha} - x_{,\alpha}v_{1,\beta}) + (y_{,\beta}v_{2,\alpha} - y_{,\alpha}v_{2,\beta})\right.$$
$$\left. + (z_{,\beta}v_{3,\alpha} - z_{,\alpha}v_{3,\beta})\right] \tag{3.71}$$

A second value for the rotation is defined in terms of the independent rotations:

$$\Omega^{(2)} = n_1\beta_x + n_2\beta_y + n_3\beta_z \tag{3.72}$$

Six SNRC are obtained by equating the two values of Ω at the six nodes of the element. Thus

$$n_{1j}\beta_{xj} + n_{2j}\beta_{yj} + n_{3j}\beta_{zj} = \Omega^{(1)}_j \tag{3.73}$$

$$j = 1,2, \ldots, 6$$

3.5.3 Linear Variation of Normal Rotation Constraints (LVNRC)

The rotation degrees of freedom at the mid-side nodes are eliminated by imposing a linear variation of the normal rotation along the element sides, leading to three more constraints. If β_s denotes the component of the rotation vector along the tangent to the curvilinear side of the element, the LVNRC are given by the equation

$$\beta_{sk} = \frac{1}{2}(\beta_{si} + \beta_{sj}) \tag{3.74}$$

where k is the mid-node on the side joining the corner nodes i,j. When expressed in terms of the components of the rotation vector, Eq. (3.74) takes the form

$$s_{1k}\beta_{xk} + s_{2k}\beta_{yk} + s_{3k}\beta_{zk} = \frac{s_{1k}}{2}(\beta_{xi} + \beta_{xj})$$

$$+ \frac{s_{2k}}{2}(\beta_{yi} + \beta_{yj}) + \frac{s_{3k}}{2}(\beta_{zi} + \beta_{zj}) \tag{3.75}$$

$$i,j = 1,2,3 \quad k = 4,5,6$$

where s_{1k}, s_{2k} and s_{3k} are the components of the unit tangent vector to the curvilinear edge at its mid-side node k. The equation of the tangent vector is derived below.

The parametric equation of the curvilinear edge passing through the corner nodes i,j, can be expressed in terms of the parameter ξ, and the α-β coordinates of the corner nodes:

$$\bar{R}(\xi) = x(\alpha,\beta)\hat{e}_1 + y(\alpha,\beta)\hat{e}_2 + z(\alpha,\beta)\hat{e}_3 \tag{3.76}$$

where the curvilinear coordinates (α,β) to any point on the curve is given in terms of the parameter ξ as

$$\alpha = \alpha_i + (\alpha_j - \alpha_i)\xi \tag{3.77a}$$

$$\beta = \beta_i + (\beta_j - \beta_i)\xi \tag{3.77b}$$

The tangent vector to the curve of Eq. (3.76) is

$$\bar{s} = \frac{\partial \bar{R}}{\partial \xi} = \frac{\partial \bar{R}}{\partial \alpha}\frac{\partial \alpha}{\partial \xi} + \frac{\partial \bar{R}}{\partial \beta}\frac{\partial \beta}{\partial \xi} \tag{3.78}$$

Using Eqs. (3.76) and (3.77)

$$\bar{s} = (\alpha_{ji}x_{,\alpha} + \beta_{ji}x_{,\beta})\hat{e}_1 + (\alpha_{ji}y_{,\alpha} + \beta_{ji}y_{,\beta})\hat{e}_2 + (\alpha_{ji}z_{,\alpha} + \beta_{ji}z_{,\beta})\hat{e}_3 \tag{3.79a}$$

The unit vector along $\bar{s}$ follows from Eq. (3.79):

$$\hat{s} = s_1\hat{e}_1 + s_2\hat{e}_2 + s_3\hat{e}_3 \tag{3.79b}$$

All of the 18 constraint conditions derived so far can be conveniently summarized as sets of linear algebraic equations for the

components of the rotation vector at each of the corner and mid-side nodes.

At the corner nodes j = 1,2,3

$$[C_1^{(j)}]\{\beta_1^{(j)}\} = \{R_1^{(j)}\} \tag{3.80}$$

At the mid-side nodes k = 4,5,6

$$[C_2^{(k)}]\{\beta_1^{(k)}\} = \{R_2^{(k)}\} \tag{3.81}$$

where the superscript indicates the node at which the matrix or the vector is evaluated. Also

$$\{\beta_1\} = \lfloor \beta_x, \ \beta_y, \ \beta_z \rfloor^T \tag{3.82}$$

$$[C_1]_{3X3} = \begin{pmatrix} a_1 & a_2 & a_3 \\ b_1 & b_2 & b_3 \\ n_1 & n_2 & n_3 \end{pmatrix} \tag{3.83a}$$

$$[C_2]_{3X3} \begin{pmatrix} \alpha_{ji}a_1 + \beta_{ji}b_1 & \alpha_{ji}a_2 + \beta_{ji}b_2 & \alpha_{ji}a_3 + \beta_{ji}b_3 \\ n_1 & n_2 & n_3 \\ s_1 & s_2 & s_3 \end{pmatrix} \tag{3.83b}$$

$$\{R_1\} = \lfloor f_1, \ f_2, \ \Omega^{(1)} \rfloor^T \tag{3.84}$$

$$\{R_2\} = \lfloor \alpha_{ji} f_1 + \beta_{ji} f_2 \qquad \Omega^{(1)} \qquad s_1\beta_{xm} + s_2\beta_{ym} + s_3\beta_{zm} \rfloor^T \tag{3.85}$$

where a_i and b_i (i = 1,2,3) are defined in Eqs. (3.48), and $\Omega^{(1)}$ in Eq. (3.71). Also, β_{xm}, β_{ym} and β_{zm} stand for the mean value of the corresponding corner values. Typically

$$\beta_{xm} = \frac{1}{2}(\beta_{xi} + \beta_{xj}) \tag{3.86}$$

Also

$$f_1 = -(n_1 v_{1,\alpha} + n_2 v_{2,\alpha} + n_3 v_{3,\alpha}) \tag{3.87a}$$

$$f_2 = -(n_1 v_{1,\beta} + n_2 v_{2,\beta} + n_3 v_{3,\beta}) \tag{3.87b}$$

It is observed that the rotation degrees of freedom at any of the nodes can be expressed in terms of the displacement degrees of freedom at the corner nodes by solution of Eqs. (3.80) at the corner nodes followed by that of Eqs. (3.81) at the mid-side nodes. Thus, we can eliminate the rotation degrees of freedom, leading to a finite element with a total of 30 degrees of freedom of the vector $\{V_{(T)}\}$, consisting of the values of the displacements and their derivatives at the corner nodes and the centroidal displacements. The imposition of the constraint conditions not only results in an improved performance of the element, but also helps to reduce the number of element degrees of freedom leading to lower computational costs.

3.6 Calculation of Element Matrices

3.6.1 The Element Stiffness Matrix and Load Vector

The element stiffness matrix and the load vector are obtained by use of the principle of minimum potential energy. The total potential energy in an element is

$$\Pi_p^{(e)} = U^{(e)} + H^{(e)} \tag{3.88}$$

where $U^{(e)}$ is the element strain energy given by Eq. (3.62), and $H^{(e)}$ is the potential energy of the external loads. If the components of the external distributed loading in the cartesian directions are denoted as p_i $(i = 1,2,3)$, then

$$H^{(e)} = - \int_{\text{Area}} (p_1 v_1 + p_2 v_2 + p_3 v_3)\sqrt{a}\, d\alpha d\beta \tag{3.89}$$

In view of Eq. (3.43), Eq. (3.62) for the element strain energy takes the form

$$U^{(e)} = \frac{1}{2} \int_{\text{Area}} \lfloor e \rfloor\, [Q]\, \{e\}\, \sqrt{a}\, d\alpha d\beta \tag{3.90}$$

where

$$\underset{1X6}{\lfloor e \rfloor} = \left\lfloor \underset{1X3}{\lfloor \gamma \rfloor} \quad \underset{1X3}{\lfloor \chi \rfloor} \right\rfloor \tag{3.91}$$

$$\underset{6X6}{[Q]} \begin{pmatrix} \underset{3X3}{[A]} & \underset{3X3}{[B]} \\ \\ \underset{3X3}{[B]} & \underset{3X3}{[D]} \end{pmatrix} \tag{3.92}$$

The minimization of the potential energy of the element with respect to the nodal degrees of freedom leads to the element stiffness matrix and the consistent load vector for the distributed loads. The i-jth element of the element stiffness matrix [K] is given by

$$K_{ij} = \frac{\partial^2 U^{(e)}}{\partial V_i \partial V_j} = \int_{\text{Area}} \lfloor e_i \rfloor [Q] \{e_j\} \sqrt{a}\, d\alpha d\beta \tag{3.93}$$

where $\{e_i\}$ may be interpreted as the strain vector with the ith nodal degree of freedom, V_i, taking on a value of unity, while all other freedoms are set to a zero value; i and j take on the values 1-30, and V_i is the ith element of $\{V_{(T)}\}$, Eq. (3.58). Similarly, if we denote the consistent load vector due to the jth component of the distributed load by $\{F^{(j)}\}$, then the ith element of $\{F^{(j)}\}$ is given by

$$F_i^{(j)} = \frac{\partial H^{(e)}}{\partial V_i} = \int_{\text{Area}} p_j (v_j)_i \sqrt{a}\, d\alpha d\beta \tag{3.94}$$

where $(v_j)_i$ is the value of the v_j-displacement component with the ith degree of freedom taking on a value of unity, while all other freedoms are set to zero.

Equations (3.93)-(3.94) are the basis for the calculation of the element matrices. The integration in these equations is carried out numerically in the ξ-η natural area coordinates. When the integration is transformed to the ξ-η coordinates, the above equations become

$$k_{ij} = \int_0^1 \int_0^1 \lfloor e_i \rfloor [Q] \{e_j\} \sqrt{a}\, f\, d\xi d\eta \tag{3.95}$$

$$F_i^{(j)} = \int_0^1 \int_0^1 p_j(v_j)_i \sqrt{a}\, f\, d\xi d\eta \qquad (3.96)$$

where f is the Jacobian defined by Eq. (3.7). A 13-point numerical integration scheme of Gaussian type as given by Cowper [78] is used to evaluate the integrals in the above equation. The application of the formula is facilitated by the fact that ξ and η are the two area coordinates and the third one is $(1-\xi-\eta)$. This integration scheme is completely symmetric with respect to all the area coordinates, and is of high accuracy.

3.6.2 Calculation of the Strain Vector

We need to calculate the strain vector $\{e_i\}$ in Eq. (3.95) at each Gaussian point of integration. We may recall that $\{e_i\}$ is the strain vector $\{e\}$ when the ith degree of freedom takes on the value of unity with all the other freedoms set to zero. We may also recall that all the displacement components are interpolated by same set of shape functions.

Starting from the above definition of $\{e_i\}$, when the ith degree of freedom is unity with all others set to zero, Eq. (3.16) can be used to calculate the generalized displacement vector $\{a\}$, using which we can calculate the displacement components and their derivatives at the Gaussian point as well as at the nodal points. These nodal values can be used to calculate the 18 nodal values of the rotation components at all the six nodes by solving the constraint conditions, Eqs. (3.80)-(3.81). Then, using the quadratic interpolation, Eqs. (3.28), the rotation components and their α-β derivatives

at the Gaussian point are readily obtained. The strain vector can be set up directly using the strain-displacement relations, Eqs. (3.49)-(3.50). It may be observed that the constraint equations contain the various geometric quantities evaluated at the nodal points, which are directly calculated from the parametric equations of the shell middle surface using the different formulas derived in the second chapter. However, the strain-displacement equations require the geometric quantities at the Gaussian point within the shell element. As discussed before, the geometric quantities calculated from the interpolated shell surface are used to compute the strain vector.

We may note here that the matrix [Q] in Eq. (3.95) is also a function of the shell geometric parameters, and has to be evaluated at the Gaussian point. Also, the computations are greatly reduced when one exploits the fact that same shape functions interpolate all the displacement components.

The above computational procedure leads to element matrices of 30 x 30 size directly, where the constraint conditions are implicitly incorporated, without deriving the discrete Kirchhoff shape functions explicitly. The explicit derivation of the latter shape functions is extremely tedious, if not impossible, since all the displacement components are coupled in the constraint conditions.

The element matrices are developed above with respect to the nodal degrees of freedom in a global cartesian system. In order to apply the symmetric and support conditions easily, the degrees of freedom will be transformed to those referred to a local orthogonal

curvilinear coordinate system. The transformation details are presented in the next section.

3.7 Transformation to Orthogonal Curvilinear Coordinates

3.7.1 Local Orthogonal Vector Triad

The curvilinear coordinates describing the shell middle surface, in general, are not orthogonal. It would be convenient to construct a triad of orthogonal unit vectors at each grid point in the finite element mesh, and to refer the displacement components to these vectors.

We have the unit vectors in the directions of the covariant base vector $\bar{a}_1$, and the surface normal as

$$\hat{t}_i = \frac{\bar{a}_1}{\sqrt{a_{11}}} = \hat{t}_{1i}\hat{e}_i \tag{3.97a}$$

$$\hat{n} = \frac{\bar{a}_1 \times \bar{a}_2}{\sqrt{a}} = n_i\hat{e}_i \tag{3.97b}$$

$$(i = 1,2,3)$$

The unit vector normal to the vectors $\hat{t}_1$ and $\hat{n}$ which forms a right handed triad in the order $(\hat{t}_1, \hat{t}_2, \hat{n})$ is

$$\hat{t}_2 = \hat{n} \times \hat{t}_1 = t_{2i}\hat{e}_i \qquad (i = 1,2,3) \tag{3.97c}$$

The $\hat{t}_1$ and $\hat{t}_2$ vectors lie in the tangent plane to the middle surface. It may be noted that the directions of these unit vectors are functions of the curvilinear coordinates. The derivatives of these vectors are required to transform the derivatives of the cartesian

components to those of the curvilinear components. The derivatives of the normal vector are given by Weingarten formula, as given by Eq. (2.24):

$$\hat{n}_{,\mu} = n_{i,\mu}\hat{e}_i = -b_\mu^\lambda \bar{a}_\lambda \qquad (\mu,\lambda = 1,2) \tag{3.98}$$

Using Eq. (2.62) for $\bar{a}_\lambda$ we obtain

$$n_{i,\mu} = -b_\mu^\lambda x^i{}_{,\lambda} \qquad (i = 1,2,3) \tag{3.99}$$

In the conventional notation, the α-derivatives are

$$n_{1,\alpha} = -(b_1^1 x_{,\alpha} + b_1^2 x_{,\beta}) \tag{3.100a}$$

$$n_{2,\alpha} = -(b_1^1 y_{,\alpha} + b_1^2 y_{,\beta}) \tag{3.100b}$$

$$n_{3,\alpha} = -(b_1^1 z_{,\alpha} + b_1^2 z_{,\beta}) \tag{3.100c}$$

Similarly the β-derivatives are

$$n_{1,\beta} = -(b_2^1 x_{,\alpha} + b_2^2 x_{,\beta}) \tag{3.101a}$$

$$n_{2,\beta} = -(b_2^1 y_{,\alpha} + b_2^2 y_{,\beta}) \tag{3.101b}$$

$$n_{3,\beta} = -(b_2^1 z_{,\alpha} + b_2^2 z_{,\beta}) \tag{3.101c}$$

To derive expressions for the derivatives of the t_1 vector, consider Eq. (3.97a).

$$\hat{t}_1 = \frac{\bar{a}_1}{\sqrt{a_{11}}} = \frac{x^i{}_{,1}\,\hat{e}_i}{\sqrt{a_{11}}} \tag{3.102}$$

where

$$a_{11} = x^j{}_{,1} x^j{}_{,1} \qquad (j = 1,2,3) \tag{3.103}$$

Differentiating Eq. (3.102) with respect to x^μ,

$$\hat{t}_1{}_{,\mu} = t_{1i}{}_{,\mu}\hat{e}_i = \frac{1}{\sqrt{a_{11}}}(x^i{}_{,1\mu} - B_\mu x^i{}_{,1})\hat{e}_i \qquad (\mu = 1,2) \tag{3.104}$$

where

$$B_\mu = \frac{x^j{}_{,1} x^j{}_{,1\mu}}{a_{11}} \qquad \text{sum on } j \tag{3.105}$$

In conventional notation, the α derivatives are

$$t_{11}{}_{,\alpha} = \frac{1}{\sqrt{a_{11}}}(x_{,\alpha\alpha} - B_1 x_{,\alpha}) \tag{3.106a}$$

$$t_{12}{}_{,\alpha} = \frac{1}{\sqrt{a_{11}}}(y_{,\alpha\alpha} - B_1 y_{,\alpha}) \tag{3.106b}$$

$$t_{13}{}_{,\alpha} = \frac{1}{\sqrt{a_{11}}}(z_{,\alpha\alpha} - B_1 z_{,\alpha}) \tag{3.106c}$$

where

$$B_1 = \frac{1}{a_{11}}(x_{,\alpha} x_{,\alpha\alpha} + y_{,\alpha} y_{,\alpha\alpha} + z_{,\alpha} z_{,\alpha\alpha}) \tag{3.106d}$$

Similarly the β-derivatives are

$$t_{11}{}_{,\beta} = \frac{1}{\sqrt{a_{11}}}(x_{,\alpha\beta} - B_2 x_{,\alpha}) \tag{3.107a}$$

$$t_{12\ ,\beta} = \frac{1}{\sqrt{a_{11}}}\left(y_{\ ,\alpha\beta} - B_2 y_{\ ,\alpha}\right) \tag{3.107b}$$

$$t_{13\ ,\beta} = \frac{1}{\sqrt{a_{11}}}\left(z_{\ ,\alpha\beta} - B_2 z_{\ ,\alpha}\right) \tag{3.107c}$$

where

$$B_2 = \frac{1}{a_{11}}\left(x_{\ ,\alpha} x_{\ ,\alpha\beta} + y_{\ ,\alpha} y_{\ ,\alpha\beta} + z_{\ ,\alpha} z_{\ ,\alpha\beta}\right) \tag{3.107d}$$

Finally, the derivatives of $\hat{t}_2$ vector are obtained by differentiating Eq. (3.97c) with respect to x^{μ}.

$$\hat{t}_{2\ ,\mu} = t_{2i\ ,\mu}\hat{e}_i = (\hat{n} \times \hat{t}_1)_{\ ,\mu} \tag{3.108}$$

where

$$(\hat{n} \times \hat{t}_1)_{\ ,\mu} = \hat{n}_{\ ,\mu} \times \hat{t}_1 + \hat{n} \times \hat{t}_{1\ ,\mu} \tag{3.109}$$

Substituting for various vectors in terms of their components in Eq. (3.109), the α-derivatives of t_2 vector in the conventional notation are found to be

$$t_{21\ ,\alpha} = (n_{2\ ,\alpha} t_{13} - n_{3\ ,\alpha} t_{12}) + (n_2 t_{13\ ,\alpha} - n_3 t_{12\ ,\alpha}) \tag{3.110a}$$

$$t_{22\ ,\alpha} = (n_{3\ ,\alpha} t_{11} - n_{1\ ,\alpha} t_{13}) + (n_3 t_{11\ ,\alpha} - n_1 t_{13\ ,\alpha}) \tag{3.110b}$$

$$t_{23\ ,\alpha} = (n_{1\ ,\alpha} t_{12} - n_{2\ ,\alpha} t_{11}) + (n_1 t_{12\ ,\alpha} - n_2 t_{11\ ,\alpha}) \tag{3.110c}$$

The β-derivatives of t_2 vector are obtained by replacing α with β in Eqs. (3.110).

3.7.2 Transformation Matrices

The components of the displacement vector resolved along the local vector triad are denoted as u, v and w, where u and v are the tangential components and w is the normal component. Thus, the displacement vector in the two coordinate systems is given by

$$\bar{U} = u\hat{t}_1 + v\hat{t}_2 + w\hat{n} \tag{3.111a}$$

$$\bar{U} = v_1\hat{e}_1 + v_2\hat{e}_2 + v_3\hat{e}_3 \tag{3.111b}$$

Substituting for the unit vectors in terms of their components in Eq. (3.111a), the relation between the two sets of components is obtained. Thus

$$\{u^{(C)}\} = [\lambda_1]\{u^{(L)}\} \tag{3.112}$$

$$\{u^{(C)}\} = \lfloor v_1, v_2, v_3 \rfloor^T \tag{3.113}$$

$$\{u^{(L)}\} = \lfloor u, v, w \rfloor^T \tag{3.114}$$

$$[\lambda_1] = \begin{pmatrix} t_{11} & t_{21} & n_1 \\ t_{12} & t_{22} & n_2 \\ t_{13} & t_{23} & n_3 \end{pmatrix} \tag{3.115}$$

The relation between the derivatives of the components in the two coordinate systems is obtained by partial differentiation of Eqs. (3.111a) and (3.111b), and substituting for the derivatives of the unit vectors in terms of their components from the expressions derived

earlier. Thus, taking derivative with respect to α leads to

$$\{u^{(C)}{}_{,\alpha}\} = [\lambda_1]\{u^{(L)}{}_{,\alpha}\} + [\lambda_2]\{u^{(L)}\} \tag{3.116}$$

where

$$[\lambda_2] = \begin{bmatrix} t_{11,\alpha} & t_{21,\alpha} & n_{1,\alpha} \\ t_{12,\alpha} & t_{22,\alpha} & n_{2,\alpha} \\ t_{13,\alpha} & t_{23,\alpha} & n_{3,\alpha} \end{bmatrix} \tag{3.117}$$

The β-derivatives are similarly related, and can be obtained by replacing α with β in Eq. (3.116). Denoting the matrix obtained by replacing α with β in Eq. (3.117) as $[\lambda_3]$, we can write

$$\{u^{(C)}{}_{,\beta}\} = [\lambda_1]\{u^{(L)}{}_{,\beta}\} + [\lambda_3]\{u^{(L)}\} \tag{3.118}$$

Equations (3.112), (3.117), (3.118) can be combined to obtain the transformation matrix at a node:

$$\{\bar{U}^{(C)}_{(i)}\} = [\bar{\lambda}_{(i)}]\{\bar{U}^{(L)}_{(i)}\} \tag{3.119}$$

where

$$\underset{9X1}{\{\bar{U}^{(C)}_{(i)}\}} = \left\lfloor \left(u^{(C)}\right)_{(i)} \right\rfloor, \left\lfloor \left(u^{(C)}{}_{,\alpha}\right)_{(i)} \right\rfloor, \left\lfloor \left(u^{(C)}{}_{,\beta}\right)_{(i)} \right\rfloor^T \tag{3.120}$$

$$\underset{9X9}{[\bar{\lambda}_i]} \begin{bmatrix} [\lambda_{1i}] & [0] & [0] \\ [\lambda_{2i}] & [\lambda_{1i}] & [0] \\ [\lambda_{3i}] & [0] & [\lambda_{1i}] \end{bmatrix} \tag{3.121}$$

where the index i in Eqs. (3.120)-(3.121) indicates the node number at which the quantity is evaluated. The $\{\bar{U}^{(L)}_i\}$ vector in Eq. (3.119) is obtained by replacing the superscript C with L in Eq. (3.120). Finally, the nodal displacement vector for an element in the two coordinate systems can be related by combining the transformations of Eq. (3.119) at the corner nodes, and the transformation of Eq. (3.112) at the centroid. Thus, we obtain the transformation matrix for an element as

$$\{U^{(C)}\} = [\bar{\lambda}]\{U^{(L)}\} \tag{3.122}$$

where

$$\underset{30X1}{\{U^{(C)}\}} = \left\lfloor \lfloor \bar{U}^{(C)}_{(1)} \rfloor, \lfloor \bar{U}^{(C)}_{(2)} \rfloor, \lfloor \bar{U}^{(C)}_{(3)} \rfloor, \lfloor u^{(C)}_{(G)} \rfloor \right\rfloor \tag{3.123}$$

and the index G stands for the centroid. The $\{U^{(L)}\}$ vector in Eq. (3.122) is obtained from Eq. (3.123) by replacing the superscript C with L. Also we have the diagonal super matrix

$$\underset{30X30}{[\bar{\lambda}]} \quad \left[\underset{9X9}{[\bar{\lambda}_{(1)}]}, \underset{9X9}{[\bar{\lambda}_{(2)}]}, \underset{9X9}{[\bar{\lambda}_{(3)}]}, \underset{3X3}{[\lambda_{4(G)}]} \right] \tag{3.124}$$

The stiffness matrix and the load vector in the local orthogonal curvilinear coordinates is obtained by the transformations

$$\underset{30X30}{[K^{(L)}]} = [\bar{\lambda}]^T[K][\bar{\lambda}] \tag{3.125}$$

$$\underset{30X1}{\{F^{(L)}\}} = [\bar{\lambda}]^T\{F\} \tag{3.126}$$

Care should be taken to arrange the stiffness matrix [K] and the load vector {F} in the order of the nodal degrees of freedom suggested by Eq. (3.123).

As the last step, the centroidal degrees of freedom are eliminated by static condensation resulting in element matrices of size 27X27. This completes the derivation of the element matrices.

In the next and the final section a brief description of the computer program is presented.

3.8 The Computer Program

The new curved triangular shell element and the associated computer program have been given the acronym KSHARA. The program KSHARA was implemented on the CDC CYBER 175 system using FORTRAN language. The program is of the "dynamic storage allocation" type, where the high-speed core memory is dynamically reallocated during the various stages of computation. This allows for the very efficient use of the limited core memory, and renders the dimensioning of the various arrays problem independent. The program is a collection of a number of subroutines; their names and logical relationships are shown in Figure 5.

The main program DRIVE sets the working array lengths and reads the control variables. GENDRI is the driver program which calls a number of subroutines to perform various steps in the finite element static analysis procedure. The principal operations include: primary input-output operations directly; the assignment of equation numbers and band-width calculation using BAND; the stiffness generation and

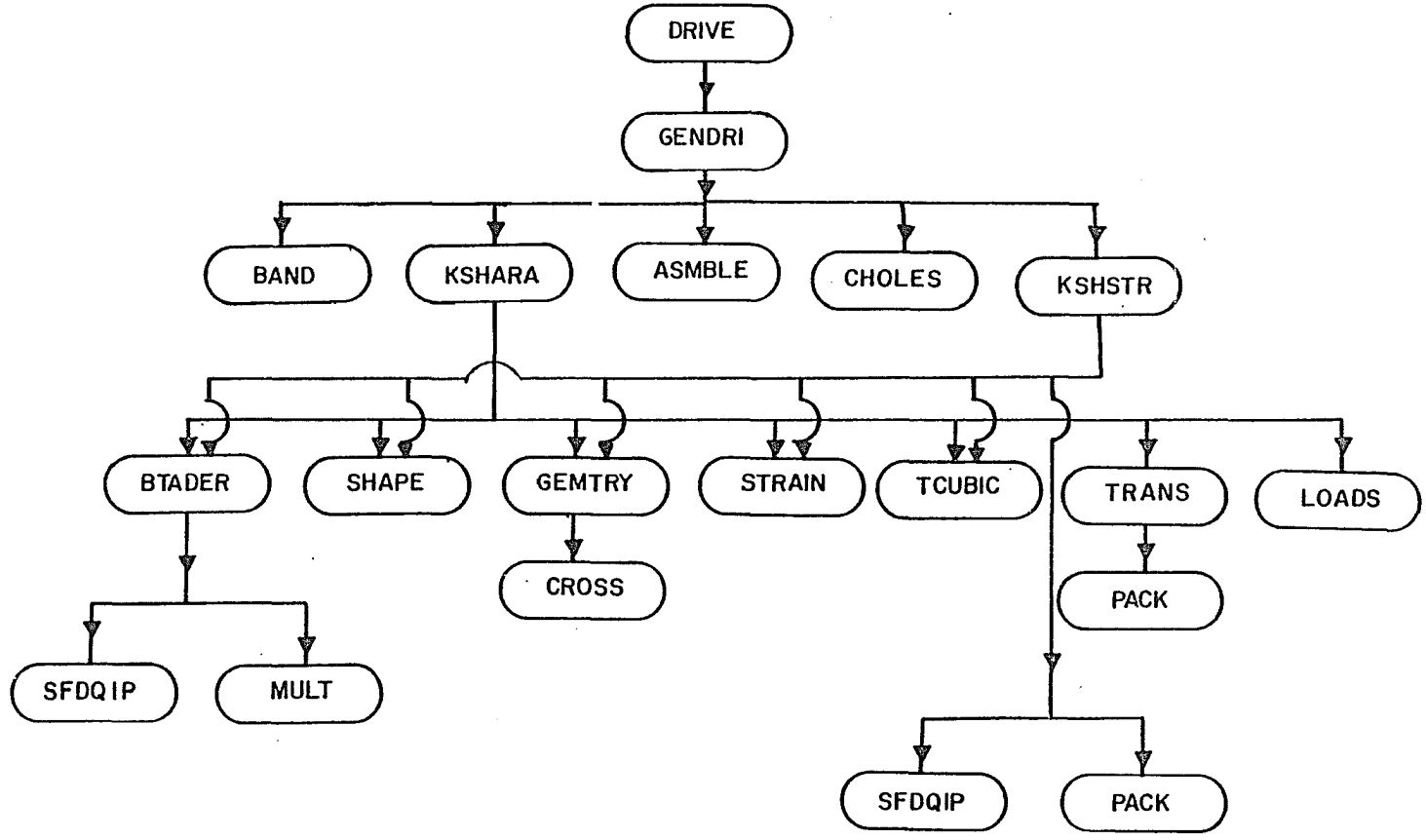

Figure 5. Subroutine structure of the KSHARA program.

its assembly through the routines KSHARA and ASMBLE; the direct assembly of concentrated loads and the modification of the stiffness matrix for the prescribed displacements; the solution of equations by Cholesky decomposition through CHOLES; and, finally, the stress recovery by calling KSHSTR.

A typical output includes an echo of the input data, the displacement components and their derivatives in tangent and normal directions at the corner nodes and element centroid, and the membrane stress and bending moment resultants at the corner nodes and the element centroid. The nodal stress values are the average of the values from all the elements sharing that node.

The program can be run optionally in the data-check mode to avoid costly data errors. The element matrices can be stored permanently on a secondary storage medium by invoking the restart option. The latter option will be useful to study the effects of various boundary conditions, or for the future non-linear analysis.

The actual computation of the element matrices is performed in the KSHARA subroutine. The user-supplied routine SHAPE returns the position vector and its derivatives up to second-order with respect to the curvilinear coordinates, to any point on the shell middle surface. To accommodate variable distributed loading, the user can supply the LOADS subroutine which would return at any point on the middle surface the tangential and normal components of the external loads. The gravity loading may be automatically included by activating the "gravity switch."

The computation of the element matrices proceeds along the lines described under Section 3.6. The GEMTRY routine computes geometric quantities including the metric and curvature tensors, and optionally returns the transformation matrices associated with the transformation from cartesian to local curvilinear coordinates. The cubic and quadratic interpolation over the triangle is accomplished by the TCUBIC and SFDQIP routines. The computation of strain vectors with each of the freedoms taking on a value of unity, and that of the laminate constitutive relations and the subsequent stiffness and load vector calculation is performed within the 13-point Gaussian integration loop.

The formulation and solution of the constraint equations to obtain the nodal values of the rotation components, and their quadratic interpolation at the Gaussian point is carried out in the BTADER subroutine. The strain vector at the integration point is set up in STRAIN subroutine. The element matrices are transformed to tangent and normal directions by the TRANS routine which utilizes PACK to form the element transformation matrices.

As a last step, the centroidal freedoms are removed by static condensation procedure. The user has also the option either to transform the stiffness matrix to tangent and normal directions at the boundary nodes alone or to have the stiffness in the cartesian direction itself. The latter options are useful in problems where the two coordinate systems coincide (for example, plate problems) or in a large problem where the boundary nodes form a small percentage of total number of nodes. In such problems, the computationally-expensive

transformation may be limited to a few boundary nodes for the easy application of the boundary conditions.

The stress recovery procedure is carried out in the KSHSTR subroutine. The membrane stress resultants and bending moment resultants are computed at the corner nodes and the centroid of every element. At the mesh point where more than one element meet, an average value for the nodal stresses is calculated.

The program was tested by solving a number of problems with alternative solutions. The element performance-studies were carried out to bring out the computational efficiency, the accuracy and versatility of the new element. The results from the numerical experiments are reported in the next chapter.

CHAPTER 4

NUMERICAL RESULTS

The results of numerical evaluation of the KSHARA element are presented in this chapter. In order to assess the solution accuracy and the computational efficiency of the KSHARA element, and to examine its versatility to model thin-shells of various shapes, a number of practical shell problems were analyzed. The choice of the example problems includes thin shells of zero, positive and negative Gaussian curvatures. Solution comparisons are made with alternative analytical or numerical solutions for various support and loading conditions, and, in some problems, over a range of values for the geometric parameters.

Another aspect of the evaluation is focused on the ability of the present element to accurately represent the membrane stress and inextensional bending states, and deformation states associated with large rigid body displacements. In literature, these problems are referred to as "patch test" problems. Patch test examples are presented for shells with positive Gaussian curvature.

Results are also included for anisotropic plates and cylindrical shells.

4.1 Cylindrical Shell Problems

Cylindrical shells belong to the class of shells with zero Gaussian curvature. They are extensively used in engineering applications. Many comparison solutions are available for cylindrical shell problems under different support and loading conditions. The problems studied include an infinite fixed-free quarter cylinder under separate loadings of a uniformly distributed bending moment at the free edge and a uniform internal pressure, the cylindrical shell roof problem under gravity loading, and the pinched cylinder with free and supported edges.

4.1.1 Infinite Fixed-Free Quarter Cylinder

The first example considered is a case where the shell is in a state of pure bending accompanied with large rigid body displacement. A quarter of an infinitely long cylinder with one end fixed and the other end free is selected as the shell configuration. Due to the symmetry about any plane normal to the axial direction, a strip of the cylinder with one element subdivision along the length and varying number of divisions along the circumferential direction was analyzed. The element orientations along with the geometric and material properties of the shell are shown in Figure 6.

Two types of loading are applied on the shell: a uniformly distributed line bending moment, M, along the free edge, and a uniform internal pressure, P. The boundary condition option, where the degrees of freedom associated with the boundary nodes are only transformed into the local coordinates, was invoked.

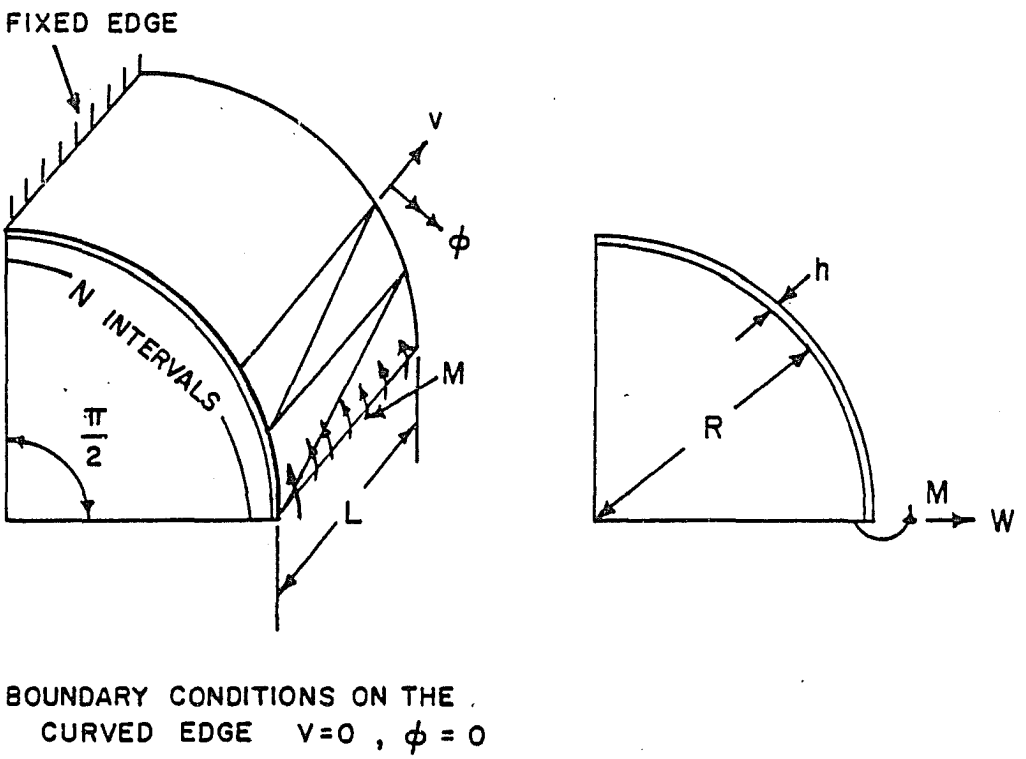

Figure 6. Fixed-free quarter cylinder under uniform edge moment.

Results for the case of uniform bending moment are shown in Table 1, in which the convergence of the normal displacement at the free edge for different values of the h/R ratio, along with the analytical solution reported in Ref. [50], is presented. In all the cases, the circumferential bending moment at all the nodal points was almost exactly equal to the applied bending moment.

Table 1. Convergence of normal displacement at the free edge of the fixed-free quarter cylinder under distributed edge moment.

		$wEh^3/(R^2M)$	
N[a]	h/R = 0.001	0.01	0.1
4	10.77	11.59	11.79
8	10.96	11.67	11.88
32	10.97	11.72	11.93
Analytical Solution[b]	10.92	10.92	10.92

[a] N = No. of circumferential divisions.

[b] Analytical solution is [50]: $wEh^3/(MR^2) = 12(1 - \nu^2)$.

The non-dimensional normal displacements for the cylinder with h/R = 0.001 converges to the analytical solution within 0.5 percent error. The same displacement for the cylinders with h/R = 0.01 and 0.1 converges to a higher value. The cylinder under the present loading is in a state of pure inextensional bending with constant bending strains. The present finite element model is able to recover the constant

bending moment at all the points in the cylinder. The discrepancy in the displacement results for the higher values of h/R ratio might be attributed to the neglected strain energy due to transverse shear deformation inherent in the present model, which is relatively higher in the thicker shells.

Results for the uniform pressure loading along with the analytical solution are displayed in Table 2. In this case, although the bending action of the shell is predominant, a significant membrane action is also present. The results in Table 2 indicate excellent agreement with the analytical solution for all the values of the h/R ratio. The maximum error is less than one percent, and occurs in the cylinder with h/R = 0.1.

Table 2. Convergence of normal displacement at the free edge of the fixed-free cylinder under uniform pressure.

		$wEh^3/(pR^4)$	
N[a]	h/R = 0.001	0.01	0.1
4	5.2902	5.4006	5.4660
8	5.4401	5.4600	5.4812
16	5.4576	5.4624	5.4785
Analytical Solution[b]	5.4600	5.4599	5.4327

[a] N = No. of circumferential divisions.

[b] Analytical solution [50] is: $wEh^3/pR^4 = 6(1 - h^2/12R^2)(1 - \nu^2)$

4.1.2 Cylindrical Shell Roof Problem

The cylindrical shell roof problem shown in Figure 7 has been used by many authors to compare their elements. The shell is loaded by its dead weight, being supported by diaphragms at the ends and free along the sides. Due to symmetry, only one quarter of the shell is analyzed, and various uniform gridworks of elements are used with orientations shown. The numerical data are given in Figure 7. Consistent load vectors for both the tangential and normal components of the loading are calculated considering the exact trigonometric variations of these load components.

Two solutions are customarily used for comparison. One is the so-called exact solution of Scordelis and Lo [60], which is essentially a shallow shell solution, as noted in Ref. [57]. The second one is the deep shell solution originally reported by Forsberg and Hartung [79]. The latter results must be read from a graph and are therefore not very accurate. Furthermore, the particular deep shell theory used is not mentioned. Hence, it was decided to generate an alternative deep shell solution using specified shell theory. Such solutions were obtained using the high-precision arbitrary shell element, CURSHL, of Cowper [33], using Donnell and Koiter-Sanders (K-S) deep shell theory. The loading representation in these calculations was identical to the one used in the present element. A converged solution was determined by comparing the 5X5 and 8X8 grid solutions in one quarter of the shell.

In Figure 8, the vertical deflection at the center of the free edge is plotted against the total number of degrees of freedom (before

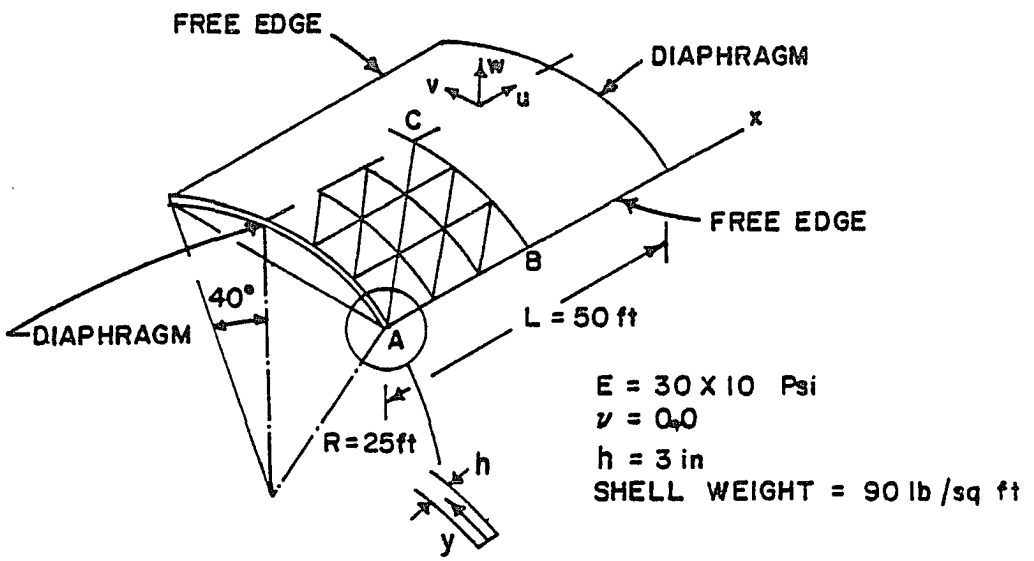

Figure 7. Cylindrical shell roof.

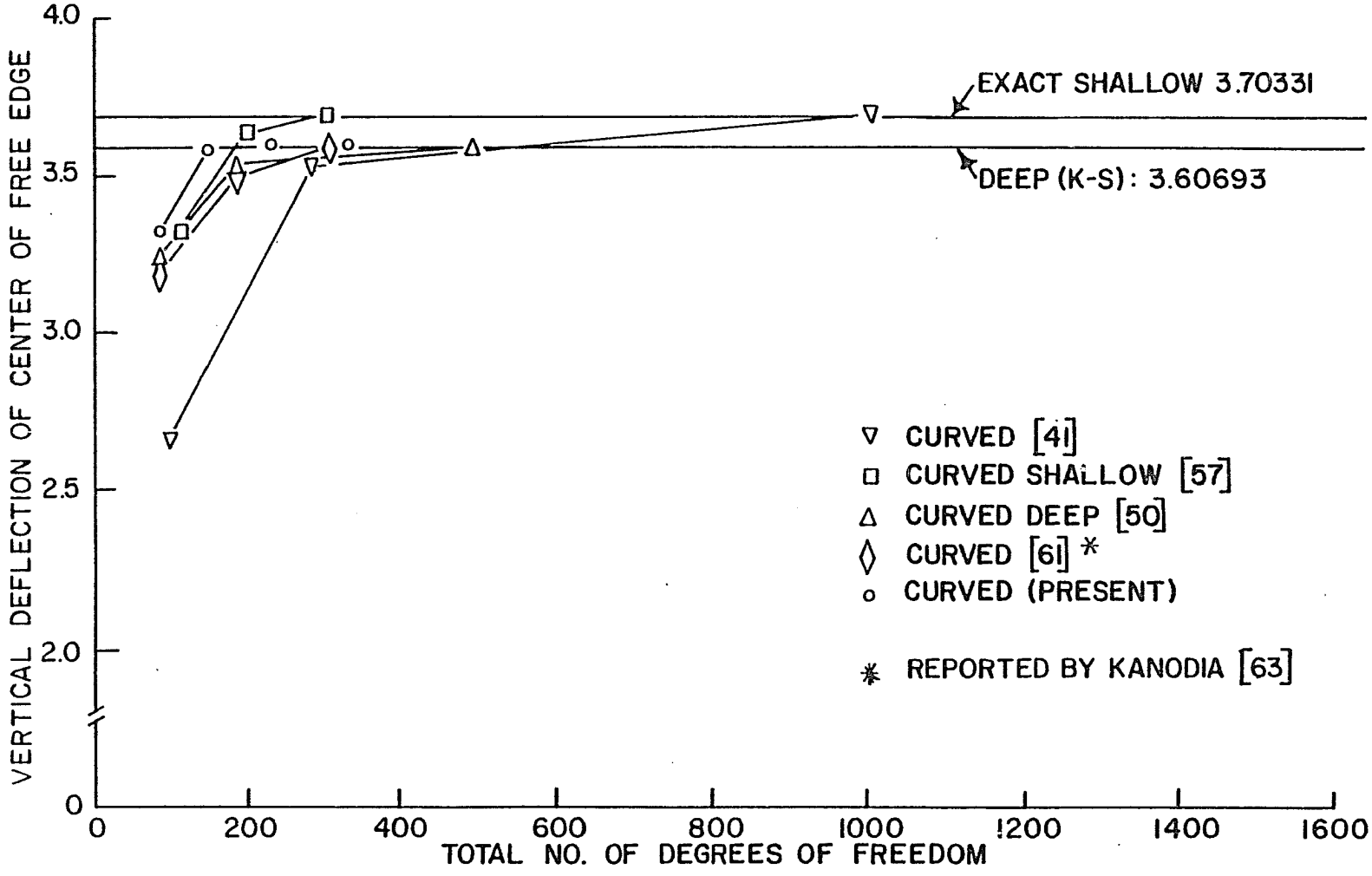

Figure 8. Comparison of vertical deflection for the cylindrical shell roof.

boundary conditions are imposed) along with the other finite element solutions. It is seen that the present element converges monotonically to the Koiter-Sanders deep shell solution, and, for a given number of equations, is the most accurate among all the elements compared. Tables 3 and 4 show the convergence of the displacements and stress resultants at various points in the shell. Again, it is observed that all the quantities compared converge to the deep shell solution based on Koiter-Sanders theory; and very good accuracy is achieved for both displacements as well as stress resultants.

4.1.3 Pinched Cylinder with Free Edges

The pinched cylinder problem, where a cylinder with free edges is subjected to two pinching loads at the center of the cylinder, is analyzed using the present element. A finite element solution using curved shell element will converge to the analytical solution if the element is able to represent the rigid body motions accurately. In the past, many authors [61, 80-81] have used this problem to check their element formulations for correct representation of rigid body modes.

Figure 9 shows the cylinder with dimensions and material properties acted upon by the pinching loads, P. Two cases are considered: the first case is that of a thick cylinder with h = 0.094 in (R/h = 52.6915), and P = 100 lb; the second case is one of the thin cylinder with h = 0.0155 in (R/h = 320), and P = 0.1 lb. In view of the symmetry, an octant of the cylinder is modeled using uniform meshes with orientations as shown in Figure 9. Some preliminary

Table 3. Comparison of displacements for the cylindrical shell roof problem.

Grid size in quarter shell	No. of equations[a]	10 u_A in	w_B in	10 v_B in	10 w_C in	Vertical deflection of pt. B
2X2	49	1.3779	3.4633	7.7276	3.8930	3.1495
3X3	100	1.4775	3.9055	8.4808	5.1571	3.5369
4X4	169	1.4911	3.9706	8.6031	5.3641	3.5947
5X5	256	1.4935	3.9856	8.6323	5.4054	3.6080
8X8	625	1.4930	3.9894	8.6396	5.4071	3.6114
shallow shell [60]		1.5133	4.0992	8.7615	5.2494	3.7033
deep shell[b] (k-s)		1.4900	3.9847	8.6257	5.4085	3.6069

[a] After boundary conditions.

[b] Generated by the author.

Table 4. Comparison of stress resultants for the cylindrical shell roof problem.

Grid size in quarter shell	No. of equations[a]	$N_{xxB} \times 10^{-3}$ lb/in	$M_{yyC} \times 10^{-3}$ lb-in/in	$M_{xxC} \times 10^{-2}$ lb-in/in
2X2	49	5.9148	1.4815	0.4087
3X3	100	6.2271	1.8899	1.1052
4X4	169	6.2965	2.0049	1.3559
5X5	256	6.3258	2.0407	1.3685
8X8	625	6.3409	2.0566	1.1869
shallow shell [60]		6.4124	2.0562	0.9272
deep shell[b] (k-s)		6.3138	2.0581	0.9634

[a] After boundary conditions.

[b] Generated by the author.

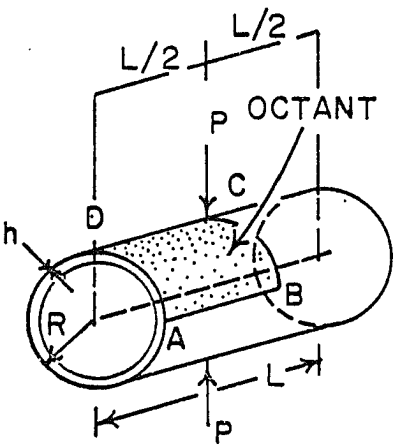

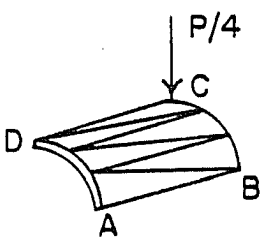

MESH IN OCTANT

R = 4.953 in.
L = 10.35 in.
E = 10.5×10^6 PSI
ν = 0.3125

THICK CYLINDER

h = 0.094 in. (R/h = 52.6915)
P = 100 lbf.

THIN CYLINDER

h = 0.01547813 in. (R/h = 320)
P = 0.1 lbf.

Figure 9. Pinched cylinder with a typical mesh in the octant.

results revealed that, while the results for the thick cylinder are sensitive to mesh size along the cylinder length, the thin cylinder is not. Hence, the convergence study was carried out with various mesh sizes in the octant of the shell as displayed in Tables 5 and 6, where the normal displacement under the pinching load is compared against other finite element and analytical solutions. The results in Tables 5 and 6 are also plotted in Figures 10 and 11, where the normal displacement of the loaded point is plotted against the total number of degrees of freedom after the boundary conditions are imposed.

An analytical solution based on inextensional theory is given by Timoshenko and Woinowsky-Kreiger [82]. Although Ashwell and Sabir [80] report an improved solution taking in to account the bending effects in the vicinity of the load, the inextensional solution is a good approximation for the thin cylinder. The bending energy neglected in the case of the thick cylinder, however, results in a stiff solution. Hence the converged solution of Dawe [83], which is based on a high-order triangular deep shell element, is considered to be more accurate for the case of a thick cylinder.

Results for the thick cylinder indicate monotonic and fast convergence to Dawe's finite element solution and almost exact agreement with it. It is also observed that the present test solution is reached using 141 degrees of freedom compared to the 412 freedoms required by Dawe's solution. The results for the thin shell also follow the same trend, and the analytical solution is approached monotonically with a modest number of freedoms.

Table 5. Convergence of normal displacement for the thick pinched cylinder.

Mesh size in octant	Normal displacement of the point under load		
	Thomas and Gallagher [61]	Wu [50]	Present
1X3	0.0048(19)	0.1052(73)	0.1082(44)
1X4	0.1107(67)	0.1086(97)	0.1131(58)
1X6		0.1100(145)	0.1131(86)
1X8	0.1119(131)	0.1104(193)	
2X4			0.1126(95)
2X6			0.1141(141)
2X8			0.1136(187)
FEM Solution of Dawe [83]			
4X4		0.11364(412)	

Note: Nos. in the parentheses are no. of d.o.f.

Table 6. Convergence of normal displacement for the thin pinched cylinder.

Mesh size in octant	Normal displacement of the point under load			
	Ashwell and Sabir [80]	Thomas and Gallagher [61]	Wu [50]	Present
1X1	0.2301(20)	0.00003(9)		
1X2		0.01582(35)		
1X3			0.0198(73)	0.0204(44)
1X4		0.02327(67)	0.0228(97)	0.0223(58)
1X6		0.02440(99)	0.0240(145)	0.0239(86)
1X8	0.02406(90)	0.02467(131)	0.0243(193)	0.0244(114)
2X6				
2X8	0.02414(135)			
3X8	0.02418(180)			
8X8	0.02431(405)			
Analytical [82]	0.02439			

Note: Nos. in parentheses are no. of d.o.f.

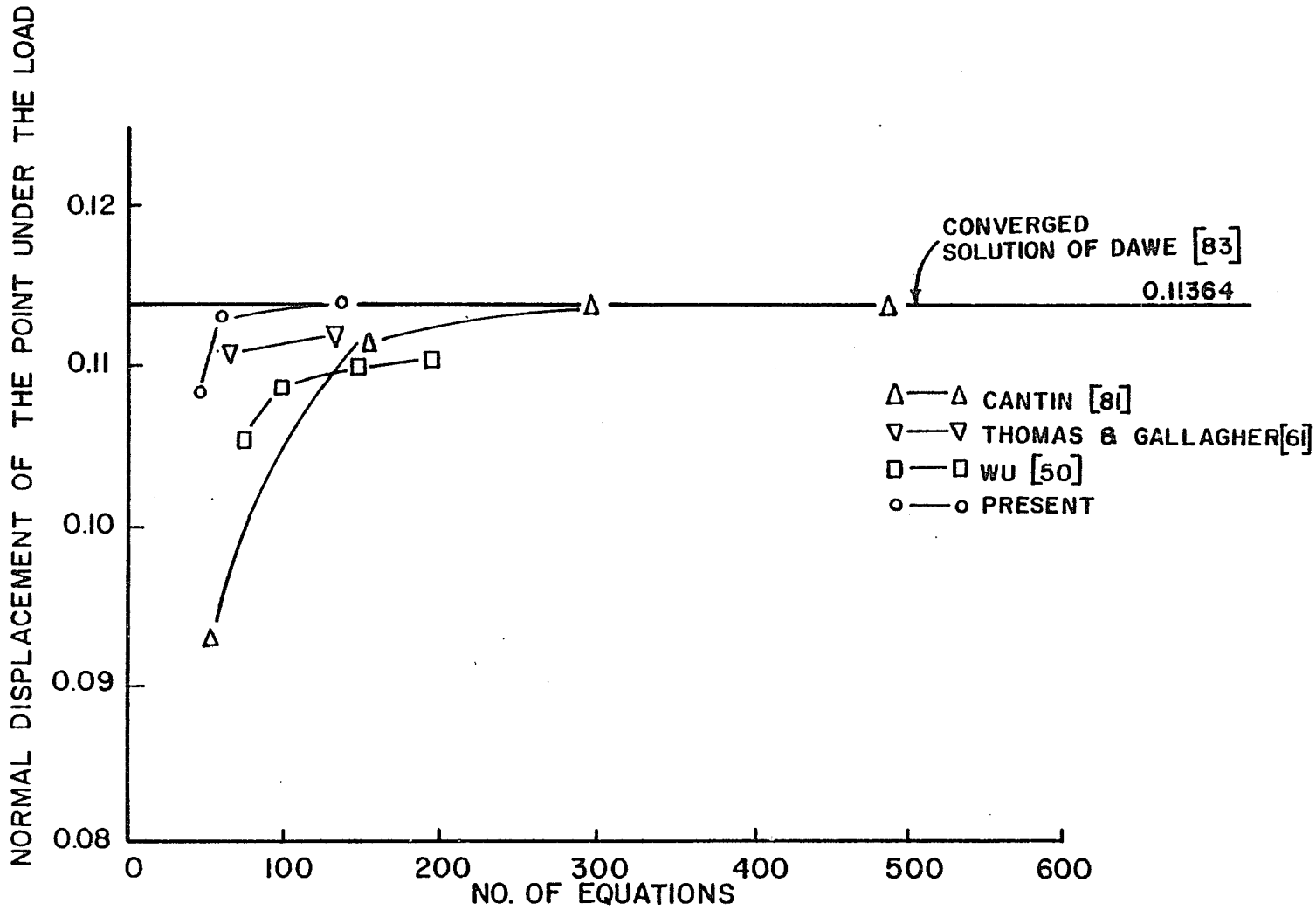

Figure 10. Comparison of normal displacement for the thick pinched cylinder.

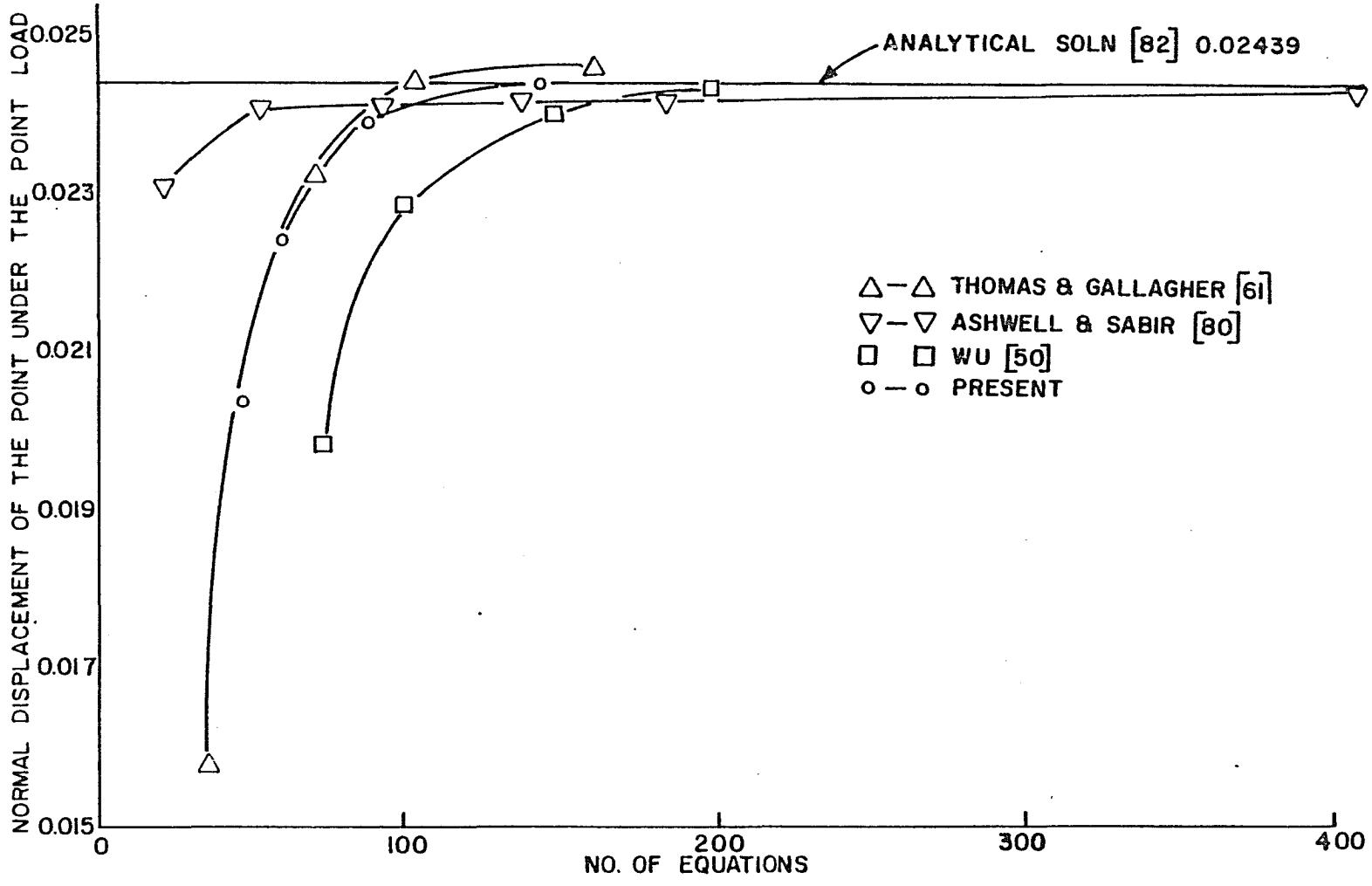

Figure 11. Comparison of normal displacement for the thin pinched cylinder.

It is observed from the results in Table 3 that for a given number of elements in the longitudinal direction, the normal displacement increases with the number of elements in the circumferential direction until a critical aspect ratio is reached and then begins to decrease. There seems to be an effect of the element aspect ratio on the convergence behavior, and such an effect was also noticed in the plate element based on the discrete Kirchhoff theory [68].

4.1.4 Pinched Cylinder with Supported Edges

As the next problem, a thin pinched cylinder with freely supported edges (diaphragm ends), acted upon by two pinching loads at the center of the cylinder is considered. The geometric details, and a 5X5 non-uniform grid in the cylinder octant, in view of the symmetry, are shown in Figure 12. The ratios of the successive grid side lengths to that of the smallest side are chosen to be 2, 3, 4 and 5 respectively. This problem is considered to be a critical test case, due to the combined effects of the concentrated loads and the support conditions. The latter effects are more pronounced because of the small L/R ratio of the cylinder.

Table 7 shows the comparison of the displacements at various points in the cylinder with the alternative finite element and analytical solutions, for two grid sizes. The finite element solution is based on the high-precision transformed shallow shell element of Lindberg, Olson and Cowper [84]. The analytical solution is from a double Fourier series solution of Flügge's equations [85], using 80 terms in each direction, also reported in Ref. [84]. It is seen that the normal

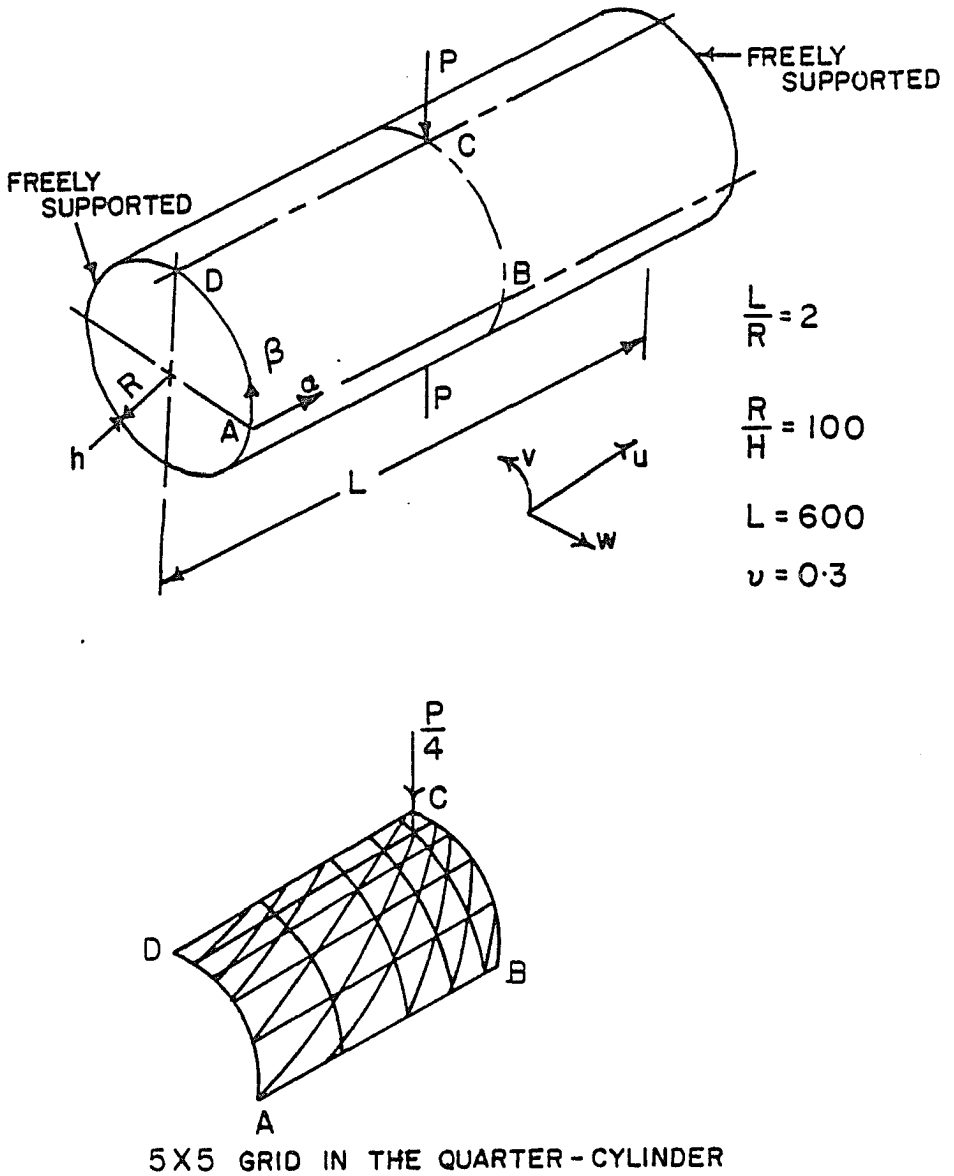

Figure 12. Pinched cylinder with supported edges.

Table 7. Comparison of displacements for the pinched cylinder with supported edges.

Grid size in quarter shell	$\frac{Ehw_C}{P}$	$\frac{Ehw_B}{P}$	$\frac{Ehu_D}{P}$
5X5	-157.3470	-7.8647	3.9804
8X8	-160.7760	-5.5209	4.0212
5X5 [84] non-uniform	-159.23	-4.63	3.954
Analytical [84]	-164.24	-0.47	4.114

deflection under the pinching load, which is proportional to the strain energy of the shell, is predicted within one percent of the comparative finite element solution, and two percent of the analytical solution. The normal displacement at the point B seems to be most difficult to predict, as also shown by the alternative finite element solution. The slow convergence toward the analytical solution, however, is encouraging. The longitudinal displacement of the point D on the diaphragm edge is within two percent of the analytical value.

The displacement distributions along various lines on the cylinder, along with the analytical solution is shown in Figure 13. The agreement between the two is satisfactory. Similarly, Figures 14 and 15 show the distributions of the membrane stress resultants and bending moment resultants, along with the analytical solution. Again, the agreement between the two is close, and a better correlation can be achieved by taking recourse to grid refinement.

4.2 Spherical Shell Problems

In this section, we present example problems of spherical shells which belong to the shells class of positive Gaussian curvature. Three problems are included in this class: a spherical cap resting on a square base under uniform pressure, a spherical shell under internal pressure, and a spherical shell subjected to pinching loads at the poles.

4.2.1 Spherical Cap Problem

A shallow spherical cap, resting on a square base with freely supported edges, is shown in Figure 16. The geometric and material

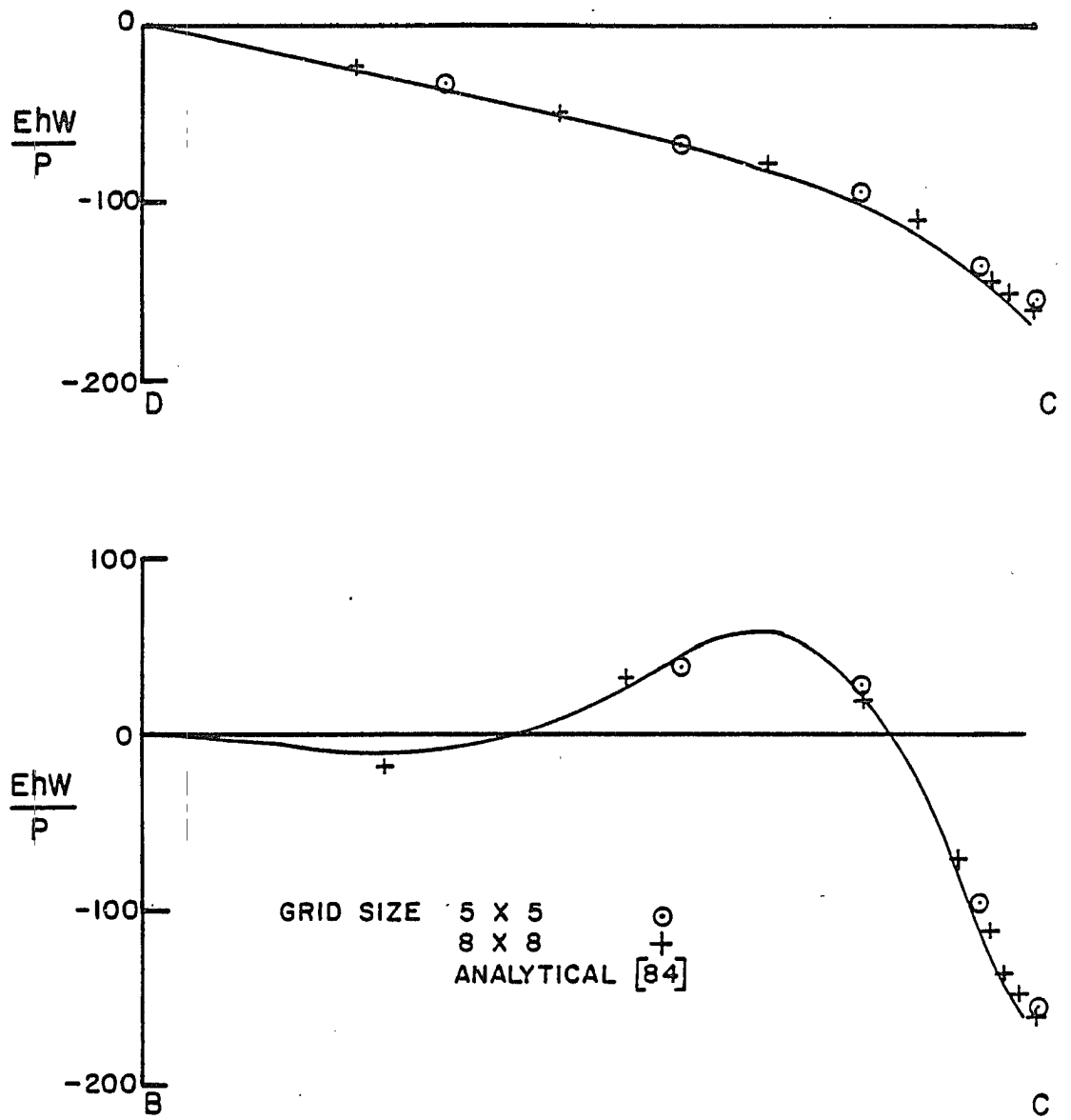

Figure 13. Displacement distributions for the pinched cylinder with supported edges.

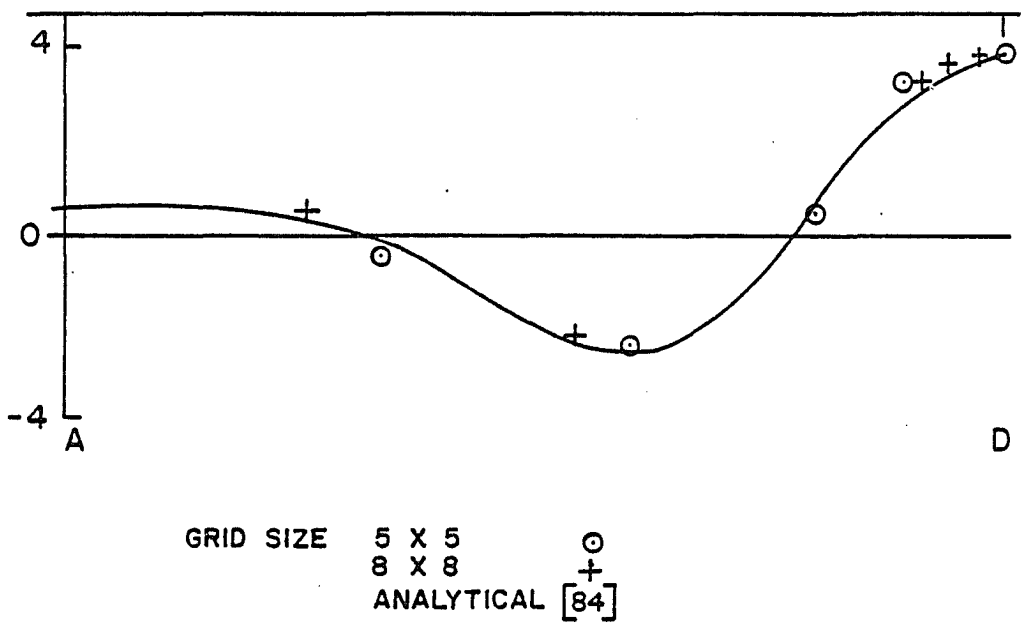

Figure 13.--Continued

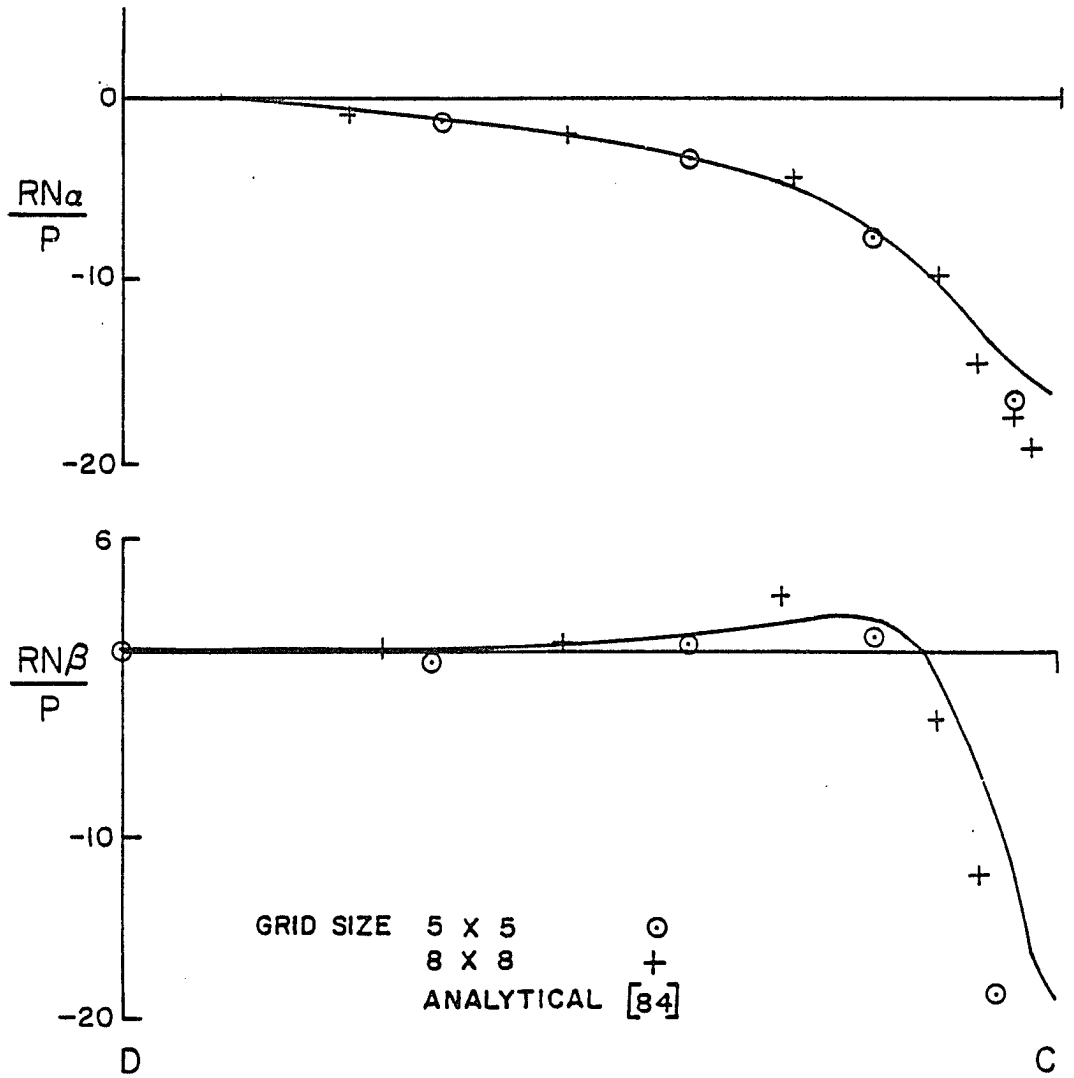

Figure 14. Membrane stress and bending moment distribution along the line DC for the pinched cylinder with supported edges.

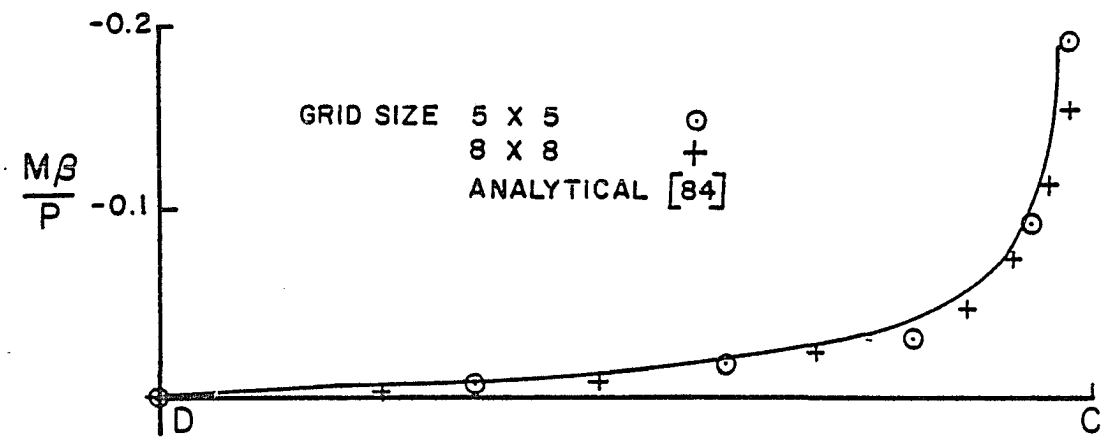

Figure 14.--Continued

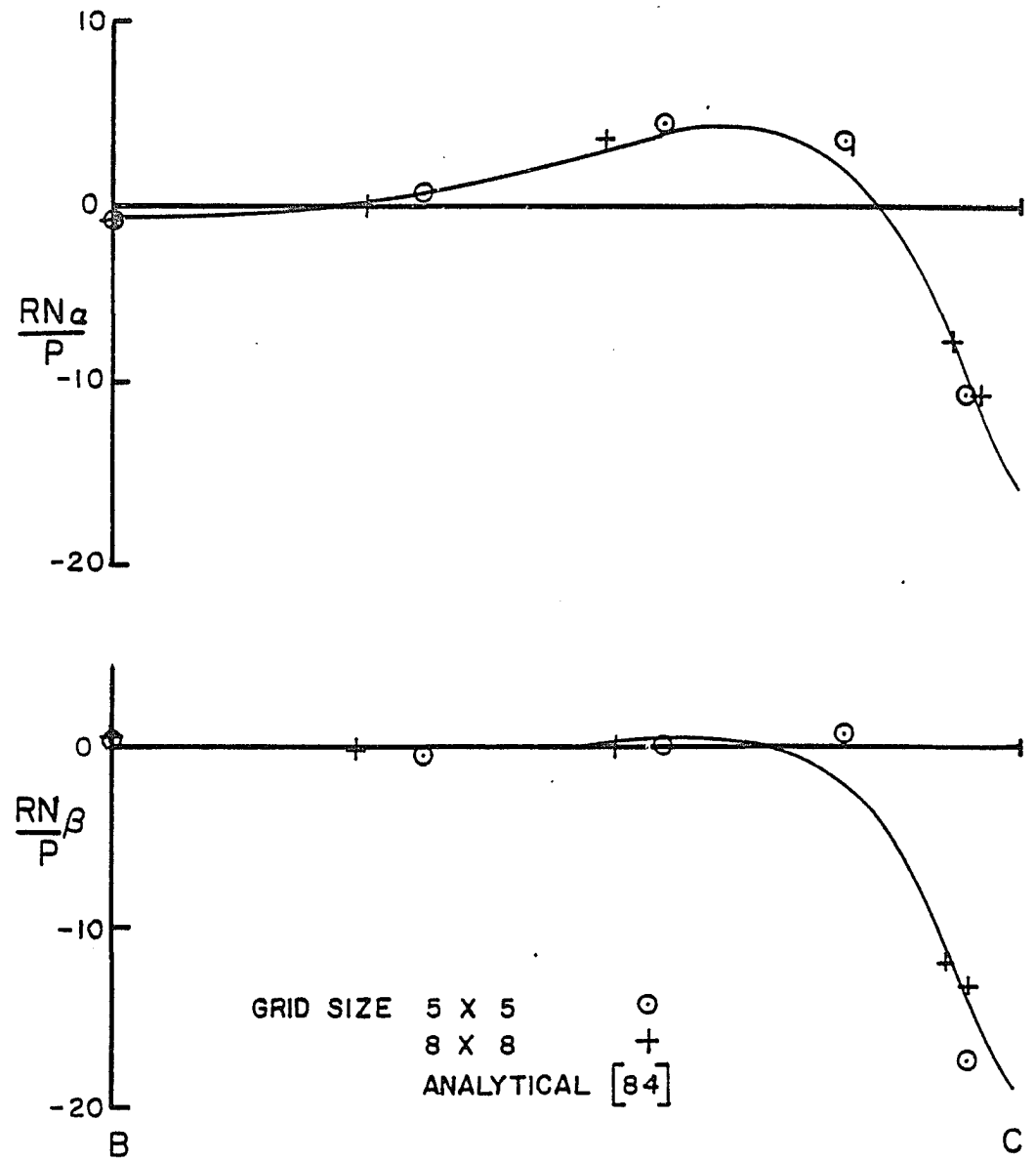

Figure 15. Membrane stress and bending moment distribution along the line BC for the pinched cylinder with supported edges.

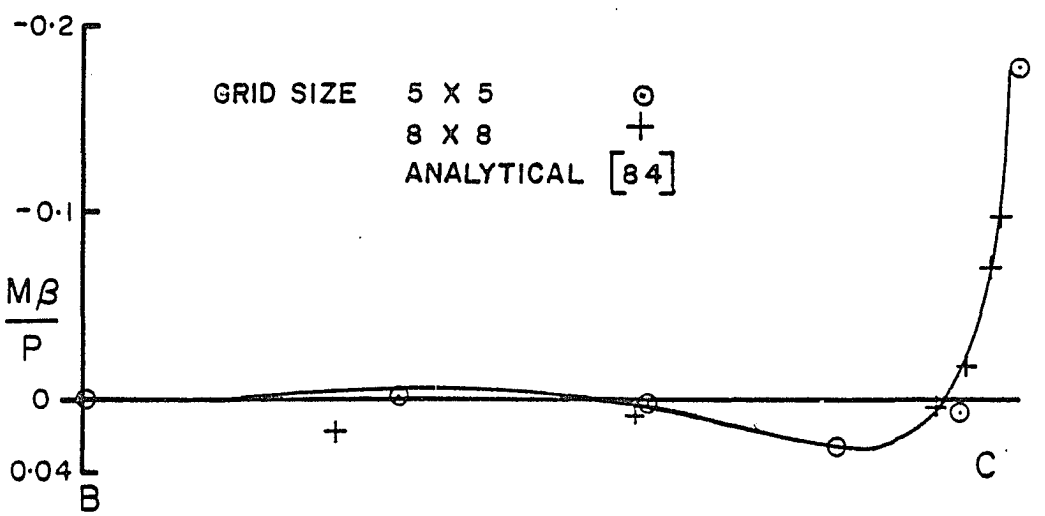

Figure 15.--Continued

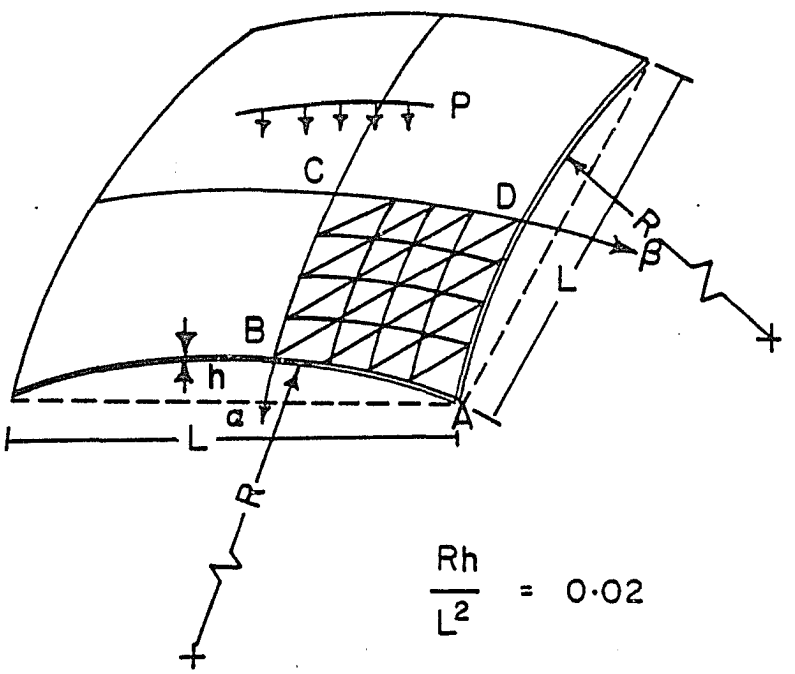

$$\frac{Rh}{L^2} = 0.02$$

$$R = 50.0$$

$$R/h = 50$$

$$E = 0.3 \times 10^7 \text{ Psi}$$

$$\upsilon = 0.3$$

Figure 16. Spherical cap under uniform pressure.

properties, and a 4X4 uniform grid in the symmetric one quarter of the shell is also shown. The cap is subjected to a uniform pressure, p. In Table 8, the displacements and stress resultants at various points on the shell are compared against the finite element solution of Cowper, Lindberg and Olson [57], and the exact solution of Ambartsumyan [86], also presented in Ref. [57]. The finite element solution is based on the high-precision triangular shallow element using 3X3 grid in the quarter of the shell. The exact solution is in the form of a double sine series.

Comparison of the results in Table 8 shows that good accuracy is obtained for displacements as well as the stress resultants. The small difference in the displacements may be attributed to the fact that in the present formulation the integration is performed over the curved surface of the shell, while the comparison solutions integrate over the base plane.

4.2.2 Spherical Shell Under Internal Pressure

A spherical shell under internal pressure is next considered. The exact solution is a pure membrane state of stress with a value of pR/2 for both the hoop and the meridional stress components at any point in the shell. The present example is a test for the element to represent a constant membrane state of stress.

The spherical shell with the α-β curvilinear coordinate system is shown in Figure 17. In view of the axisymmetric nature of the geometry and the loading, a portion of the shell between two meridians in the upper half of the sphere, as shown in Figure 17, is

Table 8. Comparison of displacements and stress resultants at various points on the spherical cap under uniform pressure.

Grid size	$\frac{Ehw_C}{pR^2}$	$\frac{10N_{\alpha\alpha C}}{pR}$	$\frac{10^3 M_{\alpha\alpha C}}{pRh}$	$\frac{10M_{\alpha\beta A}}{pRh}$	$\frac{N_{\alpha\beta A}}{pR}$	$\frac{10Ehv_B}{pRL}$	$\frac{N_{\alpha\alpha B}}{pR}$	$\frac{N_{\beta\beta B}}{pR}$	$\frac{M_{\alpha\alpha B}}{pRh}$	$\frac{M_{\beta\beta B}}{pRh}$
3X3	0.98885	5.0014	10.4206	0.8154	1.2589	3.8920	0.0046	0.0174	0.0039	0.0133
4X4	0.99438	4.9946	9.3658	0.9309	1.2392	3.8965	0.0036	0.0121	0.0035	0.0104
5X5	0.99543	4.9915	8.9718	0.9878	1.2244	3.89748	0.0026	0.0085	0.0034	0.0114
Cowper [57]	1.00982	5.1112	8.873	1.165	1.229	3.6774	0.0043	0.0144	0.0004	0.0014
Exact [86]	1.00979	5.0494	8.487	1.059	1.159	3.6794	0.0000	0.0000	0.0000	0.0000

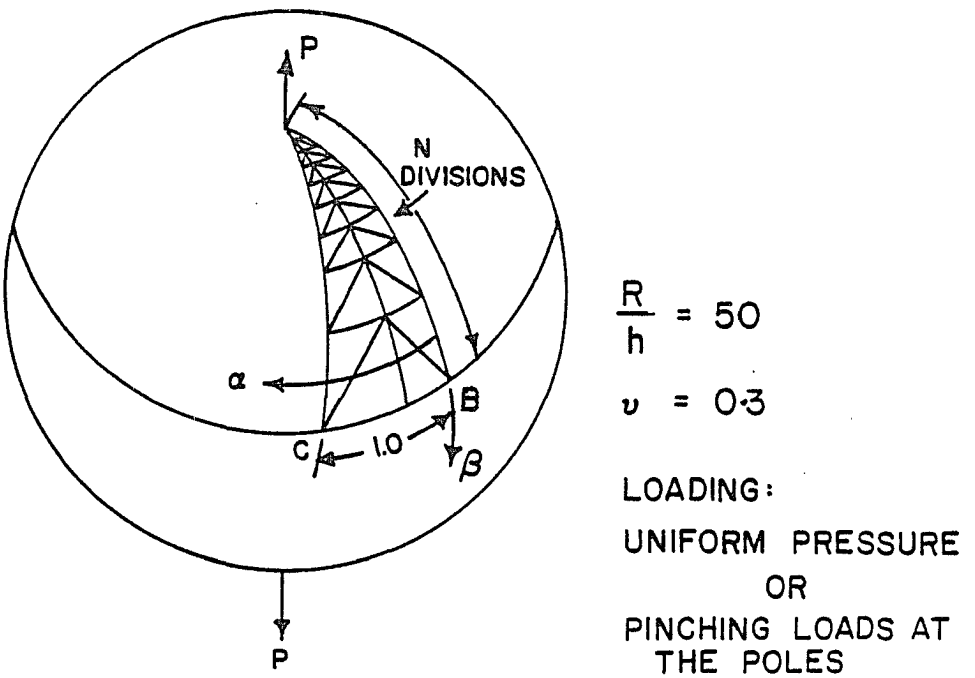

Figure 17. Spherical shell with a typical finite element mesh.

analyzed. A symmetric, non-uniform grid, with elements crowded near the pole is used.

The displacement and stress resultants at the pole and the equator are compared against the exact solution, in Table 9, for various grid sizes. A fast convergence toward the exact solution is observed. The comparison of stress resultants is apparently better than that of the displacements. The small difference in the displacements in the two solutions may be due to the approximation of the geometry of the shell within the element as a cubic polynomial. An improved result can be obtained by using a refined grid.

Table 9. Comparison of displacements and stress resultants for spherical shell under internal pressure.

Mesh size (No. of Eqs.)	Normal displacement Ehw/pR^2		Stress resultants			
			At pole		At equator	
	At pole	At equator	$\frac{N}{pR}$	$\frac{N}{pR}$	$\frac{N}{pR}$	$\frac{N}{pR}$
2X4 (57)	0.4138	0.3470	0.5276	0.4860	0.5279	0.5194
2X10 (147)	0.35321	0.3457	0.5097	0.4964	0.5173	0.5139
2X15 (222)	0.35079	0.34506	0.5056	0.5005	0.51700	0.5135
Exact	0.3500	0.3500	0.5000	0.5000	0.5000	0.5000

4.2.3 Spherical Shell Under Pinching Loads at the Poles

The problem of a pinched spherical shell poses difficulties in as much as it contains regions with predominantly bending stresses within 20 degrees from the pole, followed by the region of predominantly membrane action up to the equator. A region of high stress concentration also exists near the pole.

The geometric and material properties, and the finite element grid are same as in the case of uniform pressure. The displacements and stress resultants at various points in the shell are presented in Table 10 along with the analytical solutions.

Table 10. Comparison of displacements and stress resultants for spherical shell under pinching loads.

	Normal displacement Ehw/P		Stress resultants			
			At pole		At equator	
Mesh size	At pole	At equator	$\frac{RN_{\alpha\alpha}}{P}$	$\frac{RN_{\beta\beta}}{P}$	$\frac{RN_{\alpha\alpha}}{P}$	$\frac{RN_{\beta\beta}}{P}$
2X10	23.1573	-0.2069	12.5644	10.1333	0.16177	0.16373
2X15	22.5941	-0.2069	10.6681	9.8286	0.15895	0.15927
Comparative Solutions	21.2004 [87]	-0.2069	9.883 [56]		0.152 (Membrane [56])	
	20.654 [82]	(Membrane [56])				

Two analytical solutions are customarily considered for the region near the pole. The first one is the asymptotic solution due to Koiter [87] for the normal displacement at the pole. The displacement and stress distributions are, however, extremely difficult to calculate from Koiter's solution. Such distributions for displacements are usually calculated using the second, the shallow shell, solution of Timoshenko and Woinowsky-Kreiger [82]. The latter solution is approximately three percent lower than the Koiter solution for the normal displacement under the load. For regions of membrane action near the equator, the membrane solution is almost exact.

The results in Table 10 show the uniform convergence of the present finite element solution toward the analytical solutions. The convergence of the solutions for the points on the equator is fast. Due to the severe stress gradients, and high stress concentration near the pole, the convergence is rather slow near the poles. An improved accuracy can, however, be achieved by increasing the number of elements in the meridional direction.

The normal displacement distribution near the pole, along with the shallow shell solution of Timoshenko and Woinowsky-Kreiger [82], is shown in Figure 18. The present solution follows the trend of the shallow shell solution, and is slightly above the latter, as expected. Figure 19 shows distributions for the regions remote from the pole, along with the membrane solution, reported in Ref. [56]. The agreement between the two is almost perfect.

The bending moment distributions near the poles, along with the asymptotic solution of Flügge [88], are plotted in Figure 20.

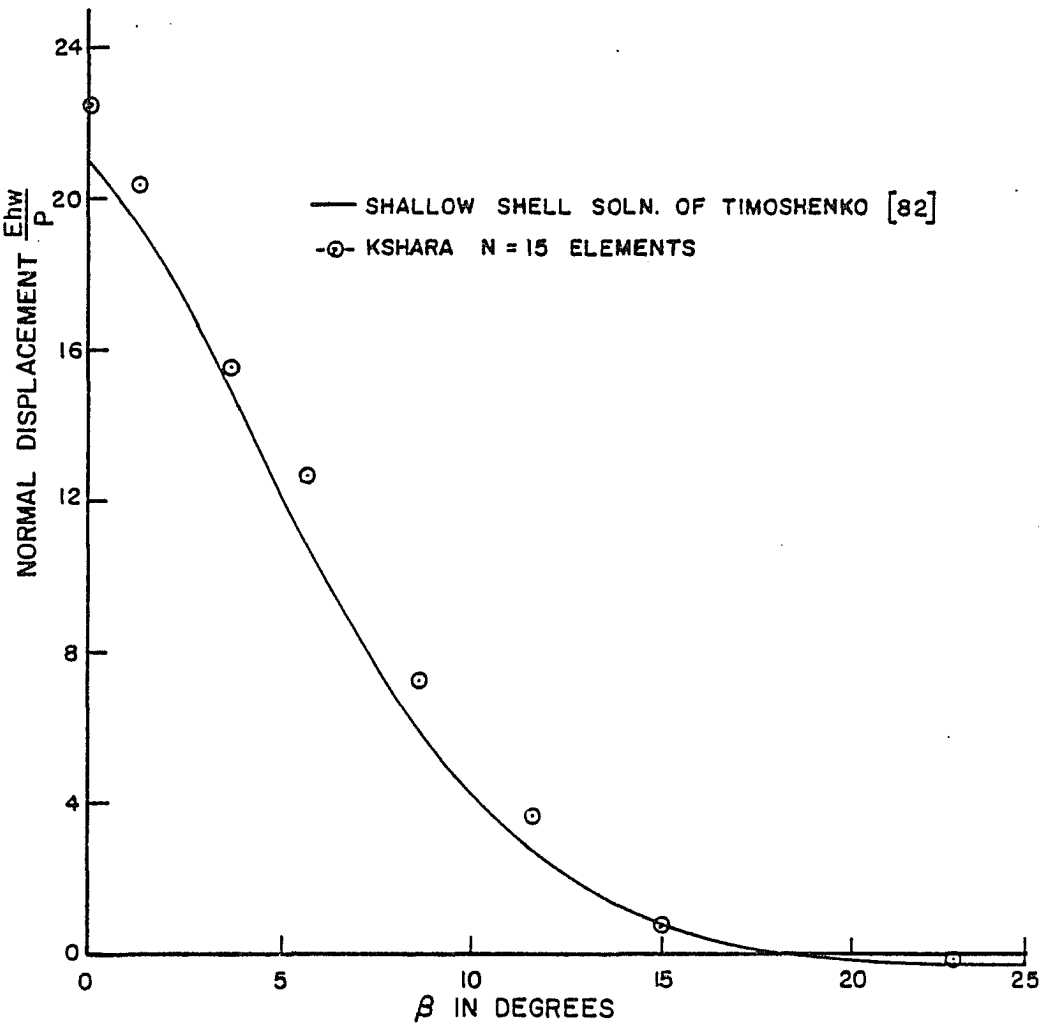

Figure 18. Normal displacement near pole of the pinched sphere.

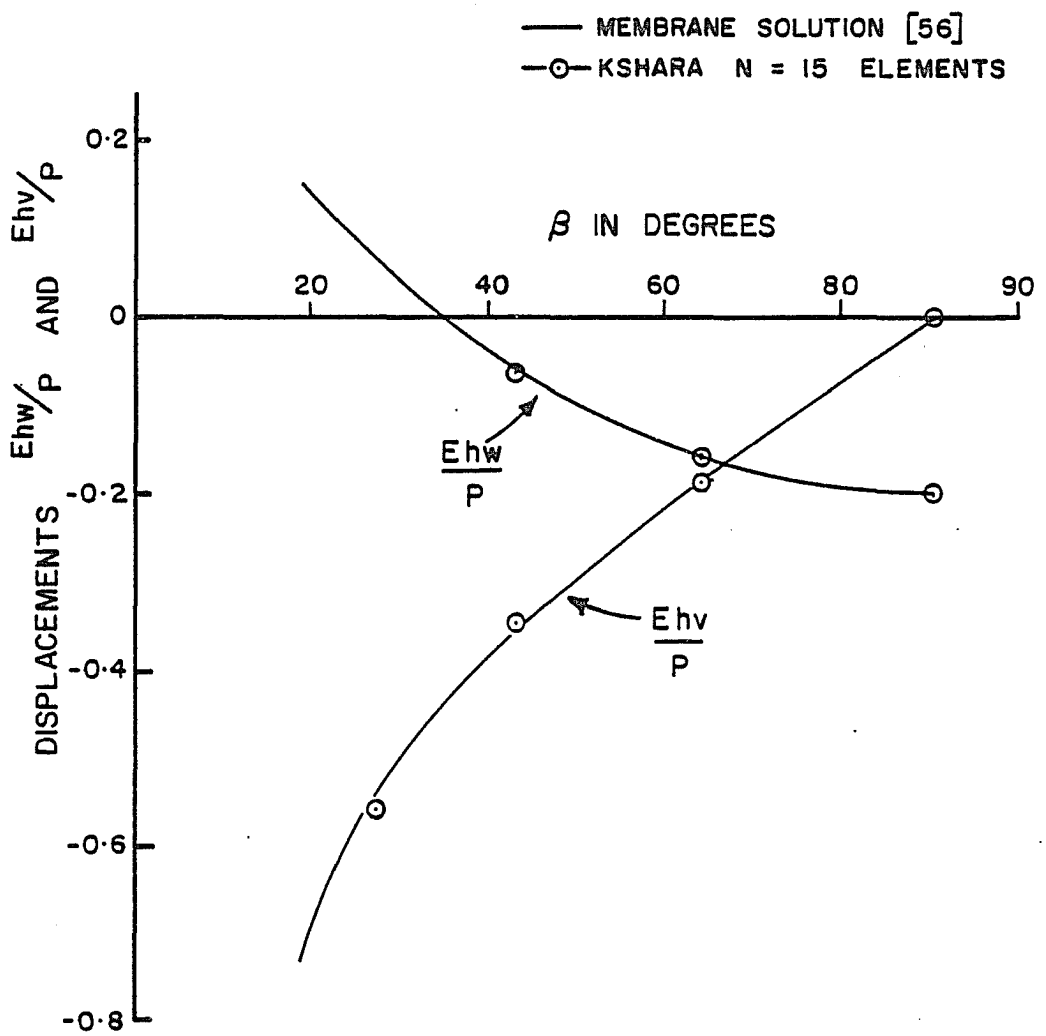

Figure 19. Displacements remote from pole of the pinched sphere.

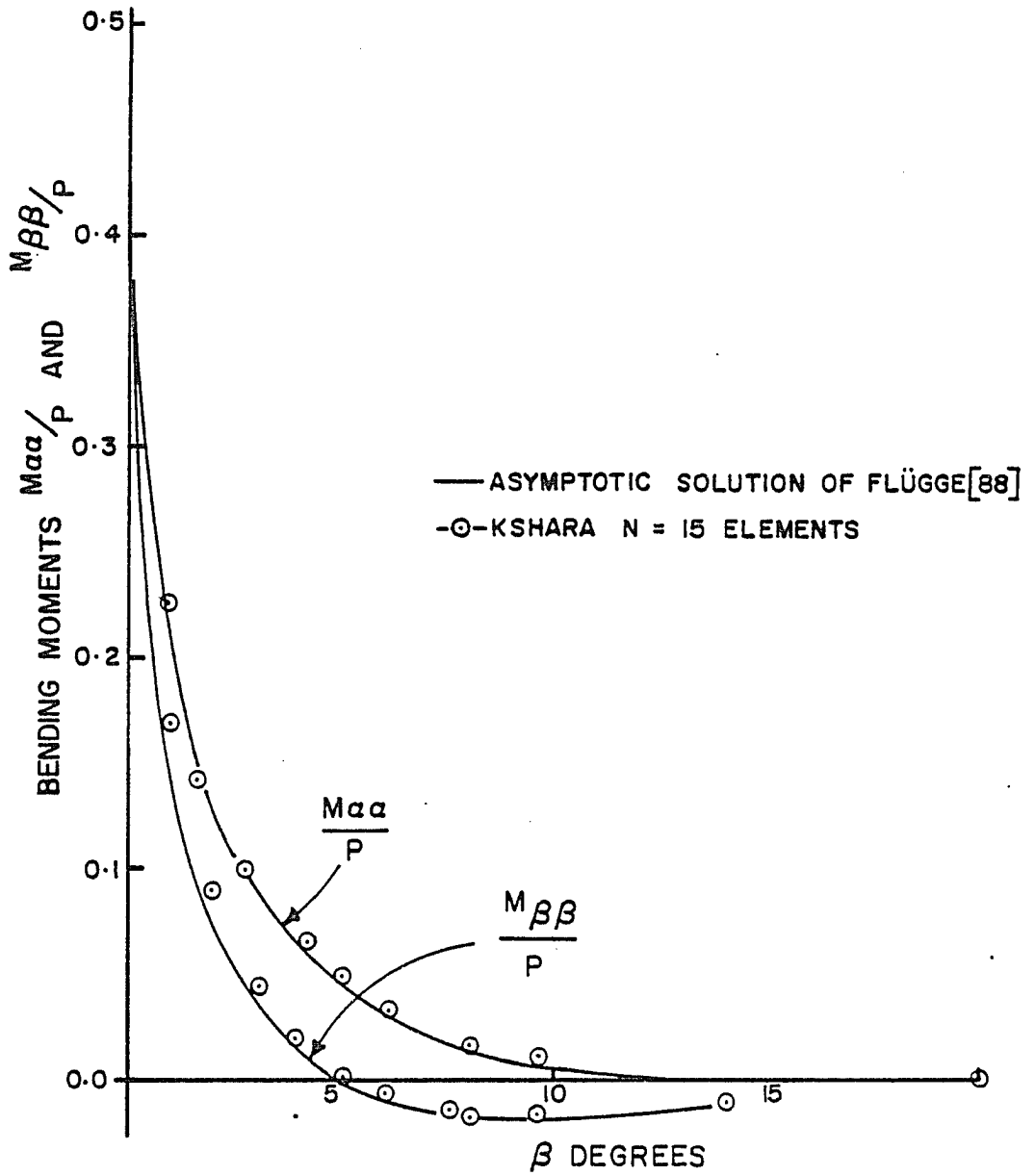

Figure 20. Bending moments near pole of the pinched sphere.

There is a close agreement between the two solutions. Such distributions are also shown for the membrane stress resultants in Figure 21. It may be noted that bending moments are predominant near the poles, and a satisfactory prediction is obtained for the same.

Figure 22 shows the membrane stress resultants for the region remote from the poles, along with the membrane solution. Again, the two solutions agree very closely.

The present example shows the ability of the new element to give good solution for problems, where regions of stress concentration and severe stress gradients exist.

4.3 Torus Under Internal Pressure

The analysis of a toroidal shell subjected to internal pressure is considered next. It is a special property of this shell that there are regions of both positive and negative Gaussian curvature.

The torus is a shell of revolution, obtained by rotating a circle about a vertical axis outside the plane of the circle, as shown in Figure 23. The parameters for the surface representation are conveniently chosen as the angles α and β, also shown in the same figure. The curves α = const. and β = const. represent the lines of curvature, and coincide with or are normal to the lines of symmetry. The torus is defined by the linear dimensions a and b shown in Figure 23, along with the geometric and material parameters of the shell considered.

In view of the horizontal plane of symmetry, and the axisymmetric loading, a sector of the shell with an included angle

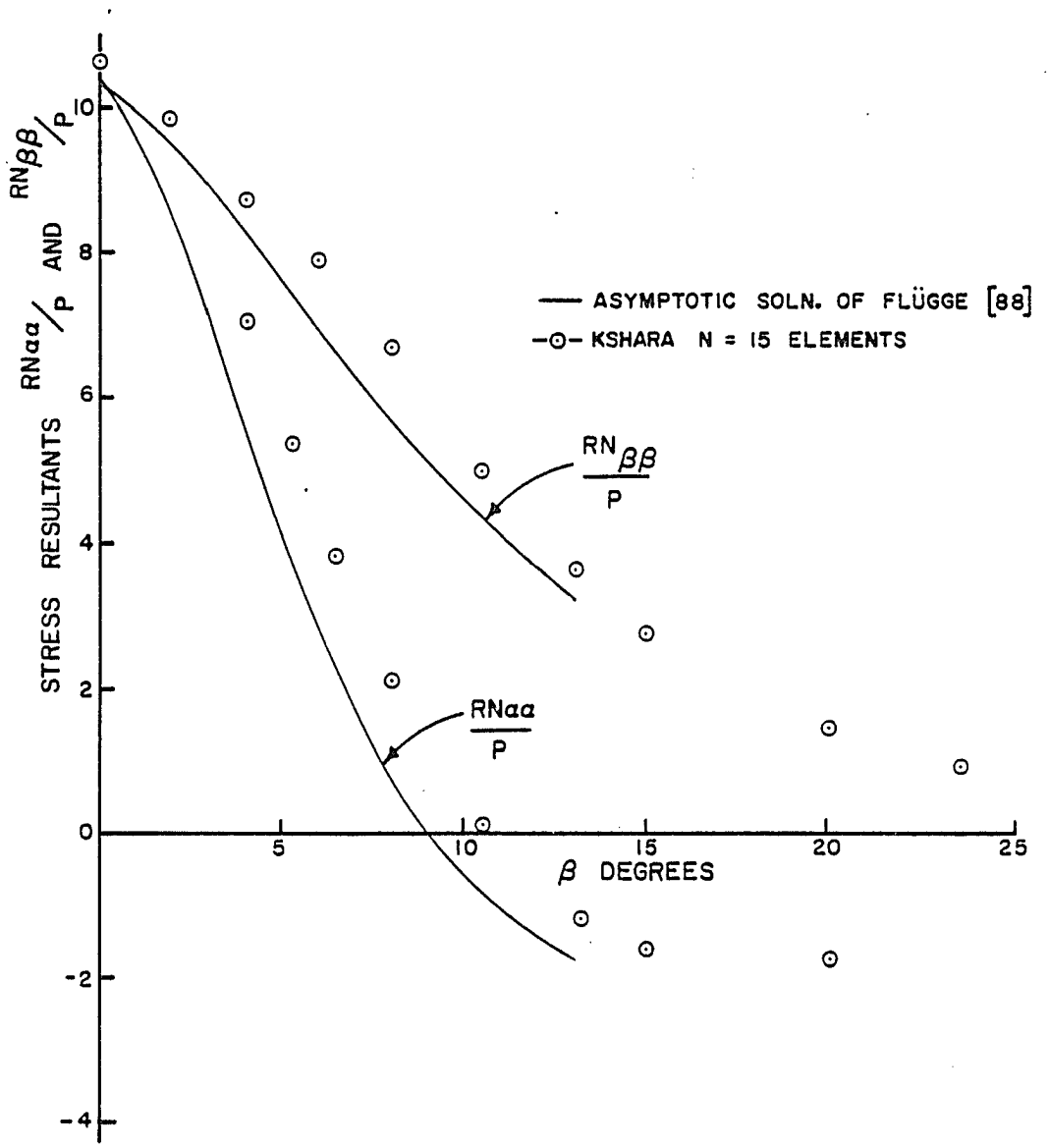

Figure 21. Membrane stresses near pole of the pinched sphere.

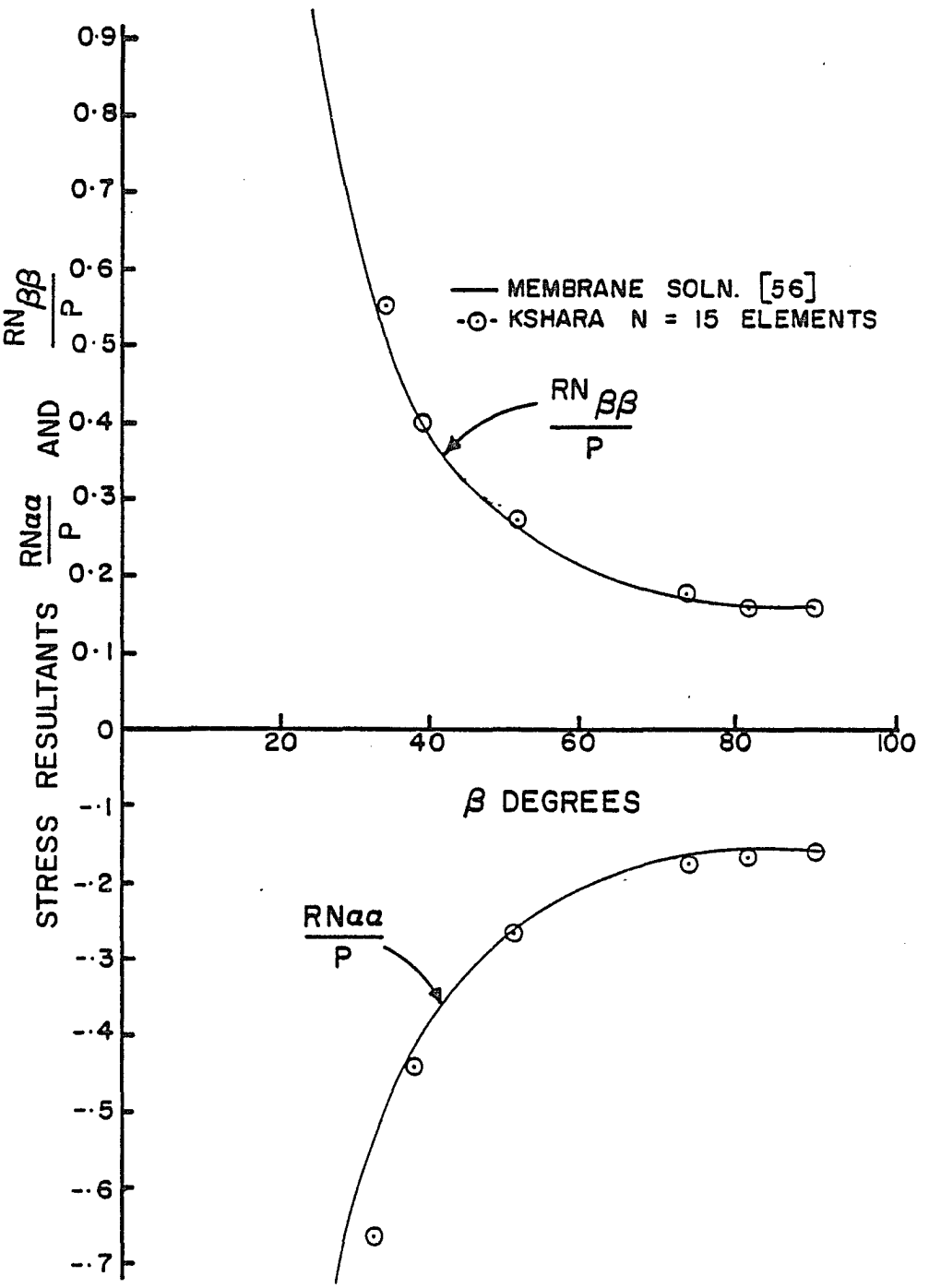

Figure 22. Membrane stresses remote from pole of the pinched sphere.

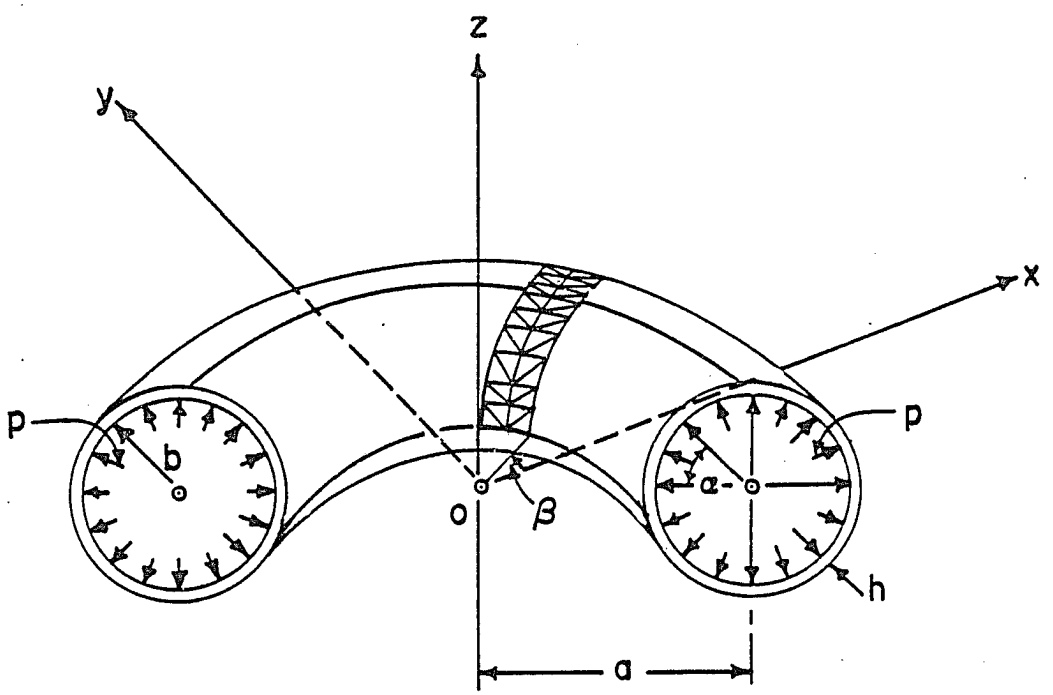

PARAMETRIC EQUATIONS

$x = (a - b \cos\alpha) \cos\beta$

$y = (a - b \sin\alpha) \sin\beta$

$z = b \sin\alpha$

$\frac{a}{b} = 1.5, \quad a = 100$ in

$\frac{h}{b} = 0.05$ & 0.005

$\frac{pb}{Eh} = 0.002$

$\nu = 0.3$

Figure 23. Torus under internal pressure.

of 8 degrees is selected for the analysis. A symmetric mesh with a total of 15 divisions in the meridional direction, with the orientations as shown in Figure 23, is considered. The mesh is nonuniform, being crowded toward the point $\alpha = 90°$, but maintaining symmetry on either side of it.

The displacements and stresses at various points in the shell are compared with the alternative numerical solution due to Kalnins [89], as displayed in Table 11. Kalnins' numerical approach is referred to as "multi-segment integration" method, where the axisymmetric shell equations are numerically solved by combining the direct-integration approach with a finite difference scheme. The comparison of results is presented for two values of the parameter h/b: 0.05 and 0.005. The maximum bending stress in the thicker shell is about 22 percent of the corresponding membrane stress, and it is about half of this for the thin shell [89].

A study of the results in Table 11 shows that very good agreement between the present finite element solution and the comparative solution has been achieved for both the displacement and stress components. In Figure 24, the normal displacement distribution along the meridian is compared with that of the Kalnins' solution.

A comparison of meridional stress distributions is presented in Figure 25. The membrane stress distribution agrees almost perfectly; the bending stress distribution is also reproduced very closely. A sharp rise in the bending stress near the region of $\alpha = 90°$ is observed. As noted by Kalnins [89], this is in agreement with the observation of Gol'denveizer [27] that, when the middle

Table 11. Comparison of displacements and stress resultants for torus under internal pressure.

Meridional angle degrees	(a) Comparison of normal displacement		(b) Comparison of meridional stresses			
	Normal displacement $\frac{w}{b}\times10^3$		Meridional membrane stress $(\sigma_{1m}/E)\times10^3$		Meridional bending stress $(\sigma_{1b}/E)\times10^3$	
	$\frac{h}{b}=0.05$	$\frac{h}{b}=0.005$	$\frac{h}{b}=0.05$	$\frac{h}{b}=0.005$	$\frac{h}{b}=0.05$	$\frac{h}{b}=0.005$
0	0.1036 (0.103)[a]	0.10055 (0.1000)	3.982	3.996 (3.997)[a]	--	--
81	4.1991 (4.208)	5.060 (5.151)	1.8573	2.170 (2.104)	2.058 (2.053)	1.509 (1.520)
180	1.2574 (1.249)	1.3017 (1.298)	1.6106	1.607 (1.601)	--	--

[a]Values in the parentheses from Ref. [89].

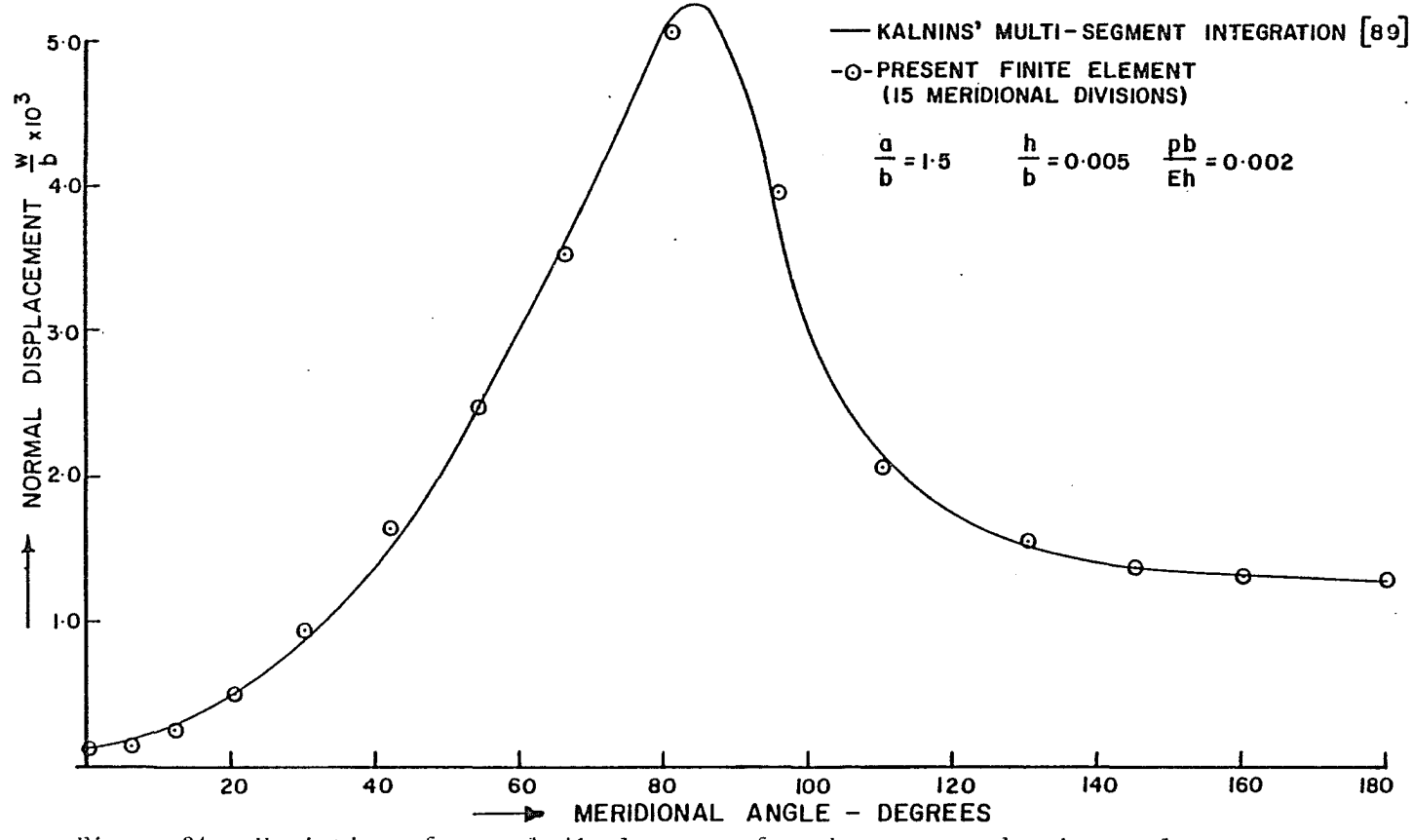

Figure 24. Variation of normal displacement for the torus under internal pressure

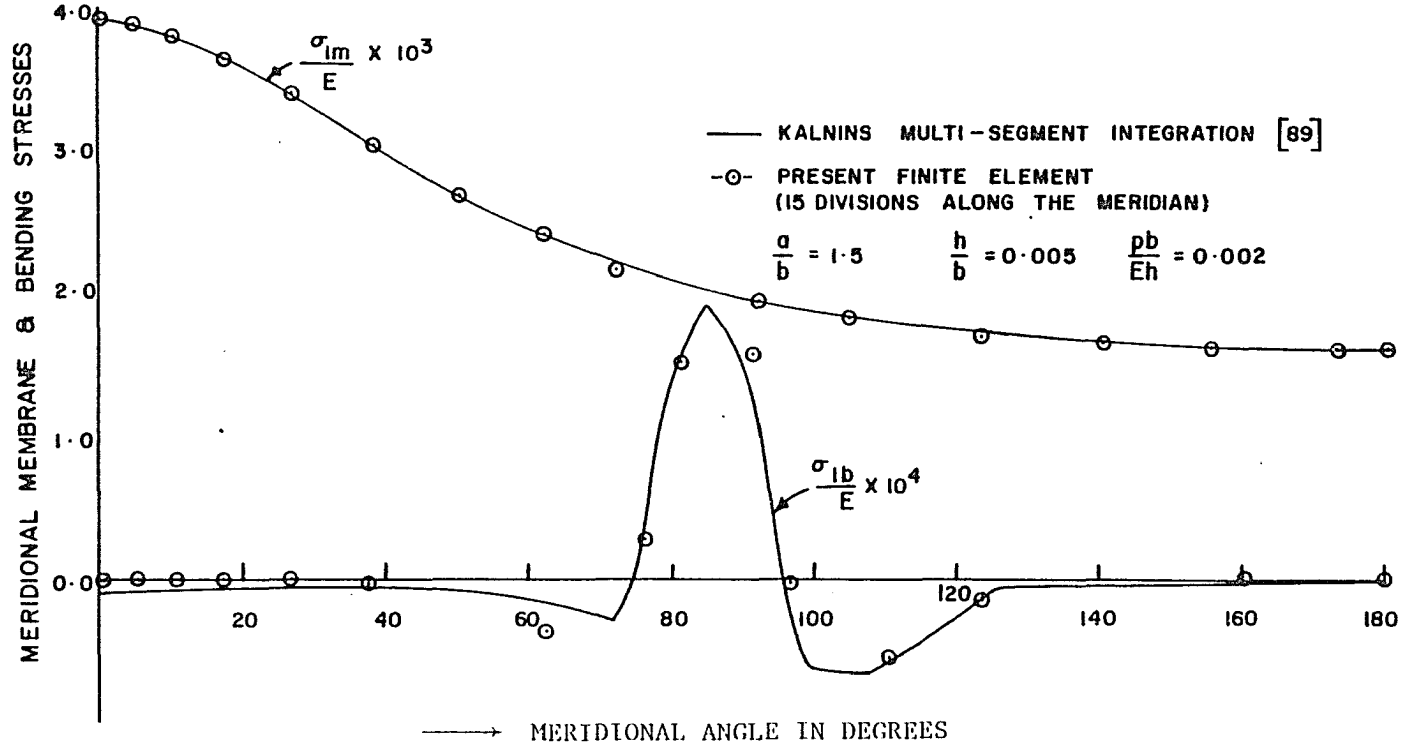

Figure 25. Variation of meridional membrane and bending stresses for the torus under internal pressure.

surface touches a plane-closed curve (which in a torus corresponds to $\alpha = 90°$), then in the vicinity of this point bending stresses should be expected, and the membrane theory is not applicable.

4.4 Hyperbolic Cooling Tower Under Wind Load

A hyperbolic cooling tower, which belongs to the class of shells with negative Gaussian curvature, subjected to wind loading is chosen as the practical shell analysis example problem. The geometry and loading of the shell shown in Figures 26 and 27 conform to that of the Central Electricity Generating Board in England. The tower is subjected to a wind loading, which is uniform over the height and symmetric around the circumference, as shown in Figure 27.

The circumferential angle, α, and the nondimensional height measured from the throat, β, are chosen as the surface parameters. The parametric curves α = const. and β = const., which are hyperbolas and parallel circles, respectively, are the lines of curvature, and hence are orthogonal.

In view of the symmetry of the loading about the vertical plane through the meridians at $\alpha = 0°$ and $180°$, one-half of the shell is discretized using a 6X11 finite element grid. The nonuniform finite element mesh is crowded near the base of the tower, as shown in Figure 28. The grid contains 132 elements with 84 nodal points, leading to 629 equations after the boundary suppressions corresponding to the clamped base.

The cooling tower is analyzed for the wind loading with the Batch and Hopley wind pressure distribution [90]. shown in Figure 27b,

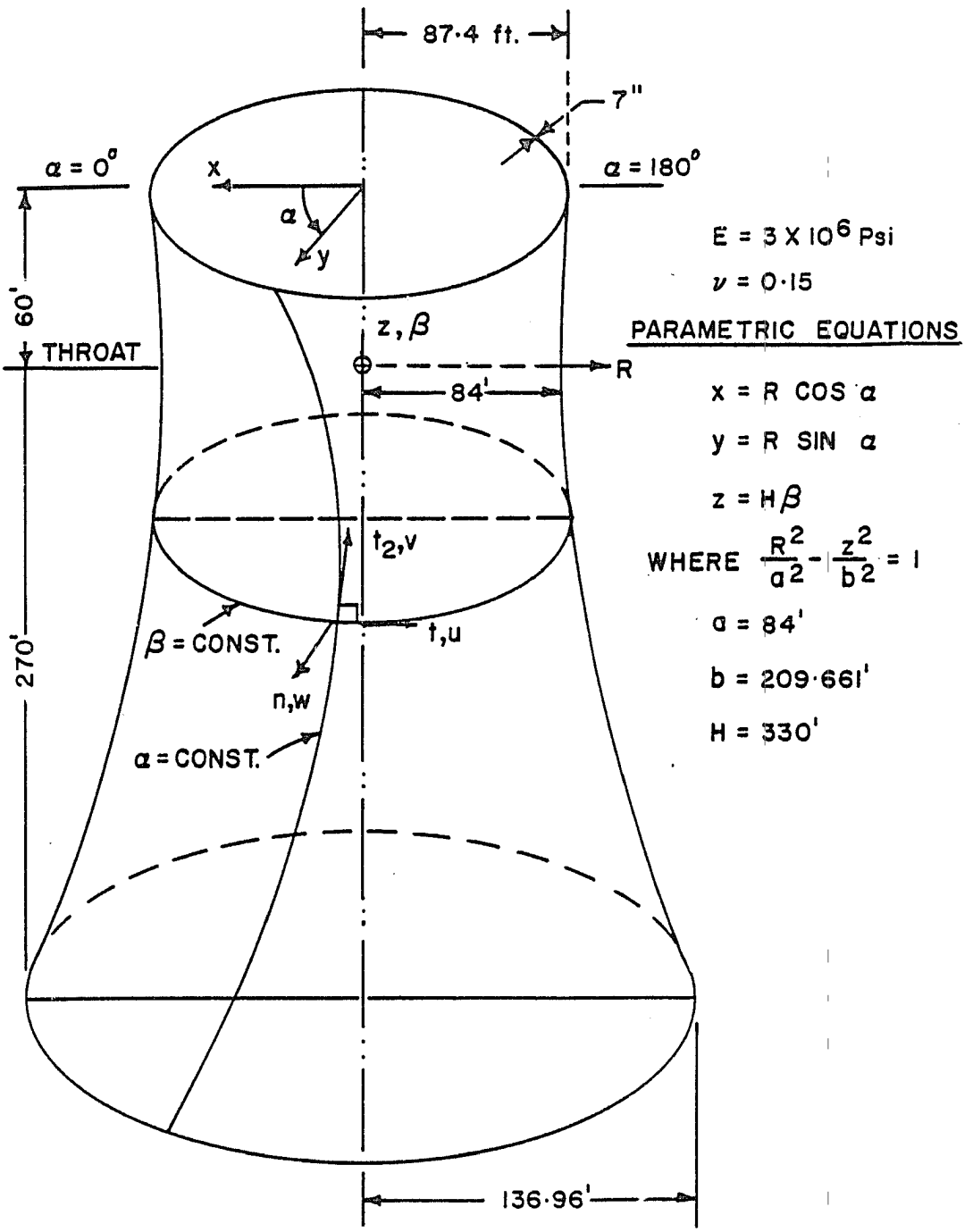

Figure 26. Hyperbolic cooling tower.

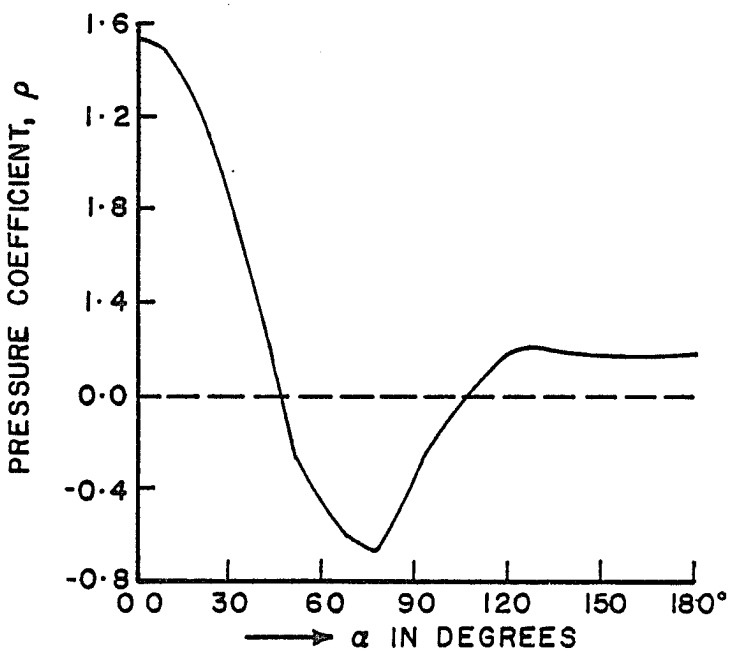

(a) LEAST SQUARES FIT TO THE BATCH AND HOPLEY DISTRIBUTION

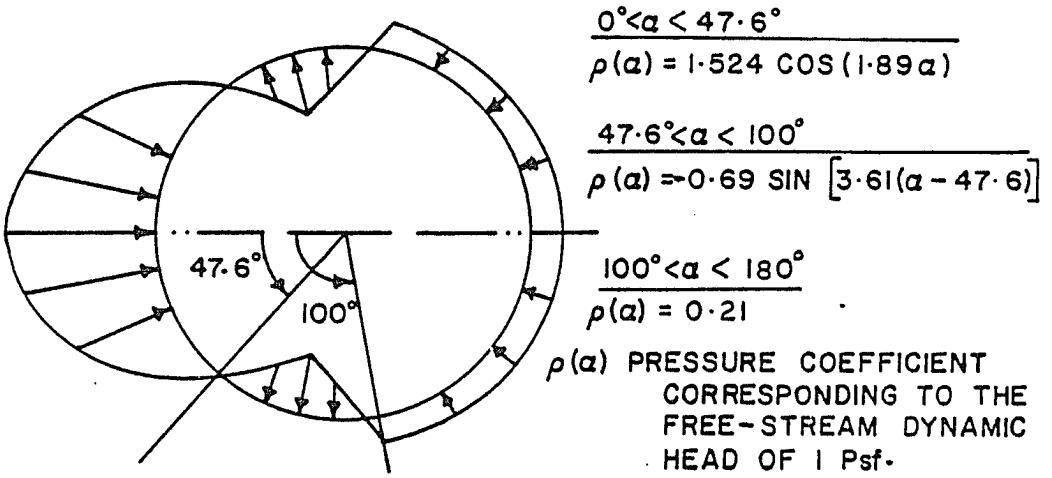

(b) ACTUAL PRESSURE DISTRIBUTION

Figure 27. Batch and Hopley wind pressure distribution.

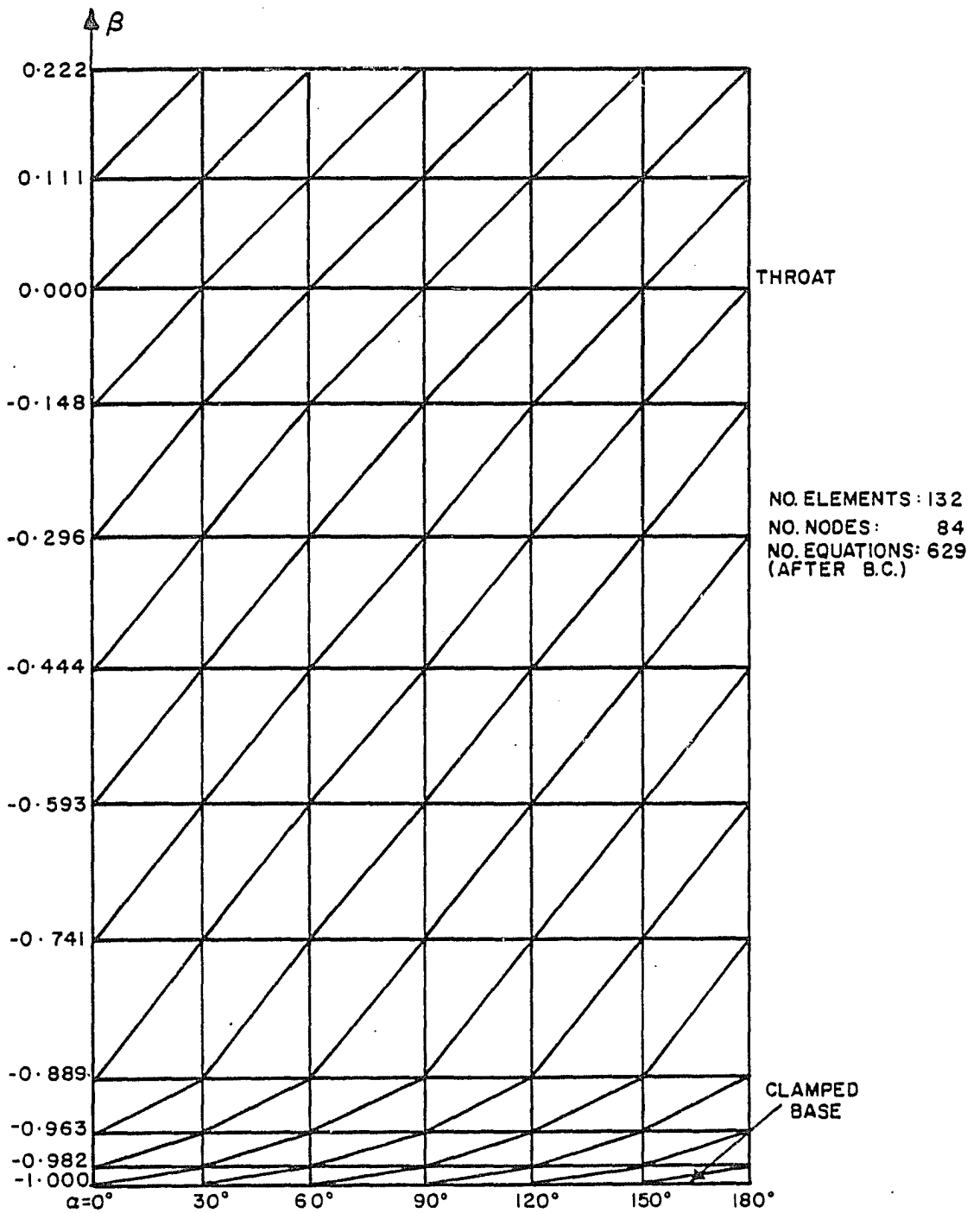

Figure 28. Finite element (6X11) grid in one-half of the hyperbolic cooling tower.

for a free stream dynamic head of = 1 psf. A least squares fit to this distribution is also shown. This pressure distribution relates to wind tunnel studies of an isolated tower without any opening at the base in a steady uniform air-stream at high Reynolds number [90].

In the present analysis, the consistent load vector corresponding to the actual Batch and Hopley distribution for a free stream dynamic head of 100 psf is calculated.

Many earlier researchers [21, 58, 90] have used this problem in their analytical or finite element investigations. The results reported, however, are all in the graphical form, and one can hardly make any meaningful comparisons. To alleviate this difficulty, an accurate alternative finite element solution was generated using the high-precision CURSHL element of Cowper [33]. A converged solution based on Koiter-Sanders theory was obtained, using a 6X13 grid resulting in 1005 algebraic equations. The loading representation in both the solutions was identical.

The normal displacement distribution along the windward meridian, along with the CURSHL solution is shown in Figure 29a. The maximum normal displacement occurs at a point approximately 30 ft below the throat. The two solutions agree very closely. The horizontal displacement distribution along the top of the cooling tower is compared in Figure 29b.

The variation of the membrane stress resultants along the windward meridian is plotted in Figure 30. The meridional component is the predominant stress, which is maximum at the base, and falls very rapidly toward the throat. It is observed that the agreement

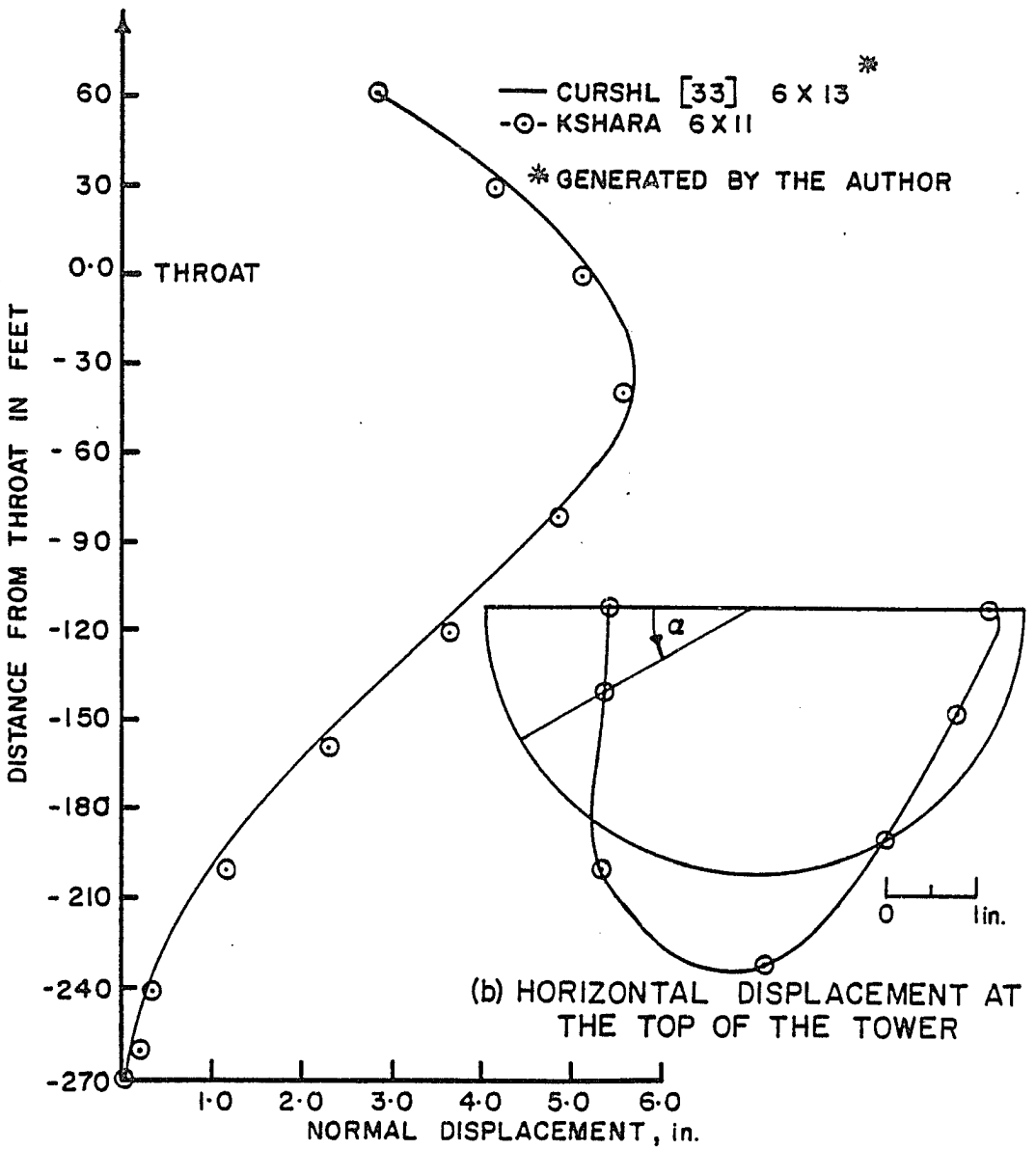

Figure 29. Distribution of normal displacement for the hyperbolic cooling tower under wind load.

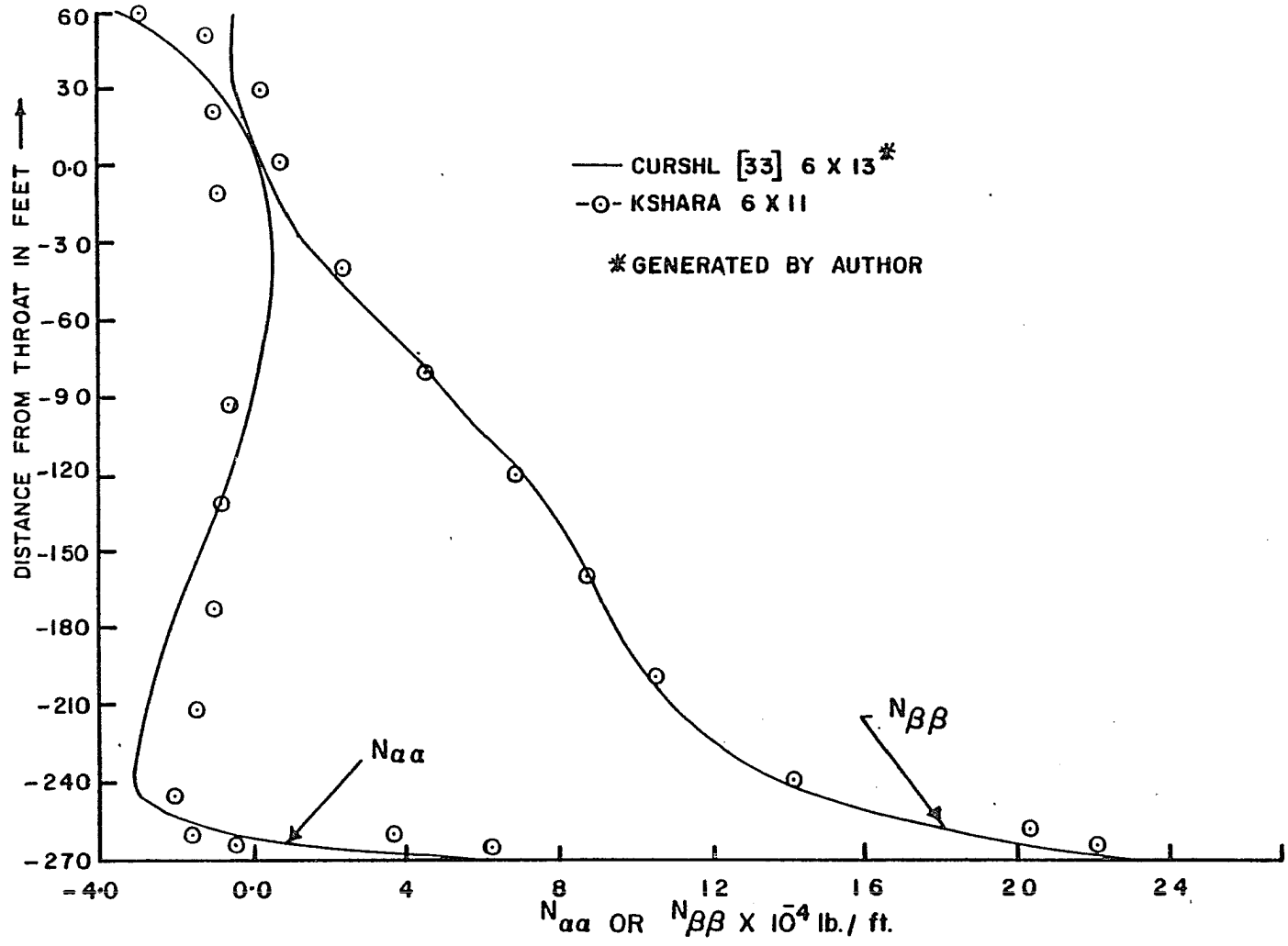

Figure 30. Membrane stress distribution along the windward meridian ($\alpha = 0°$) for the hyperbolic cooling tower under wind load.

between the two solutions for this stress component is very good. The hoop stress variation follows the comparative solution in the critical regions. The maximum hoop stress is only about 20 percent of the peak meridional stress.

The meridional bending moment distribution along the windward meridian is shown in Figure 31. There is a good agreement between the solutions compared, except for the region near the base where the variation is extremely rapid. This variation could be reproduced by using a very fine mesh in this region.

This problem demonstrates the ability of the present element to give a satisfactory solution to practical shell problems.

4.5 Pear-Shaped Cylinder Subjected to End-Shortening

To demonstrate the ability of the new element to model shells of general shape, a pear-shaped cylinder subjected to uniform end shortening of 2×10^{-5} in is considered. This problem was proposed by Hartung and Ball [91] as a bench-mark problem for new shell elements, and has been used by many researchers [34, 40, 92] to evaluate their elements.

The geometric and material parameters of the cylinder are shown in Figure 32a. The circumferential angle, α, and the non-dimensional length, $\beta = Z/L$, are used as the parameters for the surface representation. In view of the symmetry, one quarter of the shell is discretized using a 2X18 finite element mesh as shown in Figure 32b, with 72 elements and 57 nodes resulting in 364 equations after boundary suppressions.

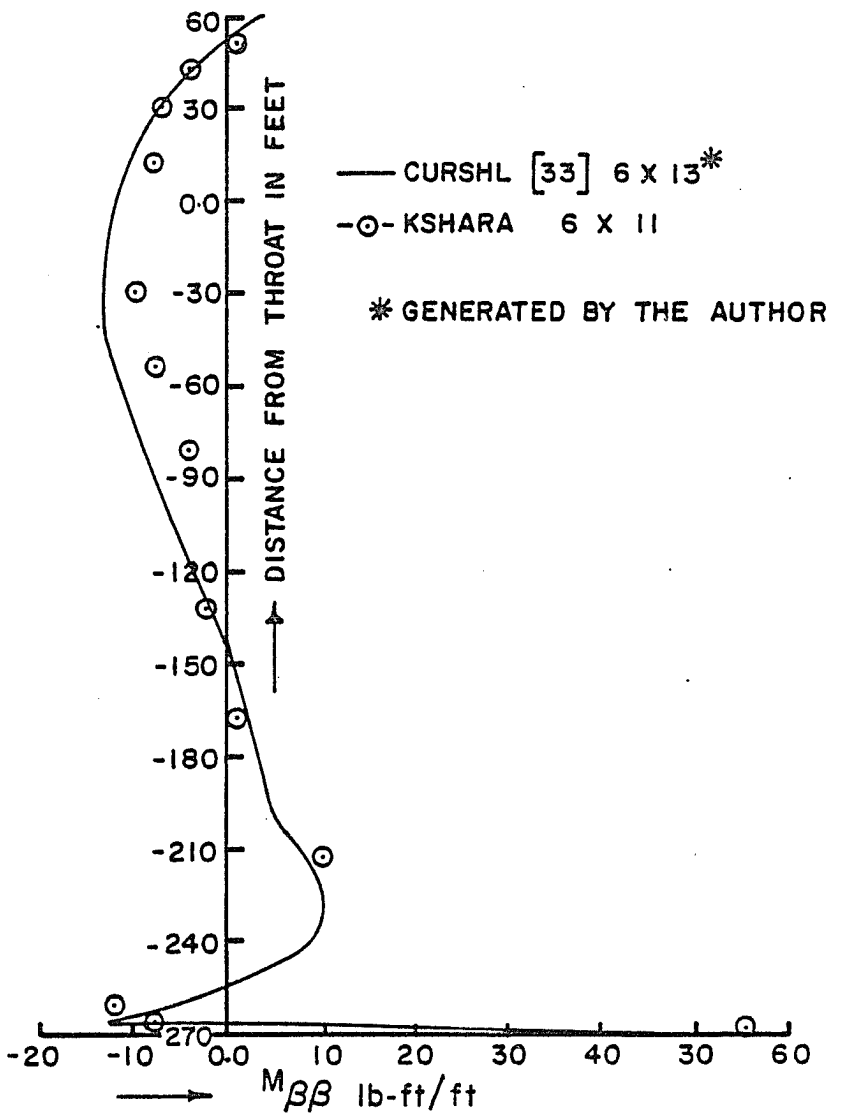

Figure 31. Meridional bending moment distribution along the windward meridian ($\alpha = 0°$) for the hyperbolic cooling tower under wind load.

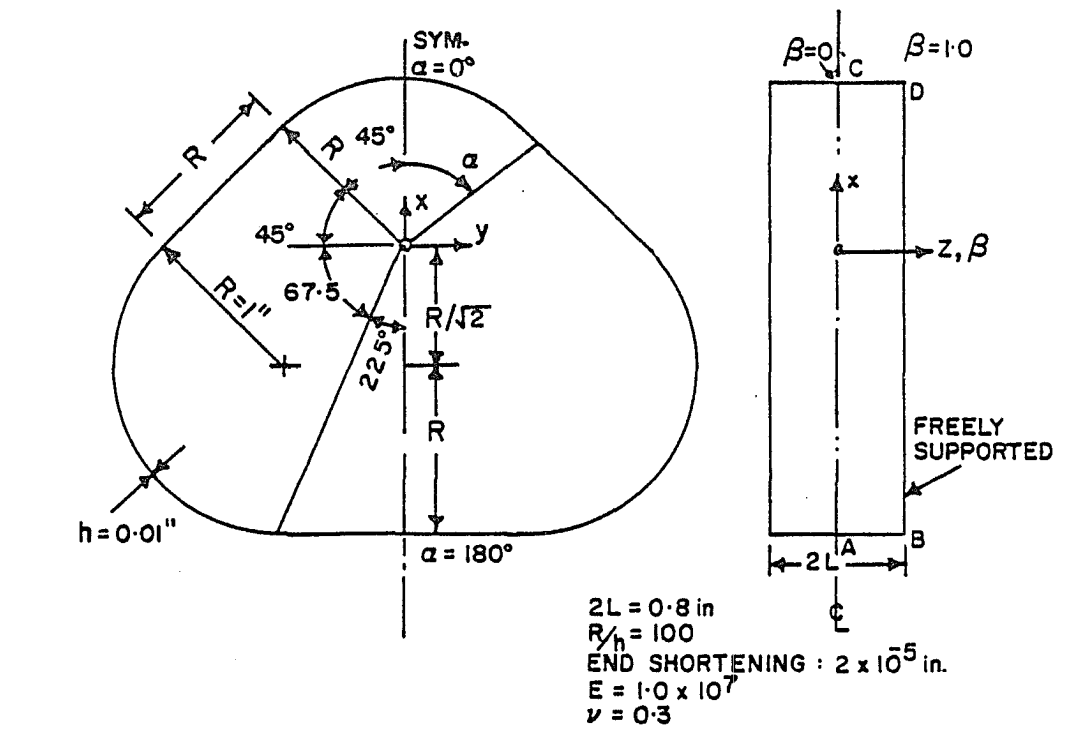

(a) GEOMETRIC AND MATERIAL PARAMETERS

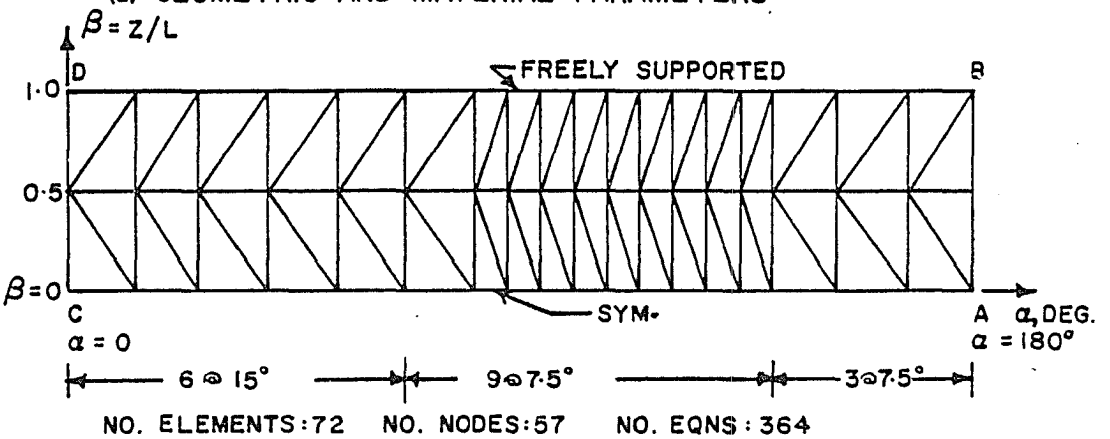

(b) 2 X 18 FINITE ELEMENT GRID IN ONE HALF OF CYLINDER

Figure 32. Pear shaped cylinder subjected to end shortening.

The cylinder ends, which are freely supported, are subjected to an inward axial displacement of $2X10^{-5}$ in at each of the ends.

It is observed from Figure 32a that the curvature in the meridional direction is discontinuous at the junctions of the flat and curved portions. The displacements and their derivatives are, however, continuous at the nodal points, and the curvature discontinuity leads to discontinuous strains and normal rotations at the junctions of flat and curved portions. This condition is not acceptable, since the normal rotations and strains are physically continuous. For convergence of displacements to their correct values, the continuity of the normal rotations and strain at all the points has to be satisfied.

A rigorous satisfaction of the continuity requirements can be achieved by choosing the discontinuous quantities as degrees of freedom, which is, however, tedious. Nevertheless the requirements can be approximately satisfied by uncoupling the degrees of freedom contained in the equations for the meridional components of the membrane strain and normal rotation.

In the present case, the derivatives $\frac{\partial u}{\partial \alpha}$ and $\frac{\partial w}{\partial \alpha}$ are to be uncoupled at the junction points. This is easily accomplished by giving separate equation numbers to these degrees of freedom for the nodes at the junction points. The continuity of other freedoms are, however, maintained as usual.

The variation of the normal displacement at the center section, along with the finite difference solution of STAGS, reported in Ref. [91], is shown in Figure 33. The STAGS solution was obtained

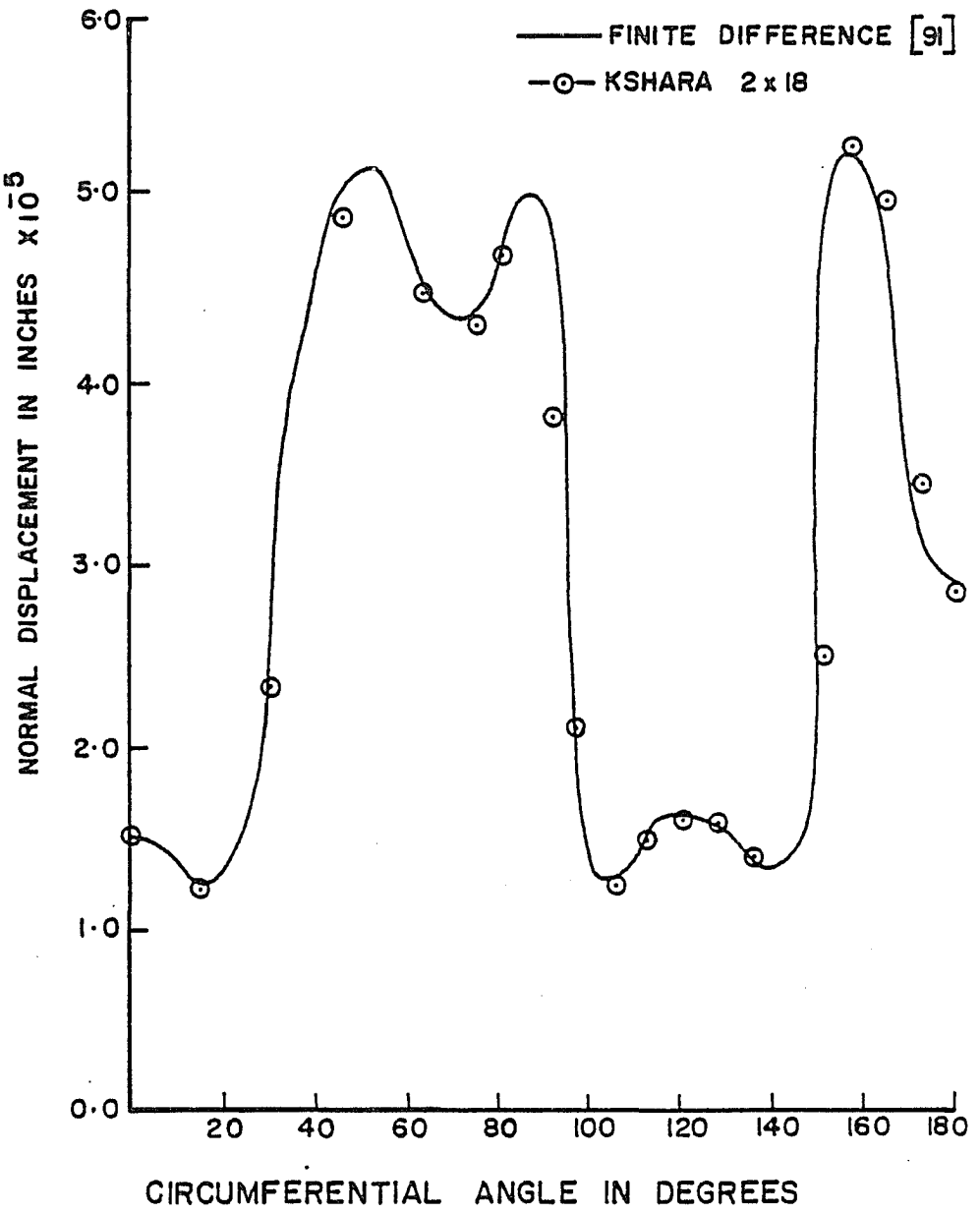

Figure 33. Normal displacement distribution at the center section for the pear-shaped cylinder subjected to end shortening.

by using a 4X40 grid work of whole stations, resulting in 756 degrees of freedom. It is observed that the agreement between the two solutions is satisfactory, and the steep gradients near the junction regions have been reproduced.

4.6 Patch Test Problems for Spherical Shells

In order to develop the confidence in a finite element shell model, it is appropriate to seek procedures for validating them. The validation becomes especially important for shell models based on intuitive or heuristic arguments, and which are not related to classical shell theory.

An indirect approach to verification of the adequacy of a finite element model is by satisfaction of certain numerical tests, which are referred to as patch tests [22]. Patch test solutions are themselves solutions to the classical theory. Very few patch test solutions for shells exist; Morley and Merriefield [93] give patch test solutions for circular cylindrical shells, and, more recently, such solutions are derived by Morley and Morris [30] for spherical shells.

The philosophy of patch test centers upon the requirement that all four characteristic solution modes corresponding to rigid body, inextensional bending, membrane and edge effects are to be properly represented, and are to be recovered by the finite element to within the limitation of accuracy of classical shell theory [30].

The application of the patch test solutions for spherical shells, as derived by Morley and Morris [30], to validate the present

finite element shell model is presented in the following sections. Also, the problem of a hemispherical shell under concentrated loads, as shown in Figure 34, in which the inextensional bending is predominate, also proposed by Morley and Morris [30], is solved.

In plane problems, the patch test concerns rigid body movements, and a set of three linearly independent constant strains and/or curvature changes. In the case of spherical shells, however, such simple state of affairs does not prevail, and one has to resort to strain and curvature changes which are only approximately constant to within the accuracy of the classical shell theory. It is noted that this gives a theoretical limitation on the size of the patch [30].

According to Koiter [6], a relative error of h/R is inherent in the classical shell theory because of the neglected transverse stresses. Since a typical stress resultant N produces a stress of N/h, and a typical stress couple M gives a maximum fiber stress of $6M/h^2$, in view of the above inherent error, it follows that

1. If RN = O(M), then N contributes negligibly to the significant fiber stress. This applies in an essentially inextensional mode.
2. If M = O(kRN), then M contributes negligibly to the significant fiber stress. This applies in an essentially membrane mode.
3. $k = h^2/12R^2$ may be ignored in comparison to unity.

For ordinary engineering purposes, the above accuracy level is too severe when assessing the finite element results; a relative error of five percent is usually acceptable. Then, the above

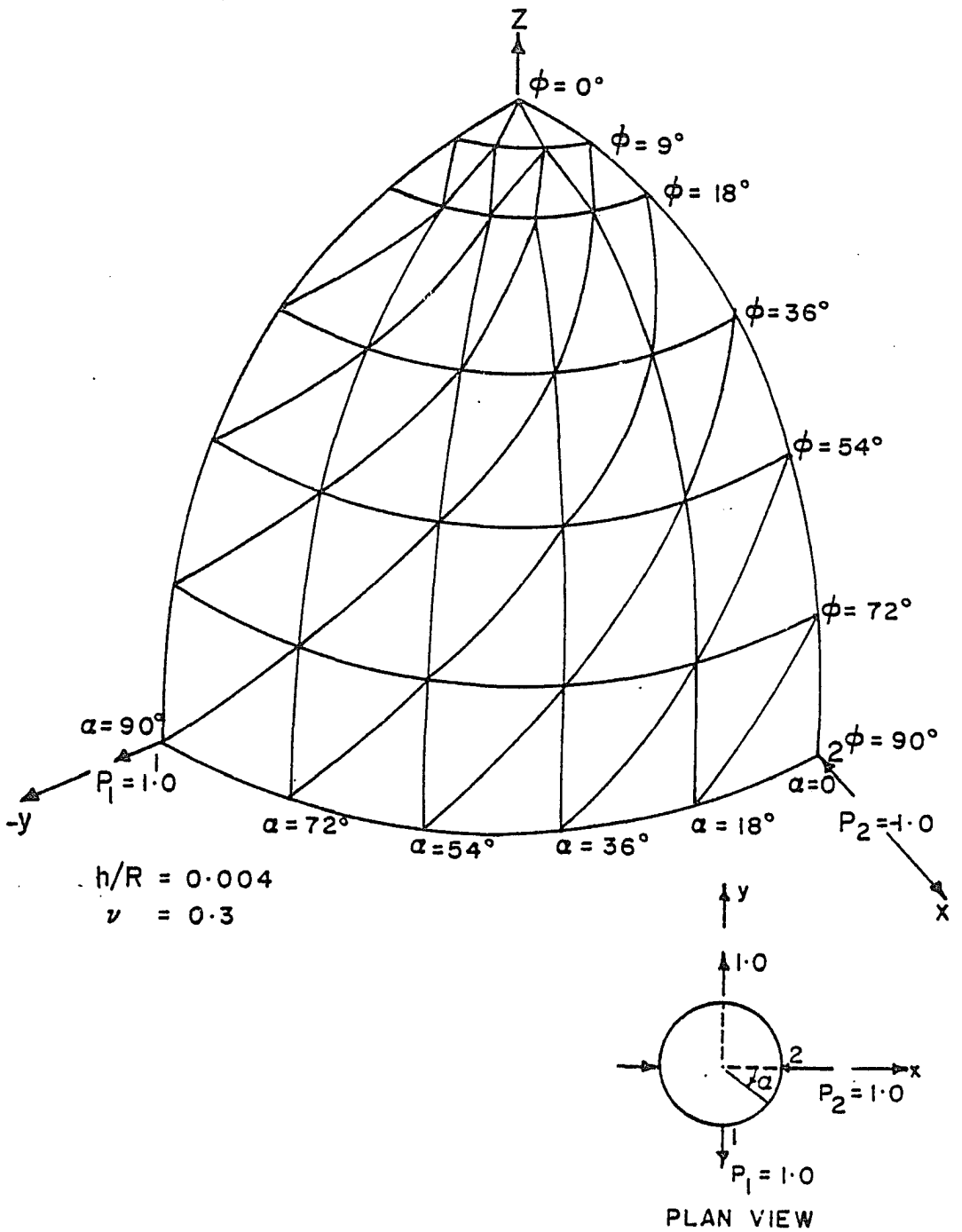

Figure 34. Hemispherical shell subjected to concentrated loads.

conditions are accordingly modified to:

1. If RN < 0.3 (R/h)M, then N contributes less than 5% to the significant fiber stress.
2. If M < 0.1 (R/h)kRN, then M contributes less than 5% to the fiber stress.

Three patch test solutions are considered: (a) inextensional bending, (b) membrane behavior and (c) rigid body motions.

4.6.1 Patch Test Solutions for Inextensional Bending

The basic solutions for the spherical shell in the orthogonal curvilinear coordinates (ϕ,θ), shown in Figure 35, for inextensional bending behavior are given by Flügge [85], and reported in Ref. [30]:

$$u = B \sin\phi \tan^n \frac{\phi}{2} \cos n\theta \tag{4.1}$$

$$v = B \sin\phi \tan^n \frac{\phi}{2} \sin n\theta \tag{4.2}$$

$$w = -B(n + \cos\phi) \tan^n \frac{\phi}{2} \cos n\theta \tag{4.3}$$

where B is an arbitrary constant and n may be positive or negative and is usually an integer. The above displacements give zero value for all the membrane strain components.

Using the above general solutions for displacements, Morley and Morris [30] have derived two patch test solutions for inextensional bending: (a) approximately constant twist curvature and (b) approximately constant bending curvatures. Both the patch test solutions are applied to the present element.

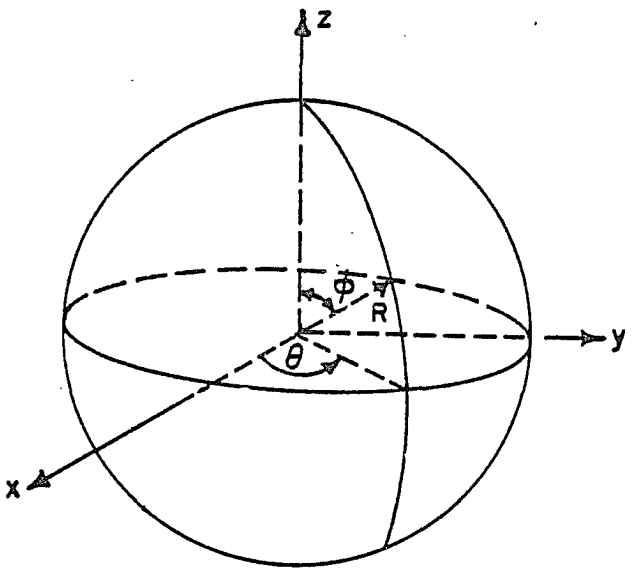

(a) SPHERICAL COORDINATES

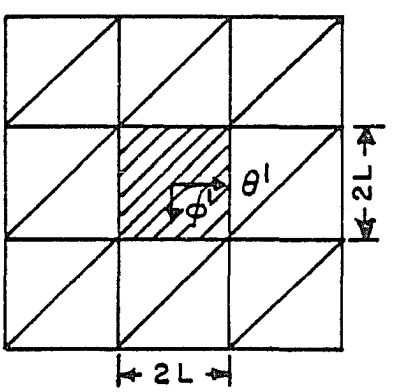

(b) ELEMENT CONFIGURATION FOR PATCH TEST

Figure 35. Spherical coordinate system and the element configuration for the patch test.

4.6.1.1 Constant Twist Curvature Case. A solution where a nearly constant curvature change state with

$$K_{\phi\phi} = K_{\theta\theta} = 0 \qquad K_{\phi\theta} \cong \text{const.} \tag{4.4}$$

is obtained from the general solutions of Eqs. (4.1)-(4.3) as [30]

$$u = -\frac{1}{6}(2 - \sin^2\phi)\,\text{cosec}\phi\,\cos 2\theta \tag{4.5}$$

$$v = \frac{1}{3}\cot\phi\,\sin 2\theta \tag{4.6}$$

$$w = -\frac{1}{6}(2 + \sin^2\phi)\,\cot\phi\,\text{cosec}\phi\,\cos 2\theta \tag{4.7}$$

The tilde above the equal sign in Eq. (4.4) stands for "approximately equal to." The curvature changes due to the above displacements are

$$R^2K_{\phi\phi} = -R^2K_{\theta\theta} = 2\cos\phi\,\text{cosec}^4\theta\,\cos 2\theta \tag{4.8}$$

$$R^2K_{\phi\theta} = (2 - \sin^2\phi)\,\text{cosec}^4\phi\,\sin 2\theta \tag{4.9}$$

From Eqs. (4.8) and (4.9) it is observed that nearly constant curvature changes occur near the origin of the coordinate system (ϕ',θ'), where

$$\phi' = \phi - \frac{\pi}{2} \qquad \theta' = \theta - \frac{\pi}{4} \tag{4.10a,b}$$

and near the origin of the new coordinate system, the curvatures behave like

$$R^2K_{\phi\phi} = -R^2K_{\theta\theta} \cong 4\phi'\theta' \tag{4.11}$$

$$R^2K_{\phi\theta} = (1 + 3\phi'^2)(1 - 2\theta'^2) \tag{4.12}$$

The accuracy of the classical theory allows us to consider

$$R^2K_{\phi\phi} = -R^2K_{\theta\theta} = 0 \qquad R^2K_{\phi\theta} = 1 \tag{4.13a,b}$$

for

$$\max \{|3\phi'^2 - 2\theta'^2|, 4\phi'\theta'\} \leq h/R \tag{4.14}$$

The condition of Eq. (4.14) requires that the dimensions of a square patch of length 2L in the ϕ-θ parametric plane, as shown in Figure 35b, is controlled by

$$L < 0.5\ (hR)^{1/2} \tag{4.15}$$

For a shell with R = 10 and h = 0.04, the curvature changes of Eq. (4.13) may be considered as accurate from the viewpoint of classical shell theory over a total arc of 3.5°. When the engineering accuracy of 5% is sufficient, the total arc length enlarges to 13°.

The application of the patch test solution is carried out on a square patch of elements, whose center is located at the origin of the (ϕ', θ') coordinates. The element configuration is shown in Figure 35b. The nodal values corresponding to the displacements of Eqs. (4.5)-(4.7) are prescribed for the nodes on the boundaries of the patch, and the curvature changes are calculated using the finite element model for the elements at the center of the patch; the average curvatures at their centroids is reported.

The results for this patch test are reported in Table 12 along with the results for other popular elements reported in Ref. [30]. It is observed that KSHARA performs excellently; the error in the stress is well below the allowable 5 percent error, and the

Table 12. Patch test results for spherical shell: inextensional bending with constant $K_{\phi\theta}$.

Element	Angle subtended by element in degrees	Max. percentage error in $K_{\phi\theta}$	Max. percentage error in outer fiber total stress
KSHARA	16	0.30	3.28
	12	0.15	0.72
	8	0.06	0.09
	4	0.01	0.01
SEMILOOF (quadrilateral)	16	0.4	25.0
	12	0.3	8.4
	8	0.2	2.0
	4	0.1	0.2
SEMILOOF (Triangular)	4	> 100	> 100
MSC/NASTRAN	8	0.3	> 100.0
	4	0.4	41.4
	2	0.0	10.2

element size even beyond 16° is acceptable. It is remarkable that even the critical requirement according to the classical theory is met, if we recall that from the classical shell theory viewpoint, the curvature change $K_{\phi\theta}$ remains constant only over a subtended angle of about 3.5° and the permitted percentage error is 0.4%. While the SEMILOOF quadrilateral up to 8° is acceptable, the SEMILOOF triangle with 4° included angle shows gross errors, and MSC/NASTRAN element has 10.2% error with an included angle of 2°.

4.6.1.2 Constant Bending Curvature Case. Another patch test solution which gives approximately constant bending curvatures is obtained from Eqs. (4.1)-(4.3):

$$u = -\frac{1}{3}\cot\phi\cos 2\theta \tag{4.16}$$

$$v = \frac{1}{6}(2 - \sin^2\phi)\,\mathrm{cosec}\phi\sin 2\theta \tag{4.17}$$

$$w = -\frac{1}{3}\mathrm{cosec}^2\phi\cos 2\theta \tag{4.18}$$

The resulting curvature changes near the origin of the coordinate system (ϕ',θ) behave like

$$R^2K_{\phi\phi} = -R^2K_{\theta\theta} \cong (1 + 3\phi'^2)(1 - 2\theta^2) \tag{4.19}$$

$$R^2K_{\phi\theta} = -4\phi'\theta \tag{4.20}$$

The accuracy of the classical shell theory allows us to consider

$$R^2K_{\phi\phi} = -R^2K_{\theta\theta} = 1 \qquad R^2K_{\phi\theta} = 0 \tag{4.21a,b}$$

for

$$\max \{|3\phi'^2 - 2\theta^2|, |4\phi'\theta|\} < h/R \qquad (4.22)$$

and once again the limiting dimensions of the square patch are same as before.

The results for this case are shown in Table 13. It is observed that the element passes the test both from the engineering and classical points of view. No comparative solutions are available.

Table 13. Patch test results for spherical shell: inextensional bending with constant $K_{\phi\phi}$ and $K_{\theta\theta}$.

Element	Angle subtended by element in degrees	Max. percentage error in $K_{\phi\phi}$ or $K_{\theta\theta}$	Max. percentage error in outer fiber total stress
KSHARA	16	3.98	8.4
	12	2.15	2.86
	4	0.2	0.02

4.6.2 Patch Test Solutions for Membrane Stretching

The membrane analysis of a sphere provides three linearly independent and nearly constant strain patch test solutions. Two of these satisfy the homogeneous equations of equilibrium (with zero external forces), and the other corresponds to constant internal pressure loading.

The basic solutions to the spherical shell for membrane behavior are given by Flügge [85], and reported in Ref. [30]:

$$u = A\{(n^2 - 1) + (n + \cos\phi)\} \operatorname{cosec}\phi \tan^n \frac{\phi}{2} \cos n\theta \tag{4.23}$$

$$v = - An(n + \cos\phi) \operatorname{cosec}\phi \tan^n \frac{\phi}{2} \sin n\theta \tag{4.24}$$

$$w = A(n + \cos\phi) \tan^n \frac{\phi}{2} \cos n\theta \tag{4.25}$$

where A is an arbitrary constant. These displacements give zero curvature changes at any point in the shell.

4.6.2.1 Constant Direct Strains (Homogeneous Solution). A patch test solution for membrane behavior with approximately constant direct strains and zero shearing strain is derived from the above general solution [30]:

$$u = - \frac{2}{3} \cot\phi \operatorname{cosec}^2\phi \cos 2\theta \tag{4.26}$$

$$v = - \frac{2}{3} \operatorname{cosec}^3\phi \sin 2\theta \tag{4.27}$$

$$w = \frac{1}{3} \operatorname{cosec}^2\phi \cos 2\theta \tag{4.28}$$

which gives rise to strains

$$R\varepsilon_{\phi\phi} = - R\varepsilon_{\theta\theta} = (2 - \sin^2\phi) \operatorname{cosec}^4\phi \cos 2\theta \tag{4.29}$$

$$R\varepsilon_{\phi\theta} = 2 \cos\phi \operatorname{cosec}^4\phi \sin 2\theta \tag{4.30}$$

and to zero slopes and curvature changes. The coordinate transformation $\phi' = \phi - \frac{\pi}{2}$ allows us to write near the origin of the coordinate system (ϕ', θ)

$$R\varepsilon_{\phi\phi} = - R\varepsilon_{\theta\theta} \cong (1 + 3\phi'^2)(1 - 2\theta^2) \tag{4.31}$$

$$R\varepsilon_{\phi\theta} \cong 4\phi'\theta \tag{4.32}$$

The accuracy of classical shell theory allows us to consider

$$R\varepsilon_{\phi\phi} = - R\varepsilon_{\theta\theta} \cong 1 \qquad R\varepsilon_{\phi\theta} = 0 \tag{4.33}$$

for

$$\max \{|3\phi'^2 - 2\theta^2|, |4\phi'\theta|\} < h/R \tag{4.34}$$

Once again the limiting dimensions of the patch within which the solution is valid is same as for the case of inextensional bending.

The results from the above patch test solution are shown in Table 14; the 16° KSHARA element is acceptable to within classical shell theory accuracy.

4.6.2.2 Constant Direct Strains (Internal Pressure). A spherical shell subjected to constant internal pressure is in a state of membrane stress with zero curvature changes. For an internal pressure p = 1.0, the solution is

$$u = v = 0 \tag{4.34a,b}$$

Table 14. Patch test results for spherical shell: membrane stretching with constant $\varepsilon_{\phi\phi}$ and $\varepsilon_{\theta\theta}$ (homogeneous solution).

Element	Angle subtended by element in degrees	Max. percentage error in $\varepsilon_{\phi\phi}$ or $\varepsilon_{\theta\theta}$	Max. percentage error in outer fiber total stress
KSHARA	16	0.29	0.24
	4	0.013	0.20

$$w = \frac{kR^4}{2D(1+\nu)} \tag{4.35}$$

where

$$k = \frac{h^2}{12R^2} \tag{4.36}$$

and D is the flexural rigidity. The resulting strains are

$$R\varepsilon_{\phi\phi} = R\varepsilon_{\theta\theta} = \frac{kR^4}{2D(1+\nu)} \tag{4.37}$$

$$R\varepsilon_{\phi\theta} = 0 \tag{4.38}$$

with zero curvature changes. The accompanying stress resultants are

$$RN_{\phi\phi} = RN_{\theta\theta} = R^2/2 \tag{4.39}$$

$$RN_{\phi\theta} = 0 \tag{4.40}$$

The patch test results for internal pressure are compared with other solutions [30] in Table 15. KSHARA element up to 16° is

Table 15. Patch test results for spherical shell: membrane stretching with constant $\varepsilon_{\phi\phi}$ and $\varepsilon_{\theta\theta}$ (internal pressure)

Element	Angle subtended by the element in degrees	Max. percentage error in $N_{\phi\phi}$ or $N_{\theta\theta}$	Max. percentage error in outer fiber total stress
KSHARA	16	0.53	0.65
	12	0.31	0.45
	4	0.03	0.26
SEMILOOF (quadrilateral)	16	0.1	0.40
	4	0.0	0.20
SEMILOOF (triangle)	16	8.30	8.50
	4	0.00	0.30
SEMILOOF (quadrilateral facet)	16	> 100.0	> 100.0
	4	0.10	0.20
SEMILOOF (triangular facet)	16	> 100.0	> 100.0
	4	15.80	49.30

acceptable to within classical shell theory accuracy, as are the 16° quadrilateral and 4° triangular SEMILOOF elements. The SEMILOOF facet elements, however, show gross errors.

4.6.3 Patch Test Solutions for the Rigid Body Movements

The finite element must remain stress free under rigid body movement. Rigid body movements for the spherical shell are given below [30]:

$$u = c_1\sin\phi + c_3(1 - \cos\phi)\cos\theta - c_4(1 - \cos\phi)\sin\theta + c_5(1 + \cos\phi)\cos\theta + c_6(1 + \cos\phi)\sin\theta \tag{4.41}$$

$$v = c_2\sin\phi + c_3(1 - \cos\phi)\sin\theta + c_4(1 - \cos\phi)\cos\theta - c_5(1 + \cos\phi)\sin\theta + c_6(1 + \cos\phi)\cos\theta \tag{4.42}$$

$$w = - c_1\cos\phi - c_3\sin\phi\cos\theta + c_4\sin\phi\sin\theta + c_5\sin\phi\cos\theta + c_6\sin\phi\sin\theta \tag{4.43}$$

where $c_1, c_2, \ldots, c_6$ are arbitrary constants.

The patch test for rigid body movements is carried out with all the six arbitrary constants in Eqs. (4.41)-(4.43) set to unity. The maximum value of the stress and moment resultants for different element sizes are displayed in Table 16. The test is successfully passed for element subtending angles up to 16° within the classical shell theory accuracy.

Table 16. Patch test results for spherical shell: rigid-body displacements.

Element	Angle subtended by the element	Max. $[N_{\phi\phi}, N_{\phi\theta}, N_{\theta\theta}]$	Max. $[M_{\phi\phi}, M_{\phi\theta}, M_{\theta\theta}]$	Max. permissible error according to classical theory
KSHARA	16°	$0(10^{-4})$	$0(10^{-4})$	$N = 0(h^2/R)$ $= 0(10^{-3})$
	4°	$0(10^{-4})$	$0(10^{-5})$	$M = 0(h^3/R)$ $= 0(10^{-4})$

4.7 A Hemispherical Shell Under Concentrated Loads at the Open Edge

A test problem proposed by Morley and Morris [30] which has an engineering appeal is considered. This problem is directed at inextensional bending through the solution of a hemispherical shell subjected to concentrated loading actions as shown in Figure 34.

The finite element discretization of the symmetric one quarter of the shell is shown in Figure 34. The finite element mesh contains 51 elements with 35 nodal points resulting in 261 equations after the boundary conditions are imposed.

In Table 17 the normal deflection of the point 2 ($\phi = \pi/2$, $\theta = 0$) is compared against the alternative finite element and numerical solutions reported by Morley and Morris [30].

Two numerical solutions using the Rayleigh-Ritz method are presented in Ref. [30]. The first solution is a single series

Table 17. Comparison of normal displacement for the hemispherical shell under concentrated loads.

Element	Angle subtended in degrees	Normal displacement of point 2 WD/P_2R^2
SEMILOOF	18	0.179
SEMILOOF FACET	18	0.184
SHEBA 6	22.5	0.175
MSC/NASTRAN	9	0.188
BAE FACET	9	0.188
KSHARA	18	0.185
Theoretical		
Double trigonometric series solution		0.185
Inextensional solution		0.173

solution which involves only the inextensional mode of behavior. Such a solution is obtained using the general inextensional solution given by Eqs. (4.1)-(4.3). The arbitrary constants in this series solution are determined from the principle of minimum potential energy. A converged solution is obtained using 302 terms of the series. This solution is a lower bound for the displacement and does not account for the membrane and edge effects. The second numerical solution is obtained by a similar procedure using double trigonometric series which attempts to include the membrane and edge effects. Once again the displacements are lower bounds.

It is observed from Table 17 that the present KSHARA element recovers the theoretical value of 0.185 exactly. All the alternative finite solutions recover the theoretical solution within at least 8% accuracy. SEMILOOF element displays exceptionally good performance particularly in its facet mode. The result for SHEBA 6 is lower than the theoretical value of 0.185. Since this is a pure displacement element and most securely founded upon classical shell theory, the lower value for the SHEBA 6 element is considered as correct [30].

4.8 Anisotropic Example Problems

The performance of KSHARA element in the presence of material anisotropy is evaluated by solving two anisotropic problems. The first problem is a symmetrically laminated graphite-epoxy orthotropic plate under uniform transverse load, and the second problem that of an orthotropic cylinder with a circular hole under axial tension.

4.8.1 An Orthotropic Square Plate Under Uniform Pressure

The geometry and the construction details of a nine-layered, symmetrically laminated graphite-epoxy composite square plate is shown in Figure 36. The plate is made up of nine layers with fiber orientation of 0 and 90 degrees in the alternate layers with 0-degree layers as outside layers. The total thickness of the 0-degree and 90-degree layers is equal. In view of the symmetry, a quarter of the plate is discretized with element orientations as shown in Figure 36.

A convergence study for both the simply supported and clamped edges under a uniform pressure is carried out.

The convergence of the normal displacement and the bending moment at the center of the simply supported plate, along with the analytical solution of Noor and Mathers [94], is presented in Table 18. The convergence is monotonic and fast; the converged solution for displacement is within one percent of the analytical solution. The corresponding accuracy for the bending moment is within two percent.

The results for the clamped plate is compared against the finite element solution of Noor and Mathers [94] in Table 19. The comparative finite element solution was obtained using a shear-flexible quadrilateral with a 8X8 grid in the quarter plate. Again, the convergence is monotonic, and the results are predicted with satisfactory accuracy for the displacement. The error in the bending moment, however, is more than that for the simply-supported case. The error can be reduced by using a refined grid.

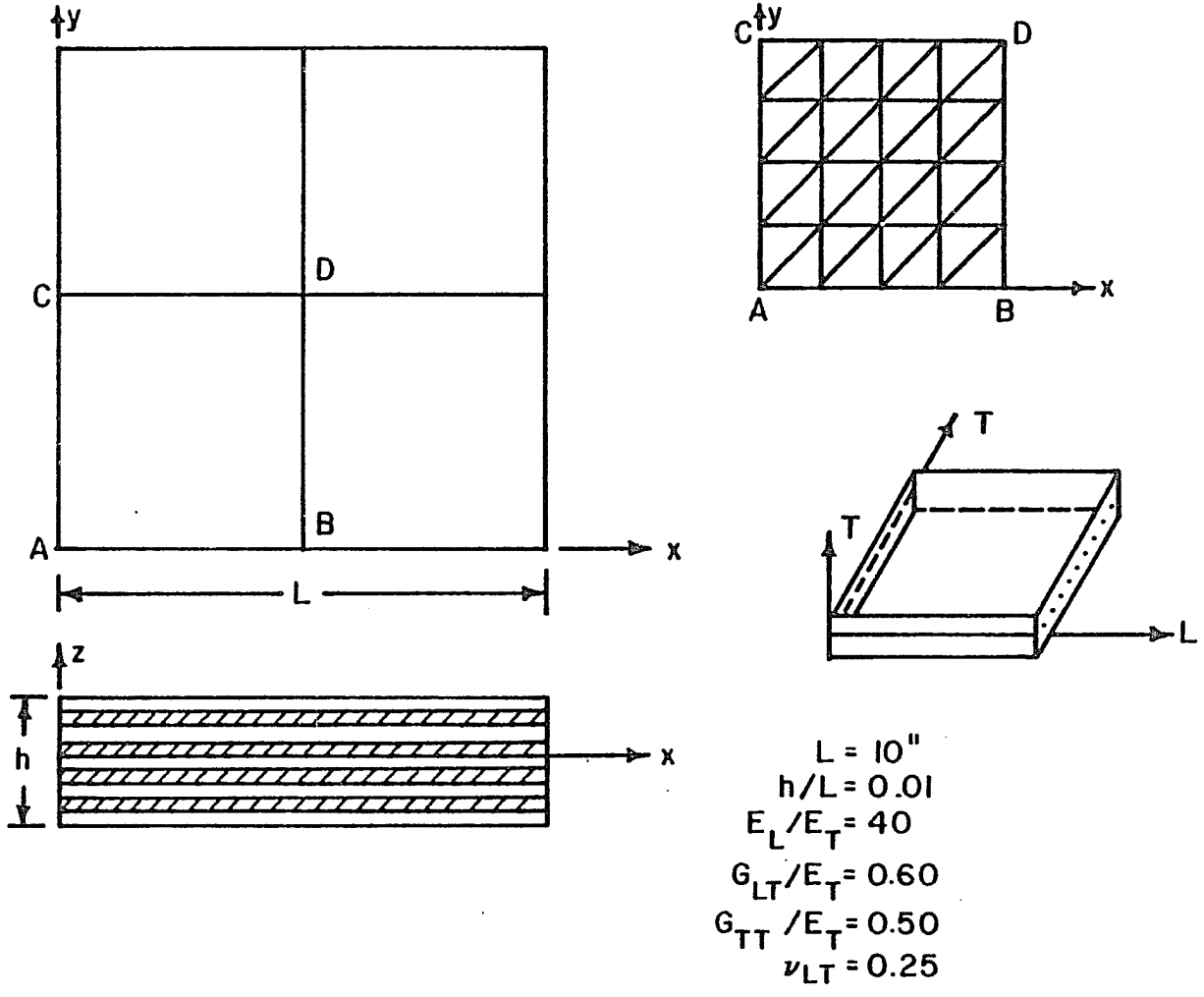

Figure 36. Nine-layered graphite-epoxy orthotropic square plate.

Table 18. Simply supported orthotropic square plate under uniform pressure: convergence of central deflection and central bending moment.

Grid size in quarter plate	No. of equations	$\bar{w}$ [a]	% Error	$\bar{M}_{xx}$ [b]	% Error
2X2	27	4.6101	2.78	9.6093	8.20
3X3	48	4.5342	1.09	9.2288	3.94
4X4	75	4.5076	0.49	9.0677	2.13
5X5	108	4.4950	0.21	8.9965	1.32
Analytical [94]		4.4855		8.8786	

[a] $\bar{w} = \dfrac{wE_t h^3}{pL^4} \times 10^2$

[b] $\bar{M}_{xx} = \dfrac{M_{xx} 10^2}{pL^2}$

Table 19. Clamped orthotropic square plate under uniform pressure: convergence of central deflection and bending moment.

Grid size in quarter plate	No. of equations	$\bar{w}$ [a]	% Error	$\bar{M}_{xx}$ [b]	% Error
2X2	27	10.498	8.97	-7.4345	12.50
3X3	48	9.976	3.55	-7.3526	11.28
4X4	75	9.772	1.44	-7.2372	9.53
5X5	108	9.676	0.42	-7.1466	8.16
F.E. Soln. [94]		9.634		-6.6074	

a $\bar{w} = \dfrac{\bar{w} \times 10^2 E_t h^3}{pL^4}$

b $\bar{M}_{xx} = \dfrac{M_{xx} \times 10^2}{pL^2}$

4.8.2 Orthotropic Cylindrical Shell with a Circular Hole Under Axial Tension

As the last example problem, an orthotropic cylindrical shell with a circular hole subjected to axial tensile load is considered. This problem is a severe test for the ability of the present element to predict accurately the stresses in the presence of severe stress gradients and the membrane-bending coupling due to the combined effects of curvature and material anisotropy.

The geometric details of the cylindrical shell are shown in Figure 37. Two cases of material properties are considered: the isotropic (aluminum) case ($E = 1.0 \times 10^7$ psi, $\nu = 0.3$), and the single-layered glass-epoxy composite case ($E_1 = 6.13 \times 10^7$ psi, $E_2 = 1.42 \times 10^6$ psi, $G_{12} = 0.53 \times 10^6$ psi, $\nu_{12} = 0.27$). In view of the symmetry one quarter of the shell is discretized as shown in Figure 38. The axial load is consistently modeled corresponding to the cubic variation of the axial displacement along the cylinder edge.

In Table 20 the membrane and total stress concentration factors at two critical locations on the hole boundary are compared with the analytical solution of Van Dyke [95] and the finite element solution of Lakshminarayana and Viswanath [96]. The alternative finite element solution uses a thirty-six degrees of freedom, high-precision cylindrical shell element.

It is observed that for the isotropic cylinder the principal stress concentration factors are predicted within 0.35 percent of the analytical solution. The present solution is more accurate than the comparative finite element solution although the number of equations

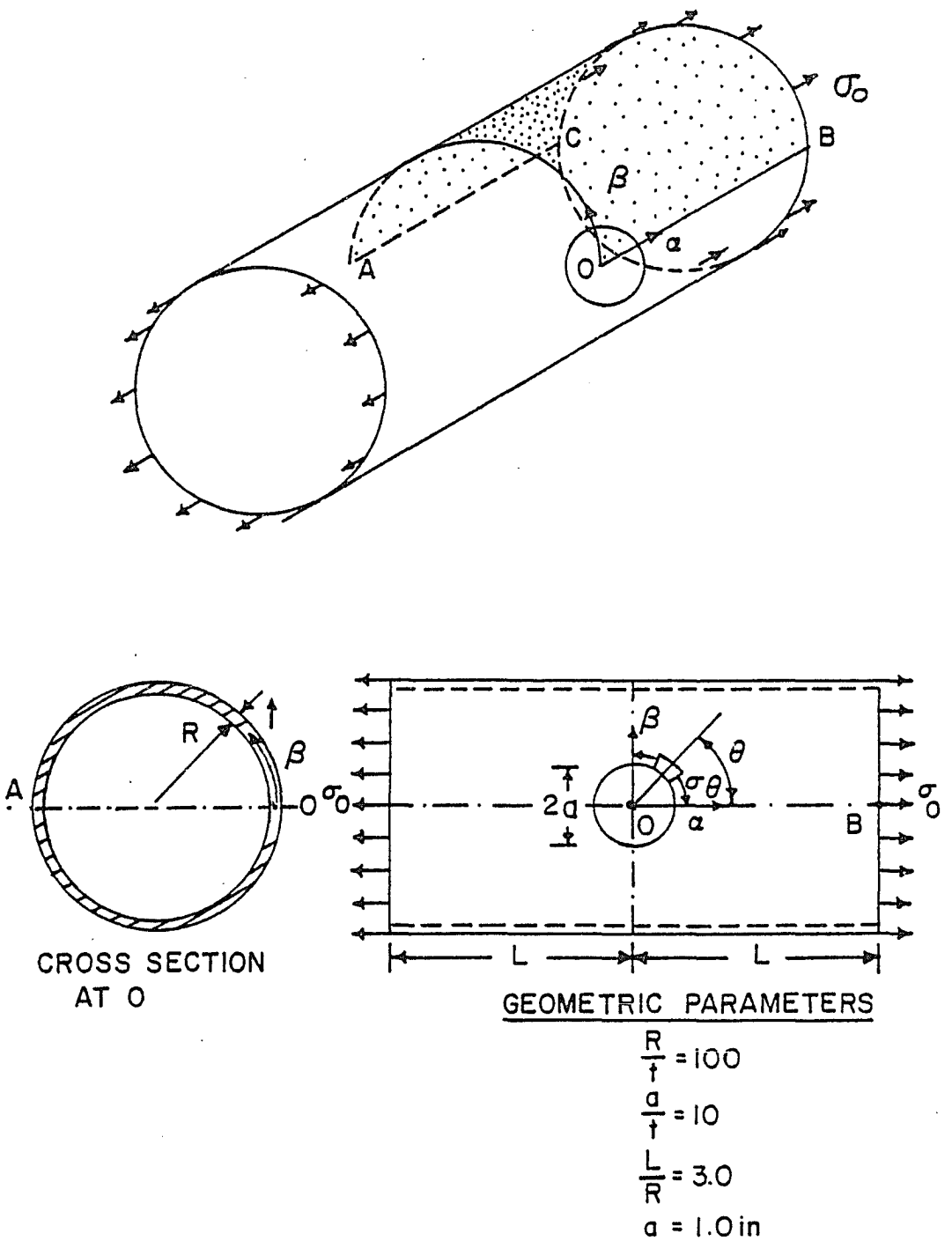

Figure 37. Cylindrical shell with a circular hole under axial tension.

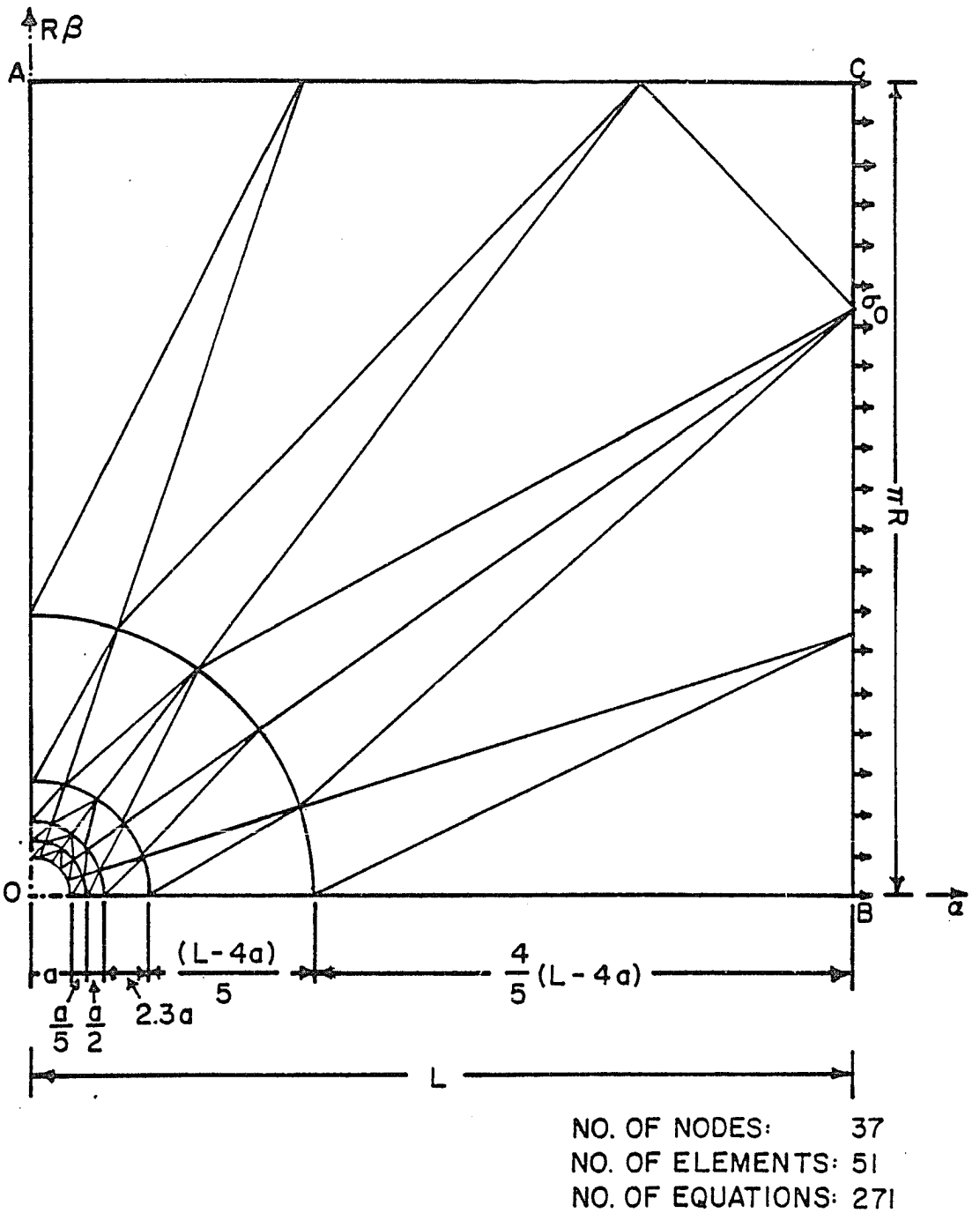

Figure 38. Finite element grid in quarter of the cylinder with circular hole under axial tension.

Table 20. Cylindrical shell with a circular hole under axial tension: comparison of stress ratios.

	Membrane stress ratio $(\sigma_\theta^m/\sigma_o)$		Total stress ratio $(\sigma_\theta^t/\sigma_o)$	
	$\theta = 0°$	$\theta = 90°$	$\theta = 0°$	$\theta = 90°$
Orthotropic shell				
Present solution	-0.5256	4.8166	-0.7645	5.1174
FEM solution [96]	-0.5037	4.9389	-0.8055	5.3780
Isotropic shell				
Present solution	-1.2205	3.5877	-1.7502	3.9174
FEM solution [96]	-1.2602	3.7042	-1.9360	4.2245
Analytical Soln. [95]	-1.25	3.6	-2.05	4.05

is less than 75 percent of the latter solution. These results also establish the adequacy of the finite element grid. In the same table the results for the orthotropic shell are compared with that of Ref. [96]. There is a good agreement between them with a maximum difference of less than five percent.

This example problem demonstrates the ability of the present element to predict the stresses within the engineering accuracy under severe adverse conditions typical of high stress gradients, material anisotropy and curvature effects.

CHAPTER 5

CONCLUSIONS

The research work presented here deals with problems associated with finite element analysis of laminated composite thin-shell structures. Their low weight and high strength-to-weight ratios have prompted their extensive use in aerospace and other industrial applications. Efficient and reliable design procedures and analysis tools are essential to establish the structural integrity and cost effectiveness of these structural forms.

The specific objective of this research was to develop a thin-shell finite element to model the linear elastic behavior of laminated composite shells, which would be efficient and simple to use by the practicing engineer. The satisfaction of mathematical requirements to ensure a sound theoretical basis was also, however, considered as equally important.

The formulation and numerical evaluation of the finite element developed herein are summarized in the following sections. An appraisal of the research work presented here, together with the concluding remarks are presented in the next section. Suggestions for future work are also included in the concluding section.

5.1 Summary of the Present Work

The issues associated with the development of thin-shell finite element, and a brief survey of the triangular thin-shell displacement finite elements in the literature were discussed in the first chapter. It was observed that the difficulties encountered in the development of curved thin-shell elements stem from the complexities of the underlying thin-shell theory, and the rigorous mathematical requirements of the finite element theory. These requirements include a satisfactory representation of the low-energy inextensional bending modes, and the required order of continuity of the assumed displacements and their derivatives across the interelement boundaries. Also, for an acceptable convergence rate a satisfactory representation of the rigid body modes must be included.

It was pointed out that the rigid body modes can be exactly represented by recourse to isoparametric representation of geometry of the shell middle surface within an element. Such a representation can be achieved by interpolation of the displacement components and the position vector to the shell middle surface by same set of shape functions in a global cartesian coordinate system.

It was also observed that Love's first-approximation shell theory, due to its established nature, forms the basis for the earlier thin-shell elements. In conjunction with the principle of minimum potential energy, this demands continuity of normal slope across the interelement boundaries for a conforming thin-shell element. It is, however, impossible to form such a shell element with simple nodal connection quantities, discounting the use of various artifices

al polynomials, sub-domain approach or
a the Lagrangian multiplier technique, among
slope continuity requirement became the
enue of search for a conforming thin-shell

proach in which the Kirchhoff hypothesis is
first for the development of plate elements
thin-shell elements. Here, the displace-
s of the middle surface are independently
the continuity of the displacement and
fficient for a conforming element. These
cessively stiff due to the transverse shear
the model, and also results in slow con-

s were surmounted by imposition of the
ype constraints at discrete number of points
eme later became known as the Discrete
nd was highly successful for plate elements.
survey of the curved triangular thin-shell
ications of the DKT were mostly
, and was, however, for deep shell
deep shell formulati approach
. This developmen
de representation.

Thus, the development of a curved triangular thin-shell element suitable for laminated composite deep shell applications, with an explicit representation of rigid body modes was sought.

The details of a linear shear deformation theory in a general curvilinear coordinate system using tensor notation was presented in the second chapter. The strain-displacement relations were transformed into a global cartesian coordinate system to enable the isoparametric representation of the shell geometry. A detailed derivation of the strain energy density in a laminated composite shell of arbitrary geometry was presented. Such a general strain energy calculation for laminated composite shells is, apparently, not available in the literature.

The finite element development was presented in the third chapter. The cartesian components of the element displacements and rotations are interpolated by simple polynomial shape functions in the natural area coordinates. The use of area coordinates renders the element behavior independent of the element orientation. Complete cubic and quadratic polynomials interpolate all three components of the displacement and rotation vectors, respectively, resulting in forty-eight generalized displacements. The position vector components are also interpolated by the same cubic polynomials.

A detailed derivation of the discrete Kirchhoff constraints and surface-normal rotation constraints is presented. The mid-side nodes used in the quadratic interpolation of the rotation components are eliminated by imposing a linear variation of the normal rotation along the element sides. Thus, a total of twenty-seven constraints,

and the static condensation of the three centroidal values of the displacements initially used, result in a three-node, twenty-seven-degree-of-freedom triangular element. The final degrees of freedom retained are the cartesian components of the three displacements and their first-order derivatives at each node.

It may be noted that the constraints were numerically implemented without deriving the DKT shape functions explicitly. Such an explicit derivation is very tedious, since all the displacement components are coupled in the constraint equations. Finally, the degrees of freedom are transformed into a local orthogonal curvilinear coordinate system to enable easy application of the support and symmetry conditions.

The results of the numerical evaluation were presented in the fourth chapter, where a number of bench mark problems as well as a few practical problems have been solved. The objective of the evaluation was two-fold: firstly, to assess the ability of the element to model shells of various shapes under different support and loading conditions; secondly, to evaluate the element under limiting states of deformation by solving the "patch test" problems.

The example problems cover the full range of values for the Gaussian curvature. The standard cylindrical shell roof problem serves to compare the alternative thin-shell elements. The problems of pinched cylindrical and spherical shells are typical of problems with low energy inextensional bending, accompanied with large rigid-body type displacements. The problem of torus under internal pressure is a special case in which the toroidal shell has regions of both

positive and negative Gaussian curvature. As a practical example problem, a hyperbolic cooling tower under Batch-Hopley wind pressure distribution has been solved. The pear-shaped cylinder is an example of a thin shell with curvature discontinuity.

Various patch test solutions applicable for spherical shell have been successfully applied to show the compliance of the conditions of conformity and convergence for this class of thin shells. Here, we may also mention the problem of a hemisphere under concentrated loads at its free edge, which was proposed in the literature as a patch-test problem having engineering appeal; the shell is in a state of predominantly inextensional bending deformation. A number of well-known elements are compared with the present element against this problem.

The chapter concludes with anisotropic example problems. A nine-layered graphite-epoxy composite plate under uniform pressure is analyzed to study the effect of membrane-bending coupling without the curvature effects. The problem of an orthotropic cylinder with a circular hole under axial tension provides the most adverse conditions with the combined effects of high stress concentration and membrane-bending coupling due to material orthotropy as well as curvature of the middle surface.

An appraisal of the thin-shell element developed herein is presented in the next section.

5.2 Discussion and Concluding Remarks

A brief discussion of the numerical results with the objective of performance evaluation is reiterated, followed by the concluding

remarks on the accomplishment of the objectives set forth in the beginning.

The cylindrical shell roof problem, which has been used in the past to compare different thin-shell elements, shows that good accuracy has been achieved for both the displacements and stresses. A fast convergence to the Koiter-Sanders deep shell solution has been achieved. The present element was found to be the most efficient among all the elements compared. Although the membrane stresses predominate, there is a significant bending of the shell; the element may be expected to perform satisfactorily in such situations.

The pinched cylinder problems, where bending predominates, have been used in the past to check the element formulation for correct representation of rigid body modes, since a large displacement occurs under the pinching loads. Again, satisfactory results for two thickness ratios have been obtained for the cylinder with free ends. The short cylinder with supported ends is a more critical problem due to strong interaction of the pinching loads and the support reactions. The variations in the displacements are satisfactorily predicted. The stress distributions also closely follow the analytical solution.

Here, we may also recall the isotropic case of the cylinder with a circular hole under axial load presented at the end of the fourth chapter. A very good accuracy was obtained for the principal stress concentration factors. Thus, we may expect the element to show good performance for shells with zero Gaussian curvature.

Two of the problems featured positive Gaussian curvature. The results for the shallow spherical cap are satisfactory. For the case

of pure membrane state of stress in an internally pressurized sphere, fast convergence toward the membrane solution has been obtained. The small discrepancy in the results near the equator may be due to the relatively large element size used, and the resulting error of cubic approximation of the surface.

The pinched sphere problem has regions with predominately bending stress near the poles, followed by membrane regions near the equator. Besides, the regions near the poles have high stress concentration. The displacements and stresses within twenty degrees from the pole are one order of magnitude more than those near the equator.

The normal displacement of the pole, which is proportional to the strain energy in the shell, is converging to the Koiter's Solution. The displacement and stress distributions near the equator agree almost exactly with the membrane solution. The displacement and bending moment distributions near the pole agree more closely with the comparative solutions than the membrane stress resultants.

Although there is a good performance for the positive Gaussian curvature shells in general, there is a need to obtain better accuracy for the stresses. The sampling of stresses at the nodes might have contributed to this low accuracy. A better accuracy may be expected if the stresses are calculated at the Gaussian points of integration. A simple modification to the element suggested in the later part of this chapter is expected to provide an improved accuracy for the stresses.

Excellent results have been obtained for the torus under internal pressure. The displacement and stress distributions agree almost exactly with the comparative numerical solution. The cubic representation of the torus geometry is apparently able to satisfactorily represent this variable curvature shell which has regions of both positive and negative Gaussian curvature.

The results for the hyperbolic cooling tower under wind loading are also encouraging. The displacements are predicted with better accuracy than the stress resultants. This problem demonstrates the ability of the element to solve practical shell problems, and those with negative Gaussian curvature.

The shell problems with curvature discontinuity can also be successfully solved, as shown by the example of the pear-shaped cylinder. There is a need, however, to uncouple certain degrees of freedom to reflect the discontinuity in certain strains and normal rotation.

The satisfactory results for the patch test problems contribute to confidence in the element. It provides an indirect verification of the satisfaction of the conditions of conformity and convergence. The patch test results show the relative superiority of the present element over other well-known elements.

Two examples show that good accuracy can be achieved in the presence of material anisotropy. There is, however, a need to solve additional problems to establish performance of the element for anisotropic shells of various shapes and different lamination parameters.

Thus, the discrete Kirchoff theory approach in conjunction with the isoparametric representation of the shell geometry has resulted in a simple conforming curved triangular thin shell element, meeting a majority of the requirements set forth in the beginning. The linear shear deformation theory for the laminated composite shells of arbitrary geometry is a novel feature of the present work. The numerical results show that the element is efficient, and is able to give results of engineering accuracy for shells of various shapes under different support and loading conditions. Also, it may be noted that, the approximation of the shell middle surface geometry within the element by cubic polynomials has been apparently satisfactory for a majority of the shell shapes encountered in practical applications. The element size, however, should be carefully selected for shells with variable curvature to avoid errors due to geometric approximation.

The present element formulation can be readily combined with a mathematical surface representation algorithm to provide an integrated solution system for arbitrary thin shells. Since the shell theory is formulated in a general curvilinear coordinate system, the surface representation algorithms which result in such a surface coordinate system can be easily accommodated.

In the next and the final section, some modifications and extensions for the present formulation are discussed.

5.3 Suggestions for Further Study

In the light of the experience accrued during the numerical evaluation of the element, two modifications may be suggested which are expected to improve the accuracy of the solution, especially for the stresses. Also, a few simple extensions are recommended, which would enhance the modeling and analysis capabilities of the element.

5.3.1 Suggestions for Modifications

As already noted in the previous section, a better accuracy for the stresses can be obtained by sampling the stresses at the Gauss points. The stresses reported here are based on the nodal averages. The numerical integration scheme used in the program uses the thirteen-point rule in the natural area coordinates. It is completely symmetric in these area coordinates. It would be convenient to evaluate the stresses at the three Gauss points symmetrically placed near the nodes, and the element centroid, which is also a Gauss point.

The second modification would involve the retention of the mid-side nodes, thus restoring quadratic variation of the normal rotation along the element sides. The mid-side nodes used for the quadratic interpolation of the rotation components were eliminated by imposing a linear variation of the normal rotation along the element sides. Although this elimination contributes to the solution efficiency in view of the reduced band width of the resulting algebraic equations, it also contributes to the lower convergence rate, since the latter depends on the order of the complete-polynomial

used for the rotation interpolation. The quadratic slope variation can be retained by having the mid-side nodes with normal rotation as the nodal variable, resulting in three more degrees of freedom for the element. This modification is simple and straightforward.

In the next section a few suggestions for extension of the present work are presented.

5.3.2 Suggestions for Extensions

Many extensions can be undertaken with the aim of enhancing the analysis capabilities, and those of the material and geometric modeling.

One of the obvious extensions is to include the effects of nonlinearities due to large deformations and those due to nonlinear elastic behavior of the material. Since it is a displacement formulation, the geometric nonlinear effects can be incorporated by recourse to nonlinear strain-displacement relations and establishing the incremental equilibrium equations which can be solved using one of the nonlinear solution algorithms. This also leads to the solution of the important problem of elastic stability of thin shells.

The element can be extended to the analysis of sandwich shells, which are finding increasing applications in the lightweight industry. Sandwich construction using composite laminates as facings, and aluminum honeycomb or foam-rubber as core material is most commonly used. The analysis of sandwich shells is usually based on the assumption that the facings resist the bending moments, and the core resists the shearing loads.

The development of an integrated surface representation system would be very useful. The technology of computer graphics and the advancements in the computer-aided design have brought structural design and analysis closer than ever before. Hence the need for such an integrated system with the ability to utilize the data bases generated during the design phase cannot be overstated.

The development of the quadrilateral version of the element also merits serious consideration.

REFERENCES

1. Lame, G., and B. P. E. Clapeyron, "Memoire Surlequilibre interieur des corps solides," Mem. Pres. Par Div. Savants, Vol. 4, 1833.

2. Beltrami, E., "Sull equilibrie delle supperficie flessibili ed inestendibili," Mem. Roy. Acad. Sci di Bologna, 1881.

3. Kirchhoff, G., "Vorlesungen über Mathematische Physik," Mechanik, Vol. 1, 1876.

4. Aron, H., "Das Gleichgewicht und die Bewegung einer unendlich dünnen, beliebig gekrümmten, elastichen schale," Zeit. reine Angew. Math., Vol. 78, 1874.

5. Love, A. E. H., "On the Small Vibrations and Deformations of Thin Elastic Shells," Phil. Trans. Roy. Sci., Vol. 179, 1888.

6. Koiter, W. T., "A Consistent First Approximation in the General Theory of Thin Elastic Shells," Proc. First IUTAM Symposium on Theory of Thin Elastic Shells (Ed. W. T. Koiter), North-Holland, 1960.

7. Sanders, J. L., "An Improved First-Approximation Theory for Thin Shells," NASA Report 24, 1959.

8. Reissner, E., "Stress Strain Relations in the Theory of Thin Elastic Shells," J. Math. Phys., Vol. 31, pp. 109-119, 1952.

9. Naghdi, P. M., "On the Theory of Thin Elastic Shells," Quart. Appl. Math., Vol. 14, No. 4, pp. 369-380, 1957.

10. Reissner, H., "Spannungen in Kugelschalen(Kuppein)," Festschrift Mueller-Breslau, pp. 181-193, 1912.

11. Meissner, E., "Das Elastizitätsproblem dünner schalen von Ringflachen-, Kugel-order Kegelform," Physik. Z., Vol. 14, pp. 343-349, 1913.

12. Reissner, E., "On the Theory of Thin Elastic Shells," H. Reissner Anniversary Volume, pp. 231-247, 1949.

13. Hilderbrand, F., "On Asymptotic Integration in Shell Theory," Proc. Symp. Appl. Math., Vol. 3, pp. 53-66, 1950.

14. Langer, R. E., "On the Asymptotic Solution of Ordinary Differential Equations with Reference to the Stokes' Phenomenon about a Singular Point," Trans. Am. Math. Soc., Vol. 37, pp. 397-416, 1935.

15. Clark, R. A., "On the Theory of Thin Elastic Toroidal Shells," J. Math. Phys., Vol. 29, pp. 146-178, 1950.

16. Naghdi, P. M., and C. N. DeSilva, "Deformation of Elastic Ellipsoidal Shells of Revolution," Proc. Second U.S. Nat. Congress Appl. Mech., pp. 333-343, 1955.

17. DeSilva, C. N., "Deformation of Elastic Paraboloidal Shells of Revolution," Uni. Mich. Engng. Res. Inst., Tech. Report 5, Project 2150, 1956.

18. Courant, R., "Variational Methods for the Solution of Problems of Equilibrium and Vibration," Bull. Am. Math. Soc., Vol. 49, pp. 1-43, 1943.

19. Argyris, J. H., and S. Kelsey, Energy Theorems and Structural Analysis, Butterworth Scientific Publication, London, 1960.

20. Turner, M., R. Clough, H. Martin, and L. Topp, "Stiffness and Deflection Analysis of Complex Structures," J. Aero. Sci., Vol. 23, No. 9, pp. 805-823, 1956.

21. Zienkiewicz, O. C., "The Finite Element Method: From Intuition to Generality," Appl. Mech. Rev., Vol. 23, No. 23, pp. 249-256, 1970.

22. Zienkiewicz, O. C., The Finite Element Method, 3rd Edition, McGraw-Hill, London, 1977.

23. Gallagher, R. H., Finite Element Analysis: Fundamentals, Prentice-Hall, Englewood Cliffs, 1975.

24. Desai, C. S., and J. F. Abel, Introduction to the Finite Element Method, Van Nostrand Reinhold Company, New York, 1972.

25. Morris, A. J., "A Summary of Appropriate Governing Equations and Functions in the Finite Element Analysis of Thin Shells," in Finite Elements for Thin Shells and Curved Members (Eds. D. G. Ashwell and R. H. Gallagher), John Wiley and Sons, London, 1976.

26. Truesdell, C., and R. A. Toupin, Encyclopaedia of Physics, Vol. III/1, Springer-Verlag, 1960.

27. Gol'denveizer, A. L., Theory of Elastic Thin Shells (Translator, G. Herrmann), Pergamon, Oxford, 1961.

28. Naghdi, P. M., "Foundations in Elastic Shell Theory," Progress in Solid Mechanics (Ed. Sneddon and Hill), Vol. IV, North-Holland, 1963.

29. Novozhilov, V. V., The Theory of Thin Shells, P. Noordhoff, Groningen, Netherlands, 1964.

30. Morley, L. S. D., and A. J. Morris, "Conflict Between Finite Elements and Shell Theory," in Finite Element Methods in the Commercial Environment (Ed. John Robinson), Vol. 2, Robinson and Associates, England, 1978.

31. Dupuis, G., "Application of Ritz's Method to Thin Elastic Shell Analysis," Trans. ASME, J. Appl. Mech., Ser. E, Vol. 38, No. 4, pp. 987-996, 1971.

32. Clement, P., and J. Descloux, "On the Rigid Body Displacement Condition," Int. J. Num. Meth. Engng., Vol. 4, No. 4, pp. 583-586, 1972.

33. Cowper, G. R., "CURSHL: A High-Precision Finite Element for Shells of Arbitrary Shape," Aeronautical Report LR-560, National Research Council of Canada, Ottawa, December 1971.

34. Thomas, G. R., and R. H. Gallagher, "A Triangular Thin Shell Finite Element: Linear Analysis," NASA CR-2482, July 1975.

35. Morley, L. S. D., "Polynomial Stress States in First Approximation Theory of Circular Cylindrical Shells," Quart. J. Mech. Appl. Math., Vol. 25, pp. 13-43, 1972.

36. Argyris, J. H., and D. Scharpf, "The SHEBA Family of Shell Elements for the Matrix Displacement Method," Aeronautical J., Vol. 72, pp. 873-883, 1968.

37. Irons, B. M., and K. J. Draper, "Inadequacy of Nodal Connections in a Stiffness Solution for Plate Bending," AIAA J., Vol. 3, p. 61, 1965.

38. Clough, R., and J. Tocher, "Finite Element Stiffness Matrices for the Analysis of Plate Bending," Proc. First Conf. on Matrix Methods in Structural Mechanics, Wright-Patterson A.F. Base, Ohio, AFFDL TR 66-80, 1965.

39. Bazeley, G. P., Y. K. Cheung, B. M. Irons, and O. C. Zienkiewicz, "Triangular Elements in Bending--Conforming and Non-Conforming Solutions," Proc. First Conf. on Matrix Methods in Structural Mechanics, Wright-Patterson A.F. Base, Ohio, AFFDL TR-66-80, 1965.

40. Harvey, J., and S. Kelsey, "Triangular Plate Bending Element with Enforced Compatibility," AIAA J., Vol. 9, No. 6, pp. 1023-1026, 1971.

41. Bonnes, G., G. Dhatt, Y. Giroux, and L. Robichaud, "Curved Triangular Elements for the Analysis of Shells," Proc. Second Conf. on Matrix Methods in Structural Mechanics, Wright-Patterson A.F. Base, Ohio, 1968.

42. Melosh, R. J., "A Flat Triangular Shell Element Stiffness Matrix," in Proc. First Conf. on Matrix Methods in Structural Mechanics, Wright-Patterson A.F. Base, Ohio, AFFDL TR-66-80, 1965.

43. Utku, S., "Stiffness Matrices for Thin Triangular Elements of Non-Zero Gaussian Curvature," AIAA J., Vol. 5, No. 9, pp. 1653-1667, 1967.

44. Key, S. W., and Z. E. Beisinger, "The Analysis of Thin Shells by the Finite Element Method," in IUTAM Symposium on High Speed Computing of Elastic Structures, TOME 1, U. of Liege Press, pp. 209-252, 1971.

45. Wempner, G. A., J. T. Oden, and D. A. Kross, "Finite Element Analysis of Thin Shells," Proc. ASCE, J. Engng. Mech. Div., No. EM6, pp. 1273-1294, 1968.

46. Coons, S. A., "Surfaces for Computer-Aided Design," M.I.T. Project Report, Mac-TR-41, 1967.

47. Ferguson, J. C., "Multivariable Curve Interpolation," J. ACM, Vol. 11, p. 221, 1964.

48. Bezier, P., Numerical Control Mathematics and Applications, Wiley, New York, 1972.

49. Lien, S., "Finite Element Elastic Thin Shell Pre- and Post Buckling Analysis," Ph.D. dissertation, Cornell University, Ithaca, New York, 1971.

50. Wu, S. C., "An Integrated System for Finite Element Shell Analysis--Surface Representation and Curved Shell Element," Ph.D. dissertation, Cornell University, Ithaca, New York, 1980.

51. Gallagher, R. H., "Problems and Progress in Thin Shell Finite Element Analysis," in Finite Elements for Thin Shells and Curved Members (Eds. D. G. Ashwell and R. H. Gallagher), John Wiley, London, 1976.

52. Gallagher, R. H., "Analysis of Plate and Shell Structures," in Proc. Symp. on Applications of Finite Element Methods in Civil Engineering, Vanderbilt University, Nashville, Tenn., pp. 155-205, 1969.

53. Dawe, D. J., "Curved Finite Elements in the Analysis of Shell Structures," Proc. of First Int. Conf. on Struc. Mechanics in Reactor Technology, Vol. 5, Part J, Berlin, 1971.

54. Gallagher, R. H., "Shell Elements," World Conf. on Finite Element Methods in Structural Mechanics, Bournemouth, 1975.

55. Bushnell, D., "Thin Shells," in Structural Mechanics Computer Program: Surveys, Assessments and Availability (Ed. W. Pilkey et al.), U. of Virginia Press, Charlottesville, Virginia, 1974.

56. Cowper, G. R., G. M. Lindberg, and M. D. Olson, "Comparison of Two High Precision Triangular Elements for Arbitrary Deep Shells," Proc. of Third Conf. on Matrix Methods in Structural Mechanics, Wright-Patterson A.F. Base, Ohio, 1971.

57. Cowper, G. R., G. M. Lindberg, and M. D. Olson, "A Shallow Shell Finite Element of Triangular Shape," Int. J. of Solids Structures, Vol. 6, pp. 1133-1156, 1970.

58. Argyris, J. H., and N. Lochner, "On the Application of the SHEBA Shell Element," Comp. Methods in Applied Mech. and Engng., Vol. 1, No. 1, pp. 317-347, 1972.

59. Dupuis, G., and J.-J. Goel, "Finite Elements with High Degree of Regularity," Int. J. Num. Meth. Engng., Vol. 2, No. 4, pp. 563-577, 1970.

60. Scordelis, A. C., and K. S. Lo, "Computer Analysis of Cylindrical Shells," J. of American Concrete Institute, Vol. 61, pp. 539-561, 1964.

61. Thomas, G. R., and R. H. Gallagher, "A Triangular Element Based on Generalized Potential Energy Concepts," in Finite Elements for Thin Shells and Curved Members (Eds. D. G. Ashwell and R. H. Gallagher), John Wiley, London, 1976, Chapter 9.

62. Thomas, G. R., and R. H. Gallagher, "A Triangular Thin Shell Finite Element: Nonlinear Analysis," NASA CR-2483, 1975.

63. Kanodia, V. L., "Finite Element Elastic Instability Analysis of Deep Shells of Double Curvature," Ph.D. dissertation, Cornell University, Ithaca, New York, 1976.

64. Birkhoff, G., and L. Mansfield, "Compatible Triangular Finite Elements," J. Math. Anal. Appl., Vol. 47, pp. 531-553, 1974.

65. Irons, B. M., and A. Razzaque, "Shape Function Formulations for Elements Other Than Displacement Methods," in Proc. Int. Conf. on Variational Methods in Engng., Southampton, 1972.

66. Irons, B. M., and A. Razzaque, "Experience with Patch Test," in Mathematical Foundations of the Finite Element Methods (Ed. A. R. Aziz), Academic Press, 1972.

67. Chang, San-Cheng, "An Integrated Finite Element Nonlinear Shell Analysis System with Interactive Comuter Graphics," Ph.D. dissertation, Cornell University, Ithaca, New York, 1981.

68. Batoz, J. L., K. J. Bathe, and L. W. Ho, "A Study of Three-Node Triangular Plate Bending Elements," Int. J. of Numer. Meth. in Engng., Vol. 15, pp. 1771-1812, 1980.

69. Batoz, J. L., and G. Dhatt, "An Evaluation of Two Simple and Effective Triangular and Quadrilateral Plate Bending Elements," in Proc. of New and Future Developments in Commercial Finite Element Method, Los Angeles, California, pp. 352-368, 1981.

70. Stricklin, J. A., W. Haisler, P. Tisdale, and R. Gunderson, "A Rapidly Converging Triangular Plate Element," AIAA J., Vol. 7, No. 1, pp. 180-181, 1969.

71. Dhatt, G., "Numerical Analysis of Thin Shells by Curved Triangular Elements Based on Discrete Kirchhoff Hypothesis," in Proc. Symp. on Applications of Finite Element Methods in Civil Engineering, Vanderbilt U., Nashville, Tenn., pp. 255-278, 1969.

72. Dhatt, G., "An Efficient Triangular Shell Element," AIAA J., Vol. 8, No. 11, pp. 2100-2102, 1970.

73. Batoz, J. L., and G. Dhatt, "Development of Two Simple Shell Elements," AIAA J., Vol. 10, No. 2, pp. 237-238, 1972.

74. Batoz, J. L., "Analyse non Linéaire Des Coques Minces Élastiques De Formes Arbitraires par Élements Triangulaires Coubés," D.Sc. dissertation, U. of Laval, Quebec, Canada, March, 1977.

75. Batoz, J. L., A. Chattopadhay, and G. S. Dhatt, "Finite Element Large Deflection Analysis of Shallow Shells," Int. J. Num. Meth. Engng., Vol. 10, No. 1, pp. 39-58, 1976.

76. Wempner, G., Mechanics of Solids with Applications to Thin Bodies, McGraw-Hill, New York, 1973, pp. 484-485, 528-529.

77. Ciarlet, Philippe G., Numerical Analysis of the Finite Element Method, Les Presses De L'Université De Montréal, Canada, 1976, Section 16, pp. 271-272.

78. Cowper, G. R., "Gaussian Quadrature Formulas for Triangles," Int. J. Num. Meth. Engng., Vol. 3, pp. 405-407, 1971.

79. Forsberg, K., and R. Hartung, "An Evaluation of Finite Difference and Finite Element Techniques for Analysis of General Shells," in IUTAM Symp. on High Speed Computing of Elastic Structures, TOME II, Univ. of Liége Press, pp. 847-859, 1971.

80. Ashwell, D. G., and A. B. Sabir, "A New Cylindrical Finite Element Based on Simple Independent Strain Functions," Int. J. Mech. Sciences, Vol. 14, p. 171, 1972.

81. Cantin, G., "Rigid Body Motions of Curved Finite Elements," AIAA J., Vol. 8, p. 1252, 1970.

82. Timoshenko, S., and Woinowsky-Kreiger, Theory of Plates and Shells, 2nd Ed., McGraw-Hill, New York, 1969.

83. Dawe, D. G., "High-Order Triangular Finite Element for Shell Analysis," Int. J. Solids Structures, Vol. 11, pp. 1097-1110, 1975.

84. Lindberg, G. M., M. D. Olson, and G. R. Cowper, "New Developments in the Finite Element Analysis of Shells," Reprint of article from DME/NAE Quarterly Bulletin, No. 1969 (4), National Aeronautical Establishment, National Research Council of Canada, Ottawa, January, 1970.

85. Flügge, W., Stresses in Shells, Springer-Verlag, Berlin, 1962, p. 221.

86. Ambartsumyan, S. A., "On the Calculation of Shallow Shells," NACA TM 1425, 1956.

87. Koiter, W. T., "A Spherical Shell Under Point Loads at its Poles," Progress in Applied Mechanics (The Prager Anniversary Volume), Macmillan, New York, 1963.

88. Flügge, W., Stresses in Shells, Springer-Verlag, Berlin, 1960, pp. 350-353.

89. Kalnins, A., "Analysis of Shells of Revolution Subjected to Symmetrical and Nonsymmetrical Loads," Trans. ASME, J. of Applied Mechanics, Series E., Vol. 86, pp. 467-476, 1964.

90. Albasiny, E. L., and D. W. Martin, "Membrane and Bending Equilibrium in Cooling Towers," Proc. of ASCE, J. of the Engng. Mech. Div., Vol. 95, No. EM3, pp. 1-17, 1967.

91. Hartung, R. F., and R. Z. Ball, "A Comparison of Several Computer Solutions to Three Structural Analysis Problems," AFFDL-TR-73-15, 1973.

92. Lindberg, G. M., and G. R. Cowper, "An Analysis of a Cylindrical Shell with a Pear-Shaped Cross Section--Lockheed Sample Problem No. 1," Report No. ST-139, National Aeronautical Establishment, National Research Council of Canada, Ottawa, 1971.

93. Morley, L. S. D., and B. C. Merrifield, "Polynomial Comparison Solutions in the Sanders-Koiter Theory of Circular Cylindrical Shells," in Finite Elements for Thin Shells and Curved Members (Eds. D. G. Ashwell and R. H. Gallagher), John Wiley, 1976, Chapter 3.

94. Noor, A. K., and M. D. Mathers, "Shear-Flexible Finite Element Models of Laminated Composite Plates and Shells," NASA TN-D 8044, 1975.

95. Van Dyke, P., "Stress About a Circular Hole in Cylindrical Shell," AIAA J., Vol. 3, No. 9, pp. 1733-1742, 1965.

96. Lakshminarayana, H. V., and S. Viswanath, "A High-Precision Triangular Laminated Cylindrical Shell Finite Element," Computers and Structures, Vol. 8, pp. 633-640, 1978.